Effects of aging on skeletal muscle stem cells revealed by single-cell transcriptomics and lineage tracing

by

J. V. Kurland

B.A., Boston University 2014

A thesis submitted to the

Faculty of the Graduate School of the

University of Colorado in partial fulfillment

of the requirements for the degree of

Doctor of Philosophy

Department of Molecular, Cellular, and Developmental Biology

2023

Committee Members:

Dr. Bradley B. Olwin and Dr. Robin D. Dowell

Dr. Justin Brumbaugh, Chair

Dr. Mary Ann Allen

Dr. Lee Nisewander

Kurland, J. V. (Ph.D., MCDB)

Effects of aging on skeletal muscle stem cells revealed by single-cell transcriptomics and lineage
    tracing

Thesis directed by Prof Dr. Bradley B. Olwin and Dr. Robin D. Dowell

Skeletal muscle is critical for overall organismal health and well-being. As individuals age, skeletal muscle function severely declines, resulting in reduced mobility, strength, and regenerative capacity. This decline results in part from intrinsic and extrinsic deficits associated with muscle stem cell function, but many open questions remain about the underlying drivers of skeletal muscle aging. Understanding how aging affects skeletal muscle function has been difficult given that aging impacts such fundamental biological processes as transcription and cell-fate determination, creating complex phenotypes that obscure the underlying drivers of aging-associated changes. Thus, to uncover the fundamental causes of skeletal muscle aging requires methodologies capable of comprehensive assessment of alterations to biological systems that occur with aging.

In my thesis work, I describe features of aging-associated muscle decline by utilizing various single-cell approaches and focusing on changes associated with muscle stem cells in aged mice. First, I developed a framework for analyzing single-cell lineage tracing data obtained from a novel barcode lineage tracing assay, from which I identified altered population dynamics during muscle stem cells expansion in aged compared to young mice. Additionally, I employed an in-depth bioinformatic analysis of single-nucleus transcriptomics to generate a comprehensive pseudotime trajectory of myogenic differentiation in young and aged mice. Through this analysis, I detected fundamental changes to temporally coordinated myogenic gene expression during aged mouse regeneration propagating from muscle stem cells into myogenic progenitors, and finally into post-fusion myonuclei, affecting gene networks critical for regenerative myogenesis. And lastly, I reveal that constitutive activation of critical myogenic signaling succeeds in recovering young-like transcriptomic signatures in muscle stem cells from aged mice, yet surprisingly this rejuvenation of muscle stem cells in aged

mice alone was not sufficient to detectably improve muscle function, supporting the role of factors extrinsic to muscle stem cells in contributing to depreciated skeletal muscle function in aging organisms. Thus, taken together, my thesis work provides important perspectives that add to the fields' understanding of skeletal muscle aging and that will help guide future studies exploring the fundamental mechanisms of skeletal muscle aging.

Dedication

To this vast and beautiful universe and all which it contains.

Acknowledgements

Since my first experiences with academic research, I've been captivated by the process of scientific training, specifically in the dedication it demands of researchers to constantly impart their knowledge, technical and otherwise, to a new generations of scientists. I am indescribably thankful for the remarkable passion and commitment to training exhibited by the individuals who played instrumental roles during my doctoral training. Their unwavering drive to guide me during this transformative process has left an indelible impact on me, shaping my growth as a scientist and reinforcing in me a profound appreciation for the pursuit of knowledge.

I'd first like to thank my two thesis advisors, Dr. Bradley Olwin and Dr. Robin Dowell. Taking me on as a 3rd year joint-student was not without risk, and this initial display of confidence in me and my capabilities was something I often pondered in low moments and which proved instrumental in carrying me through the years of my doctoral training. Ultimately, these two wonderful people provided me with such superior scientific training, as well as personal mentorship, that I cannot overstate the long-term impact they will have on my life and career.

Apart from Dr. Olwin and Dr. Dowell, a vibrant community of scientists at CU Boulder played integral roles during my educational journey. Foremost, I express my gratitude to Dr. Alicia Cutler from Dr. Olwin's lab, who provided unrivaled scientific and personal mentorship, of which without, I'm sure my story would have not turned out the the way it has. Her ability to bestow her extensive knowledge of muscle biology was remarkable enough, but it was her positive and pragmatic guidance that I am most grateful for, and that which was critical for virtually every step of my graduate school career.

I'd also like to thank Dr. Mary Ann Allen who, in addition to her unwavering and inspiring enthusiasm that continuously reinforced my own passion for science on numerous occasions, provided me with my first experiences in learning computational biology. Amazingly, Dr. Allen always has time for her students, and I am extremely grateful for her patience and dedication for teaching and the impact it has had on my doctoral training.

There is also Dr. Jacob Stanley, a post-doctoral researcher from Dr. Dowell's lab. I had the opportunity to take a course taught by Dr. Stanley, and afterward, I reached out to him for his computational expertise. Though the time Dr. Stanley and I interacted was less than of the other individuals mentioned, his contribution to my training was no less significant. I accredit Dr. Stanley with helping foster in me a more diligent and thoughtful approach to computational biology, a pivotal aspect of my training that allowed my research to reach the doctoral level it has. I am grateful for his invaluable contribution to my academic journey.

I also would like to thank the not yet mentioned members of my thesis committee, Dr. Lee Nisewander, and the chair of my committee, Dr. Justin Brumbaugh. Together, these two incredibly gifted thinkers and mentors helped guide me through the later stages of my graduate career, engendering in me the confidence as a scientist I needed to take the final steps towards graduating and completing my doctoral training.

Apart from the individuals mentioned, I want to thank all students and faculty of the MCDB department for fostering a truly wonderful environment to conduct research. Without this greater community here at CU Boulder, I can confidently say that this time spent in my doctoral training would have been far less positive. And so I am appreciative for all interactions over the years, whether brief or substantial, as each person has helped shape my journey in a meaningful way.

Contents

Figures

Figure

Supplementary Figures

Chapter 1

Introduction

In this thesis, I sought to unravel features of skeletal muscle aging through single-cell analyses of muscle stem cell transcriptomics and population dynamics in young and aged mice. My research contributes important advances towards understanding skeletal muscle decline in aging by focusing on fundamental changes to muscle stem cells and their behavior, and the effects of these changes on progenitor proliferation, myonuclear maturation, and muscle function. Altogether, my research explores novel and understudied perspectives on the underlying drivers of skeletal muscle aging and offers areas rich for further investigations into the mechanistic details.

As one of the largest, most dynamic tissues in mammalian organisms, skeletal muscle enables all physical movement including walking (locomotion), talking, eating, and breathing [1–3]. As we age, our skeletal muscle function deteriorates, contributing to significantly declining standard of living among elderly individuals [4–6]. While resident muscle stem cells play a critical role in staving off muscular decline in aging, the full extent of how aging impacts muscle stem cell function is unclear [7–10].

In this chapter, I introduce features of skeletal muscle integral for understanding and contextualizing the work comprising my dissertation. I summarize the process of regeneration whereby muscle stem cells expand after an injury to rapidly regenerate skeletal muscle tissue. I then discuss the current understanding of muscle stem cell heterogeneity and different models describing their population dynamics, as well as describe how the fields' understanding of muscle stem cell functional organization is incomplete. Lastly, I will summarize what is known about the effects of

aging on muscle stem cell function and how my work comprising this dissertation contributes to a greater understanding of skeletal muscle aging.

1.1   Skeletal muscle

Skeletal muscle is a tissue present in all vertebrates enabling movement, eating, breathing, and reproduction [1–3]. Contraction of skeletal muscle cells triggered by impulses originating in the brain make possible most physical processes we associate with life [11], where evolution of the capacity for intentional movement is proposed as a fundamental hallmark of living organisms [12].
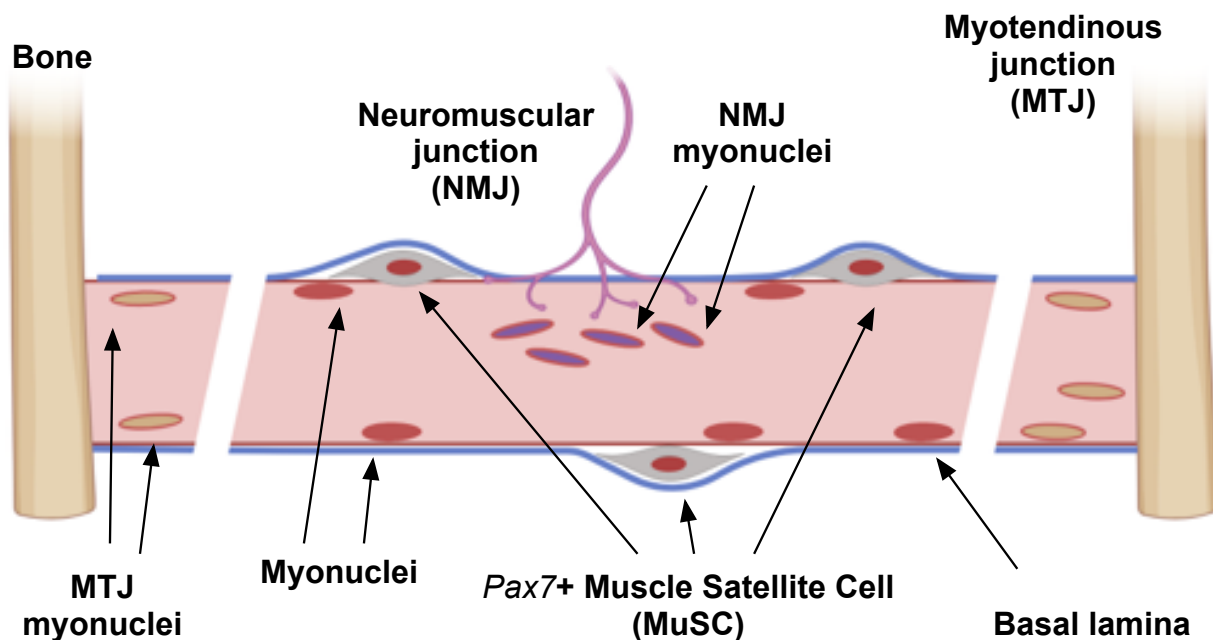
Figure 1.1: **Anatomy of a myofiber.** Cartoon schematic of a single myofiber with arrows demarking associated *Pax7*+ MuSCs, the basal lamina, myonuclei, the neuromuscular junction (NMJ), the myotendinous junction (MTJ), and myonuclei localized to either the NMJ or the MTJ.

Skeletal muscle tissue in mammals is comprised of several different cell populations. In humans and mice, the primary cell type in muscle is the known as the myofiber, long syncytial cells containing the fundamental contractile units of muscle, sarcomeres [1]. Residing on the outside of individual skeletal muscle myofibers are mononuclear myogenic cells called MuSCs, as well as non-myogenic resident fibroblasts known as fibroadipogenic progenitors (FAPs), immune cells, schwann

cells, tenocytes, endothelial cells, and others [13–17]. Altogether, these cells communicate and interact in complex and synergistic ways such to enable appropriate tissue function and maintenance.

Inside of each multinucleated myofiber are hundreds of individual myonuclei (Figure 1.1) [18,19]. Myonuclei, which are derived from myogenic progenitors during development or regeneration, are post-mitotic and express the transcripts encoding proteins forming sarcomeres, as well as other genes critical for myofiber function [16, 20–22]. In addition to sarcomeres, myofibers contain additional specialized molecular structures referred to as the neuromuscular junction (NMJ), which is the location at which nerves innervate individual myofiber, and the myotendinous junction (MTJ) where myofibers attach to bone through tendons (Figure 1.1) [23–25]. Individual myonuclei localize to these specialized structures and express transcripts specific for their formation and maintenance (Figure 1.1) [16, 26–29]. The factors driving subsets of myonuclei to acquire and maintain distinct transcriptional profiles despite existing within a common cytoplasm, as well as whether individual MuSCs are biased towards production of distinct myonuclear subtypes, is not understood.

1.2   Muscle stem cells and regeneration

Skeletal muscle possesses a remarkable capacity to regenerate following stress or severe muscle injuries [30]. Conferring the ability for muscle to regenerate are resident muscle stem cells, MuSCs [30–32]. First named muscle "satellite" cells because of their intimate positioning along the outside of myofibers, MuSCs are a distinct population of quiescent myogenic cells that reside between the basal lamina and the cell membrane of individual myofibers (Figure 1.1) [32]. MuSCs are characterized by their expression of the transcription factor (TF) *Pax7*, which regulates gene networks necessary for maintaining these cells in a quiescent state [33, 34]. Upon a stimulus such as stress or muscle injury, MuSCs become activated and enter the cell cycle, downregulating *Pax7*, and upregulating expression of genes such as *Myod1* and *Runx1* which drive MuSCs to proliferate [30, 35, 36]. While small numbers of MuSCs are activated during homeostasis in the absence of injury, it is likely that after an injury the vast majority of MuSCs become activated [37].

Immediately following a muscle injury, immune cells infiltrate muscle tissue, degrading dam-
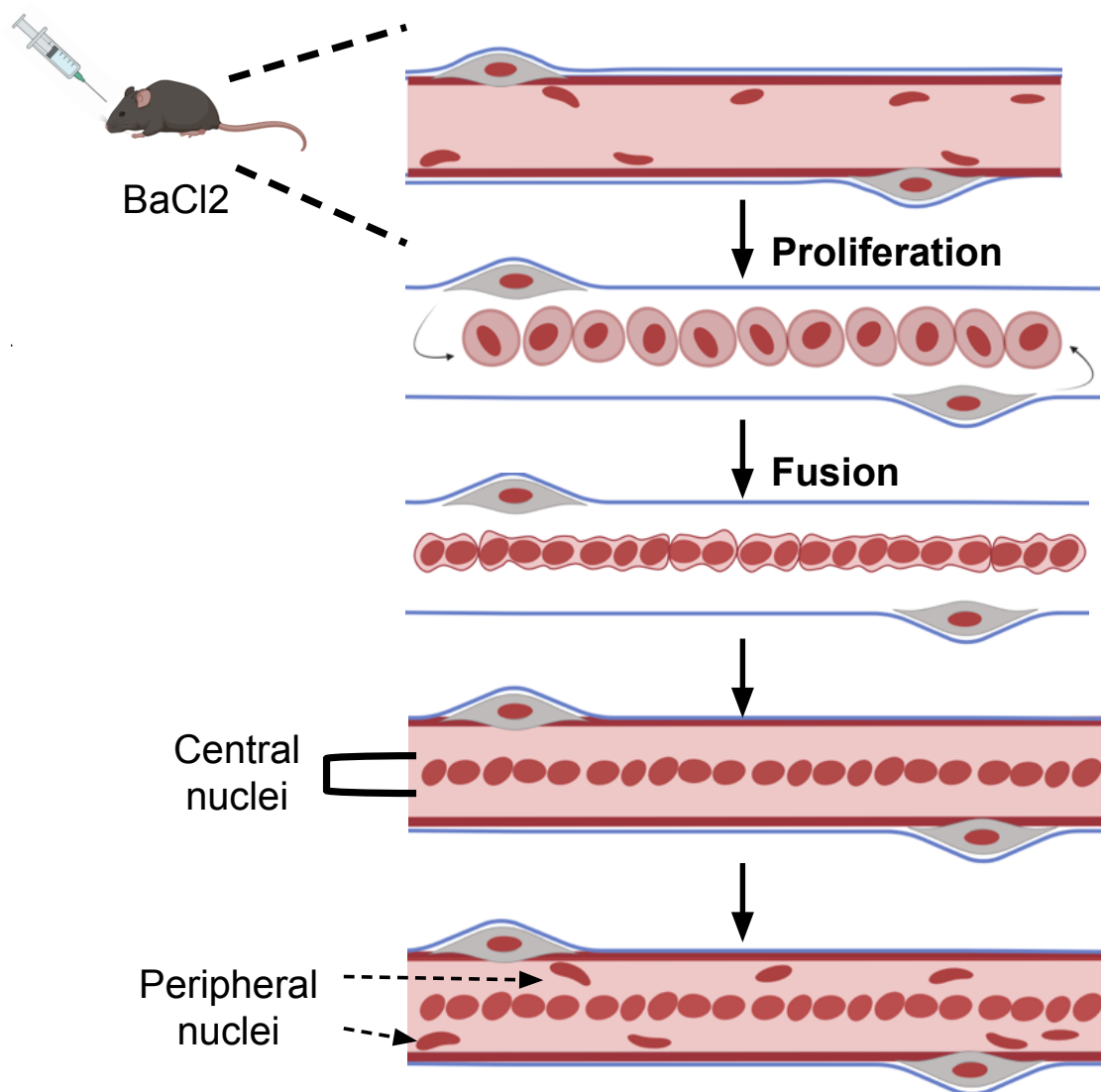
Figure 1.2: **Diagram of skeletal muscle regeneration in mice.** Quiescent *Pax7* cells are activated upon an injury, proliferate as mononuclear myogenic progenitors, before fusing to form centrally located myonuclei. When myogenic progenitors fuse, all myonuclei are initially centrally located, while myonuclei localized to the periphery of myofibers are only observed in later stages of regeneration and mature myofibers.

aged myofibers [38]. Simultaneously, MuSCs activate and expand as mononuclear myogenic progenitors (also referred to as myoblasts), where they position themselves linearly within the persisting collagen matrix (known as a "ghost-fiber") which acts as a scaffold for the regeneration of new myofibers (Figure 1.2) [39]. Eventually myoblasts exit the cell cycle and cease proliferating, differentiate, and fuse, forming a regenerated myofiber where myoblast nuclei become syncytial myonuclei

(Figure 1.2) [38]. Differentiated myogenic progenitors and maturing myonuclei express immature myosin isoforms critical during regeneration (*Myh3* and *Myh8*), before expressing mature myosin isoforms in regenerated myofibers (*Myh1* or *Myh4*) [16, 20, 40–42]. Myonuclei in newly fused myofibers are centrally located within regenerated myofibers, while in mature myofibers myonuclei are located along the periphery (Figure 1.2) [43, 44]. The factors determining and regulating this particular myonuclear organization is incompletely understood [43, 45, 46]. Additionally, while the transcriptional changes driving early activation and proliferation of MuSCs and myoblasts are well-characterized, the changes that occur within differentiated progenitors and post-fused myonuclei during regeneration is not clear given a lack of *in vivo* studies investigating myonuclear transcription once progenitor fusion has occurred during regeneration [16, 41].

While most MuSC progeny fuse and differentiate to regenerate the necessary numbers of myonuclei required for mature muscle function, a portion of MuSCs undergo self-renewal divisions to ensure the replenishment of the MuSC pool, conferring the capacity of muscle to respond to further rounds of injury [47–50]. Self-renewal is characterized by MuSC divisions producing either a progenitor cell determined for differentiation along with another another MuSC retaining its ability to produce either more MuSCs or differentiating progenitors from additional divisions, or two MuSCs [47, 49–51]. Correctly balancing these opposing cell fate choices for differentiation and production of myonuclei, or self-renewal generating additional MuSCs during regeneration, enables skeletal muscles' persistent capacity for regeneration even after multiple injuries [52].

1.3   Muscle stem cell population dynamics and heterogeneity

The regulatory mechanisms determining whether a particular MuSC lineage terminates in differentiated myonuclei or self-renewed quiescent MuSCs, and how these cell fate choices are balanced on a population level, is incompletely understood. Skeletal muscle is not the only organ system possessing adult stem cells, and to understand MuSC population dynamics, clues can be drawn from other tissues [53–57]. To understand paradigms employed by adult stem cell populations during homeostasis and regeneration, models have been proposed to explain how stem cells

maintain a balance between proliferation and self-renewal. First, there is the invariant asymmetry model, in which *all* cells proceed through identical asymmetric divisions, each resulting in a single stem cell and a single differentiating progeny (Figure 1.3). In this model, stem cell clonal diversity is maintained, and stem cell populations are not hierarchical or segregated into distinct subsets. While this paradigm characterizes several adult stem cell compartments during maintenance, this behavior is likely less well-suited for acute regenerative responses such as skeletal muscle regeneration where large numbers of differentiated progeny are produced rapidly [55, 56].

The alternative model is that of population asymmetry [53, 58, 59], which proposes that stem cells are hierarchical, such that some stem cells proliferate as transit amplifying cells before differentiating, while others proliferate as stem cells through self-renewal divisions [53, 58, 59]. This paradigm is associated with a neutral drift of stem cell clones, such that over time individual clones are lost to differentiation and there is a reduction in overall population diversity [53]. Stem cell populations adhering to this model have the benefit of generating large numbers of progenitors (as well as stem cells) rapidly but at the cost of clonal diversity [53, 56, 57].

Whether MuSCs dynamics more closely resemble that of invariant asymmetry or population asymmetry has not been thoroughly settled. Initially, MuSCs were considered to be a homogeneous population of cells [48, 50, 60, 61]. In concordance with this, asymmetric self-renewal divisions have been demonstrated as critical for maintaining MuSC pools [47, 50, 61]. On the other hand, MuSCs are shown to proliferate through symmetric expansions as well, specifically after injury [39, 48, 61]. Thus, neither population asymmetry or invariant asymmetry can fully account for the diverse range of observable MuSC behaviors. Rather, the true nature of MuSC dynamics must incorporate paradigms from both conceptual models of stem cell population dynamics, potentially accounting for a shifting of the balance between the two during different processes such as maintenance or regeneration.

Critical to unraveling MuSC population dynamics is the question of whether MuSCs exist within hierarchical subpopulations with distinct propensities for different cell fates. Since the early studies suggesting uniformity among the MuSC populations, evidence now strongly supports the
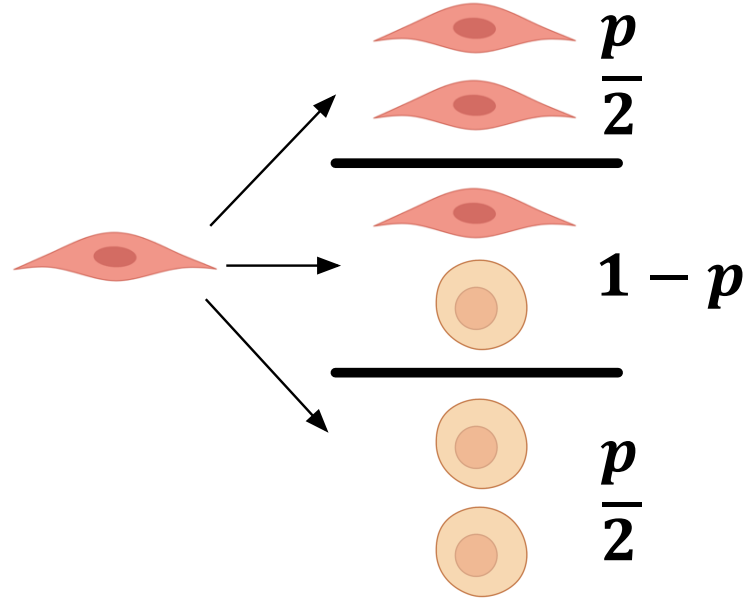
Figure 1.3: **Different types of MuSC divisions.** Representation of different types of divisions MuSCs (red) proceed through, where p is the probability of a division being symmetric and resulting in two MuSCs. When $p = 0$, a model of invariant asymmetry occurs, when $p > 0 \ \& < 1$, population asymmetry occurs where a division has a probability of $\frac{p}{2}$ of producing two MuSCs or two amplifying progenitors (beige).

contrary; that MuSCs exist within phenotypically distinct subpopulations with differing proliferative and self-renewing capacities [29, 61–66]. Subsets of MuSCs have been observed with higher or lower proliferative potential based on their retention (or non-retention) of a fluorescent tag that becomes progressively diluted during greater numbers of divisions [62]. But notably, there are contradicting reports regarding whether these distinct transcriptional states correlate with functional differences [29, 63]. For instance, expression levels of of *Pax7*, *Myf5* (a critical gene driving progenitor differentiation), and *Pax3* (a gene critical for myogenic progenitors during development), are all associated with different propensities for MuSCs to activate, proliferate, or self-renew [29, 61, 63, 64, 66]. Consistent with these findings, MuSC clonal diversity is retained during homeostasis but is lost during successive rounds of injury, suggesting clonal drift where hierarchical MuSCs are depleted as distinct lineages commit to differentiation [52]. Thus, while evidence strongly suggests functional subpopulations of MuSCs exist, it is unclear whether these differential proclivities for certain behaviors are predetermined through intrinsic differences or rather are

acquired stochastically from extrinsic factors upon stimulus such as an injury or isolation and culture. Moreover, the precise roles these different populations and their progeny have during muscle regeneration has not been fully explored.

1.4   Skeletal muscle aging

As organisms ages, tissue function universally declines, ultimately resulting in death. Because of the broad impact aging has on tissue function, to better understand the fundamental drivers of aging requires a strategy capable of evaluating changes on a global level rather than simply looking at individual genes or networks. Recent technological advances in experimental and computational techniques have enabled unprecedented insight into the processes driving aging in ways that only these systems-wide approaches can accomplish. Evidently clear through these contemporaneous studies is that aging impacts processes such as transcription and cell function in ways only observable when considering global transcription or cell populations as a whole [67–69]. Thus, applying a broad lens to studying aging is imperative to reveal its underlying drivers.

Skeletal muscle function and regenerative capacity decline dramatically as individuals age [6, 70]. Muscle in aged individuals is weaker, less resistant to injury, and less capable of adequate regeneration after an injury [6, 70]. At a molecular level, key anatomical structures within skeletal muscle are disrupted including the NMJ and MTJ, suggesting disruptions in myonuclear transcriptional regulation [16, 20, 22, 28, 71–73]. Additionally, in skeletal muscle from aged individuals, MuSCs are less abundant, less proliferative, undergo less self-renewal, are prone to premature differentiation, and are less responsive to critical myogenic signaling [8, 74–82]. However, the mechanisms for how disrupted MuSC function contributes to changes in myonuclear gene expression and mature muscle function has remained unclear.

The heterogeneity among MuSCs described in the previous section has made unraveling differences in MuSC behavior specific to aging a complicated endeavor. As the roles of different MuSC functional subpopulations is incompletely understood, it becomes increasingly difficult to determine if specific subpopulations are preferentially disrupted in aging, rather than aging uniformly impact-

ing the entire MuSC population. Nevertheless, work has demonstrated that through successive rounds of injury in aged mice, clonal complexity of MuSCs is reduced, suggesting loss of MuSC diversity and potentially loss of distinct progenitor populations [52]. Additionally, specific features of MuSC function, including quiescence, proliferation, differentiation, and population balance appear disrupted in aging [8, 52, 83, 84]. However, whether these affects are isolated to particular MuSC subpopulations and their designated roles, or result from global changes affecting all MuSCs and myogenic processes equally, has not been sufficiently investigated.

Efforts by our group and others to assess global changes to MuSCs during aging have revealed that timing of myogenic progenitor expression is perturbed in MuSCs and progenitors isolated from aged mice. These findings introduce the perspective that beyond just changes in MuSC population dynamics, there is altered timing of transcriptional events necessary for activating MuSCs and producing myonuclei drive aging-associated changes to myogenic progenitors isolated from aged mice [74, 85, 86]. In other words, while MuSC cell fate determination may generally be conserved as organisms age, the rate and trajectory at which these cell fates are acquired may be disrupted. However, up to this point all experiments revealing differences in the timing of myogenic TF expression had been done on cultured cells *ex vivo* [74,85,86]. When MuSCs are cultured, not only are the mature myogenic states achieved during mouse muscle regeneration never obtained, these systems fail to recapitulate the diversity of MuSC subpopulations and functions manifested among *in vivo* MuSCs existing within their native environment.

The questions I address in this thesis include whether rescuing aspects of MuSC signaling, which recovers MuSC number, proliferation, and capacity for asymmetric divisions, is sufficient to recover muscle function in aged mice. Additionally, I explore how altered timing of myogenic TF expression impacts myogenesis broadly in aged mice after an injury, describing a critical link between disrupted processes in MuSCs and disrupted mature muscle function. And lastly, I describe how changes in MuSC function in aging disrupts a significant expansion of a small subset of MuSCs, supporting that population dynamics during and after muscle regeneration are perturbed in aged mice. Taken together, I provide an extensive exploration of features of muscle regeneration that

are altered in aging by focusing on MuSCs. Furthermore, I reveal a vast conceptual landscape still needing to be mapped in order to gain a more comprehensive understanding of the underlying drivers of skeletal muscle aging, as well as organismal aging broadly.

Chapter 2

MuSC population dynamics during aged mouse muscle regeneration

2.1   Chapter Note

All wet-lab experiments conducted for this project were conducted by researchers in the lab of Dr. Bradley Olwin. A post-doctoral fellow in Dr. Olwin's lab, Dr. Monica Hall, along with support from Dr. Robin Dowell and Dr. Mary Ann Allen all worked together developing the barcoding strategy. All viral preparations and sequencing libraries were prepared by Dr. Hall. Dr. Olwin and Dr. Hall, with intellectual contributions from Dr. Allen, contributed to designing the novel barcode lineage tracing assay and overcoming hurdles in its development. The scripts required for the initial data processing steps, where barcode reads are aligned and scored, were written by Dr. Allen prior to my joining of the labs of Dr. Olwin and Dr. Dowell. Dr. Allen also conducted some initial analysis of the barcode sequencing experiments prior to my arrival. My contribution to this project was the development of a computational and statistical framework needed to process, analyze, and interpret results from these barcoding experiments.

In addition to the barcode lineage tracing experiments described in this chapter, there are also experiments designed and completed by a former post-doctoral fellow Dr. Brad Pawlikowski, Dr. Alicia Cutler, as well as a rotation student Rachel Gessner.

2.2   Introduction

During development and homeostasis, adult stem cells differentiate into tissue-specific terminal cell types to form and maintain mature tissues and organ systems [87]. During aging or disease,

this process of differentiation is disrupted, negatively impacting tissue maintenance and resulting in pathological conditions including failure to regenerate and cancer [88, 89]. Studies suggest a stem cells' procession through significant numbers of cell divisions occurring over an individuals' lifetime is associated with oxidative stress, accumulation of DNA damage, telomere shortening, and increased risk of disease, indicating there are likely mechanisms to limit division numbers of adult stem cells [58, 88, 89]. Thus, determining how stem cell populations balance division numbers to ensure maintenance of healthy stem cell compartments, as well as sufficient numbers of differentiated progeny to maintain tissue, is crucial for understanding how stem cell and tissue function is affected as organisms age. However, addressing this question is difficult as it requires labeling single stem cells with unique identifiers that persist in their progeny to accurately quantify their division dynamics after a process such as regeneration is complete.

Lineage tracing in molecular and cellular biology is a term for all methodologies that attempt to infer relationships between cellular lineages, diversity of lineal origins, and the cellular dynamics responsible for producing those lineages [53]. Some lineage tracing techniques rely on the inheritance of fluorescent tags, either linked to DNA, or as free diffusing molecules, to identify relationships lineal dynamics [53]. Other techniques utilize DNA barcodes to label genomes of stem cells which are sequenced following expansion and differentiation of the labeled stem cells to identify relationships between clone size and clone diversity [90–92]. In these techniques, distinct methods are employed to produce DNA barcodes themselves. One method uses endogenous barcodes, pre-existing DNA elements that become mutated as cells divide, while other methods use exogenous synthesized DNA sequences as barcodes that are virally integrated into the genomes of the cells from which progeny are hoped to be tracked [53, 90, 91]. Additionally, barcodes can be either dynamic, in which they change with successive cell divisions enabling generation of lineal trees, or static, in which barcode sequences remain unchanged through cell divisions and thus provides insight into clone sizes and population paradigms of cell lineages being tracked [53, 90–94]. While various lineage tracing techniques exist that enable exploration of cell expansion and fate decisions, none have been capable of accurately quantifying clone size and diversity of MuSCs and their progeny

during regeneration [53, 91, 93–95] .

Unlike the majority of adult stem cell compartments, MuSCs are responsible for rapidly generating large numbers of differentiated progeny (>100s) after injury, and thus may exploit unique strategies to balance the opposing cell fates choices of self-renewal and differentiation during these periods of extreme stress. Lineage tracing experiments with MuSCs have yielded intriguing results, yet none have provided direct quantification of how MuSC population dynamics are balanced during regeneration [52, 62, 89, 95]. The use of flourescent dyes that label all dividing cells by their linkage to replicated DNA, including EdU, a nucleotide analog integrated into cellular genomes during divisions, and flourescently tagged histones which label DNA and is inherited when cells divide, have identified MuSCs with distinct proliferative behaviors [62, 64, 96, 97]. However, when labeled cells undergo large numbers of divisions, EdU becomes diluted, such that cells dividing roughly 3 or more times will appear unlabeled [96]. Moreover, given these labels are present in all dividing cells, they are not true *lineage tracers*, as they do not relate dividing cells to their clonal origins.

Alternatively, experiments have been conducted using mice genetically modified to continually express one of four fluorescent proteins in all progeny of *Pax7+* MuSCs [52]. Thus, as MuSCs within these mice proliferate and fuse into myofibers, the diversity of fluorescent proteins detected in the cytoplasm of myofibers is correlated with the clonal diversity of progenitors they were derived from. This study concluded that clonal complexity of MuSCs is reduced upon successive injuries, supporting that clones are progressively lost through symmetric divisions and differentiation, indicative of a model of population asymmetry [52]. While this study provided some of the most potent evidence describing a paradigm of MuSC population dynamics during regeneration, there was insufficient diversity of fluorescent proteins to comprehensively reveal clonal diversity among MuSCs and myonuclei. For these reasons, the use of genetic barcodes, given their immense diversity of potential sequences and their persistence in progeny through any number of cell divisions, is the most promising form of lineage tracing to better understand MuSC population dynamics.

Nevertheless, most barcoding strategies are plagued by an underappreciated pitfall often unaddressed in studies employing these techniques; that being they are incapable of quantifying with

certainty that each unique barcode represents a single cell because of how barcodes are amplified for sequencing and imperfect diversity of barcode libraries [53, 93, 94, 98, 99]. This amplification step, while important for generating barcodes in sufficient numbers for detection, introduces amplification bias, such that following amplification, the pre-isolation frequency distribution of unique barcodes from the tissue is not maintained in the library that is ultimately sequenced. For these reasons, the group of Dr. Bradley Olwin, with intellectual contributions from Dr. Mary Allen, developed a novel barcoding strategy in which after individual barcodes are isolated, but prior to their amplification, an additional unique DNA tag (a unique molecular identifier, or UMI) is attached to every individual barcode. This addition of a UMI confers that after amplification, all barcodes with identical UMIs can be computationally collapsed to 1, such that every unique barcode after this collapsing can be interpreted as having derived from a single infected MuSC. This technique provides the only existing means of accurately quantifying numbers of progeny from a single cell *in vivo*, and is applied here to evaluate how MuSC populations balance lineage sizes and segregate cell fate choices.

For my thesis work, I developed a computational and statistical framework to model barcode frequency distributions after accounting for complex technical and biological variability across experiments, as well as inherent bias in the barcode library itself. My findings, in combination with additional experiments from our group and from other groups, support that subsets of MuSCs expand disproportionately relative than others, establishing the existence of distinct MuSC subpopulations in strikingly disparate proportions that exhibit opposing proliferative behavior following a muscle injury. Moreover, it appears central myonuclei, which are produced in the first 4 days post-injury (dpi), are clonally diverse and are predominantly products of only a few cell divisions, while self-renewing MuSCs are clonally homogenous having proceeded through significant numbers of divisions, a previously unknown feature of MuSC-mediated myogenesis after injury. Finally, I describe how the population dynamics appear disrupted during aged mouse regeneration, suggesting that dysregulated population balance may contribute to regenerative defects that accompany skeletal muscle aging. These results are generally consistent with current paradigms, yet provide more controversial findings as well by building on previous findings and providing the most quantitative

depiction of MuSC population dynamics in young mice, and how this balance may be perturbed in aging.

2.3   Results

2.3.1   Single-cell lineage tracing strategy

To unravel the clonal dynamics of MuSCs following an injury, Dr. Bradley Olwin and Dr. Monica Hall, with intellectual contributions from Dr. Mary Ann Allen, developed a novel barcode lineage tracing technique capable of quantifying individual myogenic cell divisions post-injury (Figure 2.1). This strategy uses a modified avian leukovirus developed into the RCAS system to insert random DNA barcodes into the genomes of quiescent MuSCs, which are then inherited by their progeny (Figure 2.1A-B). After regeneration, DNA is then isolated from the muscle, and barcode frequencies are assessed, revealing the minimal number of cell divisions the initially infected MuSC underwent prior to differentiation or isolation.

The RCASBP(A) virus (referred to as RCAS) is only able to infect avian cells expressing a TVA receptor [100, 101]. To enable MuSC infection with RCAS, mice were bred with the *TVA* receptor gene inserted into the *Rosa26* locus preceded by a lox-stop-lox sequence and possessing a mutated ATG translational start site [102]. Thus, $Pax7^{CreERT2/+}$ mice express expression of *TVA* specifically in MuSCs following recombination (Figure 2.1C) [103].

RCAS viruses were engineered to possess a random barcode library of $1.6 * 10^7$ possible barcodes as well as a gene for a fluorescent protein used to visually confirm infected cells (Figure 2.1B-C). Barcode viruses are produced by transfecting DF1 chicken fibroblast cells endogenously expressing the *TVA* receptor, expanding these cells, then harvesting and purifying virus by ultracentrifugation. The viral library is verified by infecting DF1 cells with 8-fold excess of the barcode library and performing linear amplification PCR (LAM-PCR) followed by universal PCR to attach sequencing adapters. Barcode DNA is then gel purified and prepared for Illumina sequencing at read-depths of 60,000 per nucleus (Figure 2.1A). One of the critical novel innovations of this
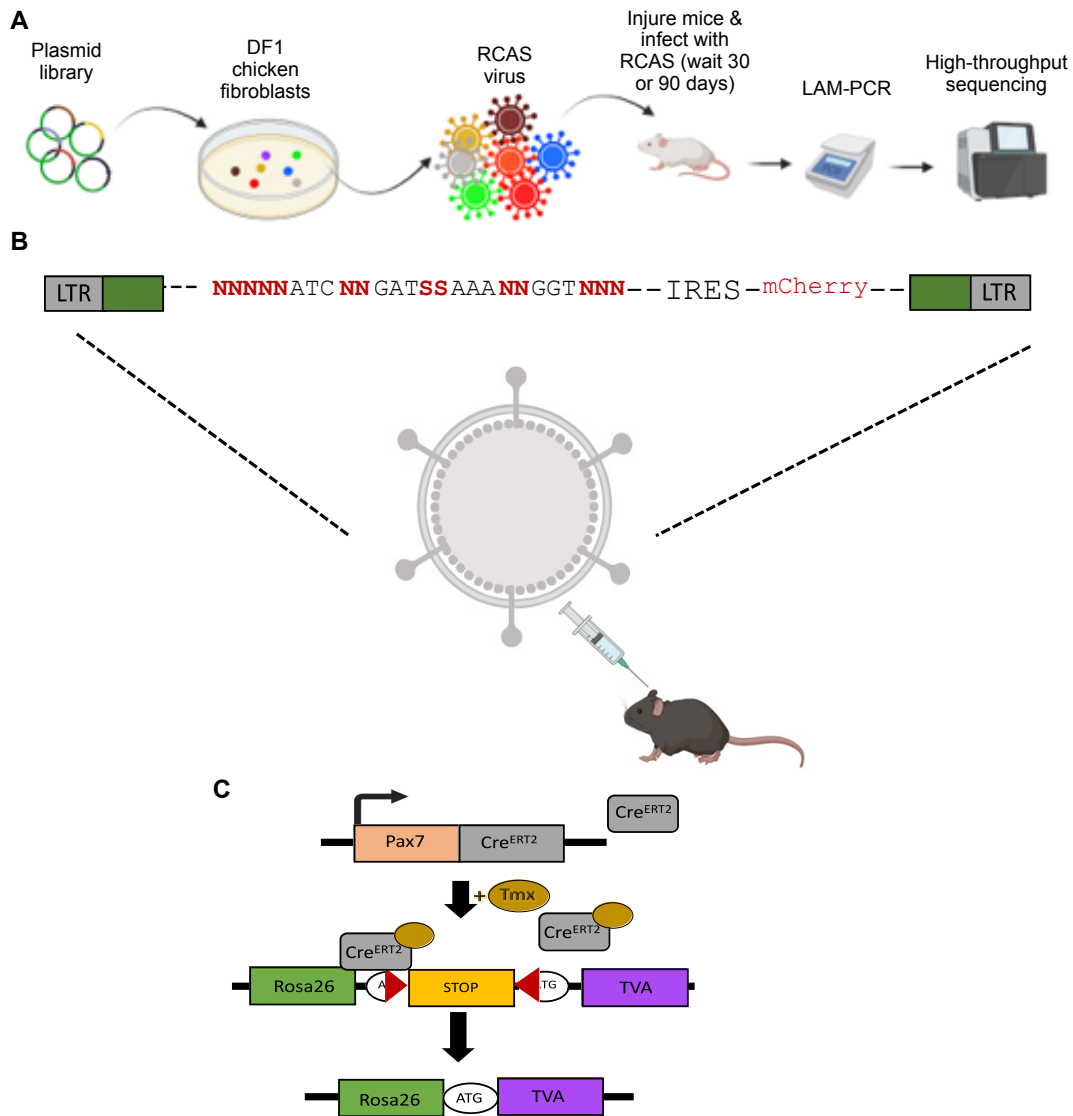
Figure 2.1: **Diagrams associated with barcoding lineage tracing strategy.** (A) Workflow diagram of RCAS barcode lineage tracing strategy. Plasmid library is infected into DF1 chicken fibroblasts, isolated, and injected into mice concomitant with a BaCl$_2$ induced muscle injury. Genomic DNA is isolated, subjected to LAM-PCR, amplified, and sequenced. (B) Diagram of the barcode cassette containing viral insertion sites (LTR), next generation sequencing adapters (green), and a barcode sequence containing degenerate and consensus bases. (C) Mouse genetics enabling expression of the TVA receptor in *Pax7*+ MuSCs. *Pax7* expression and addition of tamoxifen (Tmx) induces a Cre-mediated recombination, removing a STOP codon, and enabling the expression of the gene for the TVA receptor. Thus, *Pax7*+ cells will express TVA and can be infected by RCAS.
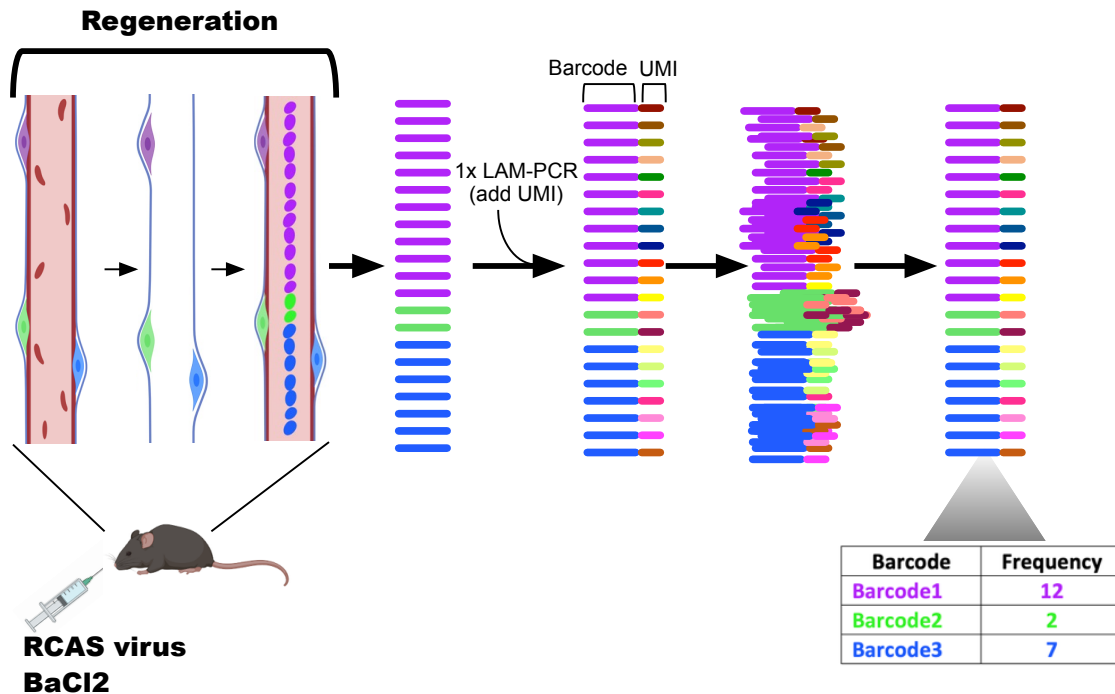
Figure 2.2: **Diagram of barcode deconvolution using unique molecular identifiers (UMIs).** Mouse is injected with RCAS library (and BaCl$_2$ for muscle injury), where individual MuSCs are labeled with a unique DNA barcode (purple, green, blue). During regeneration, MuSCs proliferate as myogenic progenitors before fusing and forming a chain of centrally located myonuclei. After regeneration, genomic DNA is isolated from the mouse TA muscle and subjected to a single round of LAM-PCR to add a unique molecular identifier (UMI) to each individual barcode. Barcode:UMI sequences are then amplified by universal PCR and sequenced. Identical barcode:UMI combinations are deemed products of PCR amplification, and every unique barcode:UMI combination represents a single cell. Groups of identical barcodes with unique UMIs are considered derived from a single infected MuSC that expanded to produce myogenic progeny during regeneration. Clone sizes can then be assessed and organized into a frequency table quantifying lineage size.

barcoding strategy differentiating it from other techniques is the linear amplification PCR (LAM-PCR) step which attaches a unique molecular identifier (UMI) to each individual barcode Figure 2.2). The step is critical in that it enables the bioinformatic deconvolution of PCR duplicates to determine the *true* frequency distribution of barcodes in the muscle and thus the quantification of the minimum number of cell divisions that occurred prior to a cell exiting the cell cycle or tissue harvest (Figure 2.2).

Following sequencing of the barcodes, alignment and scoring of all reads was accomplished using a script written by Dr. Mary Ann Allen where only barcodes with perfect matches to the

designated consensus bases would be included for further analysis. These barcodes were then organized into a frequency table once identical barcodes with identical UMIs were collapsed, and identical barcodes with unique UMIs were deemed as part of a common lineage derived from a single infected MuSC (Figure 2.2A-B).

2.3.2   Barcode frequency distributions in DF1 cells and mice

Altogether, two experiments were conducted in DF1 chicken fibroblast cells as controls where barcode virus was added at 8x the multiplicity of infection (MOI) to assess diversity of the sequence library. Additionally, 22 experiments were conducted in mice (n = 12, young; n = 10, aged; n = 17, 30 dpi; n = 5, 90 dpi). All 90 dpi samples were from young mouse experiments because of concerns of aged mice not surviving 90 days after induced injury. From all 24 experiments $\sim$700,000 unique barcodes were detected, and $2.5x10^7$ total barcodes were sequenced (Figure 2.3A). These varied across individual DF1 and mouse experiments because of changes in the sequencing depths (more below). Overall, the number of replicates and numbers of barcodes sequenced were extensive, confirming a sufficiently diverse barcode library and sufficient numbers of replicates to generate biological conclusions.

Frequency distributions were assessed for each individual mouse or DF1 control experiment. Distributions from DF1 experiments and *in vivo* mouse experiments consistently, and unexpectedly, contained dramatic right skews, albeit to varying degrees. These long right tails result from the majority of barcodes only being detected a few times in each of these experiments, while a small subset of barcodes were detected hundreds, thousands, or tens of thousands of times (Figure 2.3B-D).

2.3.3   Numbers of MuSCs in the TA muscle

The number of unique barcodes detected from the 22 mouse experiments varied widely depending on factors such as sequencing depth and yield from isolation (Figure 2.4A). That numbers of unique barcodes spanned over 50,000 in several mouse experiments posed a conceptual conun-
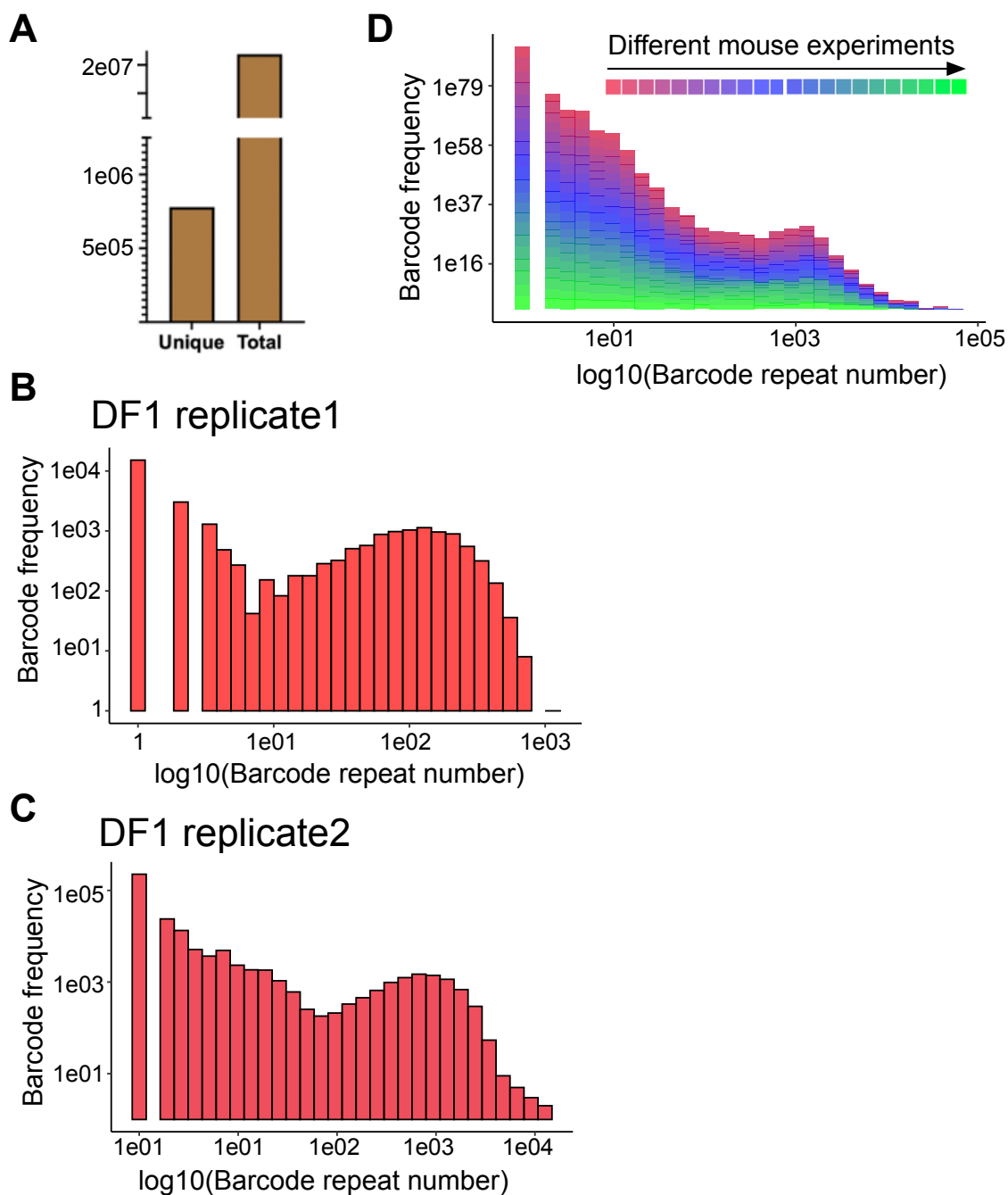
Figure 2.3: **Frequency distributions from barcode lineage tracing experiments in DF1 cells and mice.** (A) Numbers of unique and total barcodes identified from 24 experiments (n = 2 DF1, n = 22 mice). (B) Frequency distribution of barcodes isolated from replicate 1 or (C) replicate 2 of DF1 control experiments. (D) Frequency distributions of barcodes from mouse experiments where each color corresponds to an independent experiment.

drum; previously it's been proposed that between only 5-7 MuSCs exist along a given myofiber, making total MuSC numbers in a TA muscle in the range of 20,000-30,000 (roughly 5,000 myofibers per 1 TA muscle) [33, 80, 104]. The fact that numbers of unique barcodes sequenced were in and beyond the estimated range of the total number of MuSCs in a TA muscle was problematic, as this would suggest successful labeling of virtually all MuSCs in the TA muscle and sequencing of all barcodes in our experiments. This was impossible, given an estimated infection efficiency of ∼20%-30%, and that only 1/3 of the entire barcode library isolated from a given TA muscle was sequenced. However, I can reconcile high numbers of unique barcodes if prior estimations for MuSC numbers in muscle are incorrect. In fact, MuSCs on isolated myofibers may be fewer than on myofibers in their native conditions, supporting these studies may have underestimated MuSC numbers present on individual myofibers [33, 80, 104] .
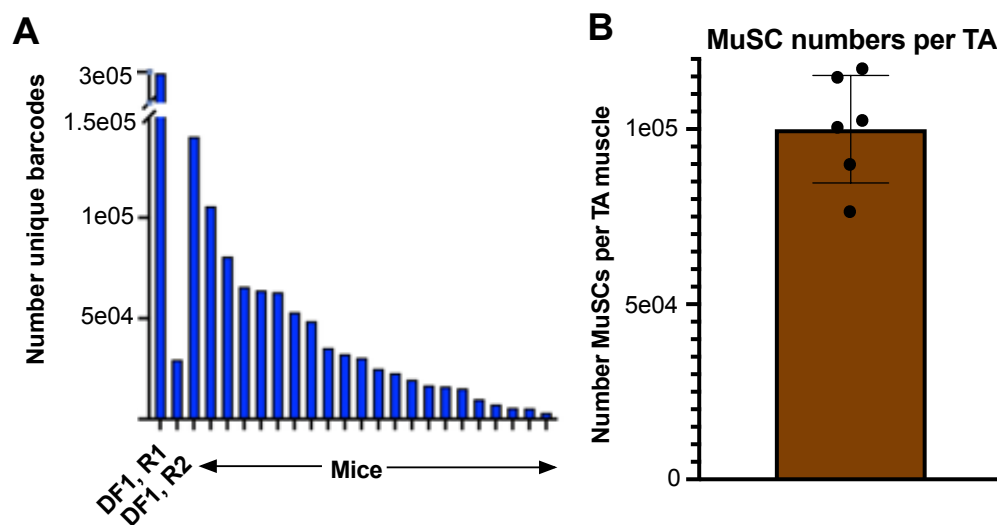
Figure 2.4: **Comparison of unique barcode numbers and MuSC numbers in a TA muscle.** (A) Numbers of unique barcodes detected from the 2x DF1 control experiments and the 22x mouse experiments. (B) Average number of MuSCs in a TA muscle quantified from PAX7^{IRESCreERT2};R26R^{floxTdTomato} mice (n = 7). Each point represents an image take from a single TA muscle.

To accurately quantify the number of MuSCs per TA muscle, I analyzed microscopy images taken by Dr. Alicia Cutler of TA muscles in PAX7^{IRESCreERT2};R26R^{floxTdTomato} mice. These mice express a nuclear localized fluorescent protein in all MuSCs expressing *Pax7*. Longitudinal cross

sections were taken of TA muscles with labeled MuSCs, allowing for quantification of MuSC numbers on native myofibers. Extrapolating these results to determine number of MuSCs present in a single TA muscle revealed that across 7 independent mice, an average of ∼100,000 MuSCs per TA muscle was observed, suggesting MuSC numbers are greater than previous estimates (Figure 2.4B). With these new data, the numbers of unique barcodes detected in our barcoding experiments become much more reasonable, as they represent the expected ∼20%-30% of all MuSCs in a TA, rather than ∼100%. The presence of a greater abundance of MuSCs in skeletal muscle than previously appreciated not only lends credence to our results but also contributes to the understanding of the MuSC populations and confers a potential for existence of large subpopulations.

2.3.4   Barcode bias and high frequency barcodes (HFBs)

From these analyses, I concluded that the numbers of unique barcodes sequenced from our experiments were an accurate representation of both the viral infection efficiency and the number of MuSCs in the TA muscle. Thus, I next sought to better understanding the *total* number of barcodes sequenced from each mouse experiment. Among all unique barcodes, a small percentage (∼1%) were detected at disproportionately large frequencies, which I termed high-frequency barcodes, or HFBs (Figure 2.3A; 2.5A). The relative distributions of HFBs and low frequency barcodes (LFBs) suggest that small subsets of MuSCs expand generating far greater numbers than an average MuSC in the bulk population. Although subsets of MuSCs possess distinct proliferative behavior, their relative distributions observed in our lineage tracking experiments support a strikingly disproportionate balance among MuSC subpopulations.

I observed that some HFBs fall within ranges from tens, hundreds, or even thousands, while others were detected with frequencies >100,000 in our dataset (Figure 2.3C; 2.5A). I considered it a reasonable assumption that some HFBs are legitimate results of cell divisions, but given what's known about cell numbers in muscle and MuSC dynamics after an injury (see Section 2.3.8 "MuSC population modeling"), I deemed HFBs on the higher end of this spectrum were most likely experimental artifacts. Because identification of HFBs challenges the current understanding of MuSC

population dynamics during regeneration, I needed to develop a method to better assess barcode bias and identify biologically relevant HFBs (i.e. resulting from significant number MuSC and progenitor divisions).

Unraveling barcode bias is confounded by several factors. First, while the barcode library was constructed to possess a theoretical diversity of $1.6x10^7$ possible sequence permutations, and thus every unique barcode detected in our experiments would theoretically correspond to a single infected MuSC, the true diversity of the library packaged into RCAS particles prior to infection into DF1 cells was never directly assessed. Moreover, library generation and sequencing fidelity is imperfect, so sequenced barcodes may erroneously appear at high frequency due to their overrepresentation in the library (such that they exist in higher numbers of viruses), bias in terms of sequencing, or some other more subtle source of bias occurring within the mice.

Additionally, initial mouse experiments were conducted at different sequencing depths compared to later experiments, such that the total numbers of barcodes sequenced varied significantly across experiments (Figure 2.4A; Figure 2.5B-C). When sequencing is less deep, more of the total barcodes detected in a given experiment will be comprised of the highest frequency barcodes. However, as sequencing depth increases, the overall frequency distributions shift, where HFBs comprise a lower proportion of all barcodes as more LFBs would theoretically be detected. To ask which experiments were conducted at theoretically sufficient depths where the distribution of HFBs, LFBs, and the numbers of unique barcodes, is an accurate representation of the true distribution of MuSC lineal sizes, barcodes were subsampled from each independent mouse experiment for a bootstrapping analysis, and numbers of unique barcodes were assessed in each bootstrapped sample (Figure 2.5D). If an experiment was conducted at this theoretically sufficient depth, numbers of unique barcodes would not decrease as bootstrap size decreases (which in this case is analogous to sequencing depth). However, if sequencing depth was insufficient, where greater depth would theoretically result in more unique barcodes, as bootstrap subsample size decreases, numbers of unique barcodes would decrease proportionally.

I observed through this analysis that, qualitatively, it appears few, if any, of the mouse
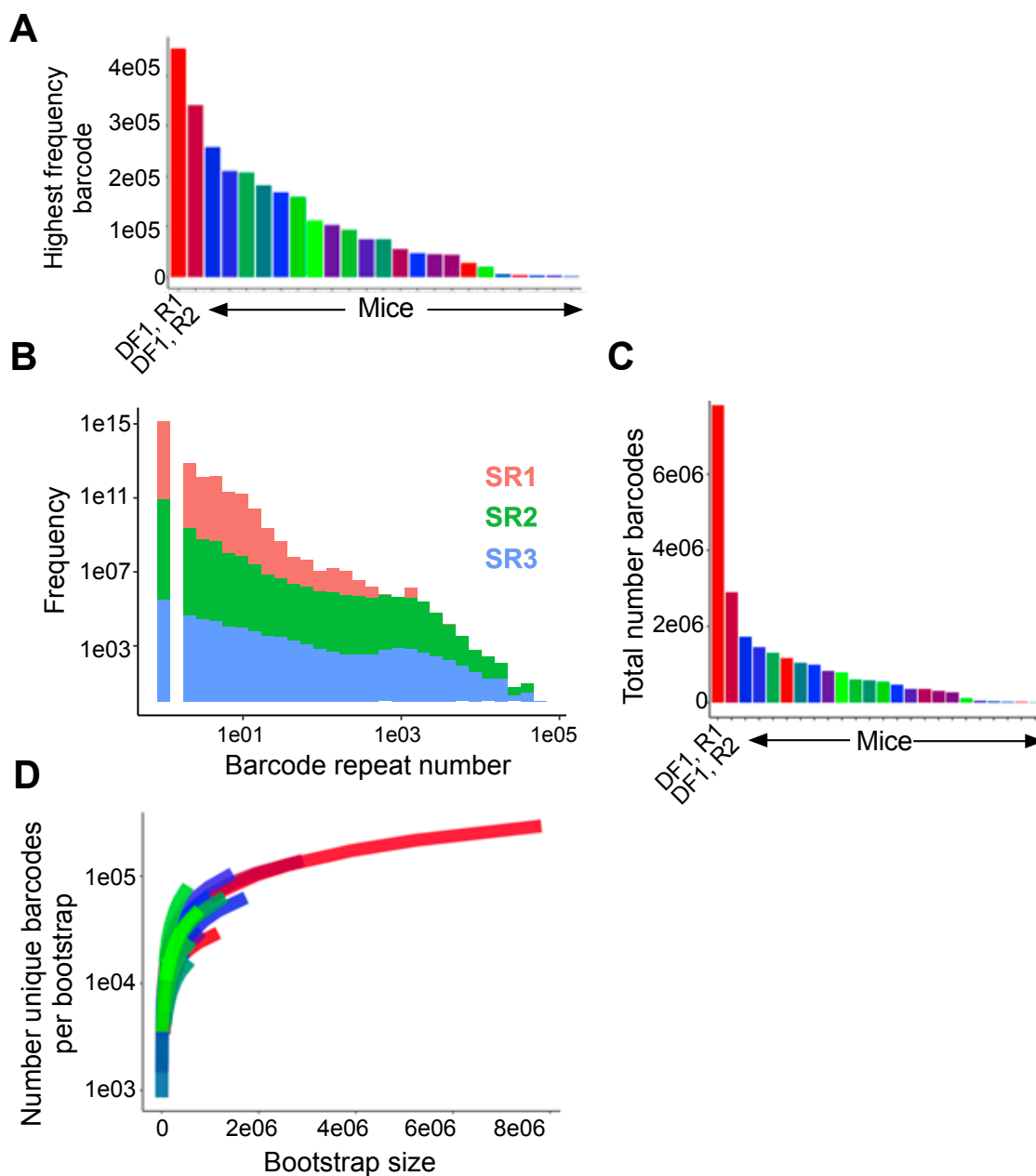
Figure 2.5: **High-frequency barcodes (HFBs), barcode bias, and sequencing depth.** (A) Highest frequency barcodes from each DF1 or mouse sample. (B) Barcode frequency histogram split by which round of sequencing barcodes were derived from. (C) Numbers of total barcodes sequenced from each DF1 or mouse experiment. (D) Results from bootstrapping analysis of barcode sequencing depths.

experiments were conducted at demonstrably sufficient depth, as curves associated with these plots are changing proportionally to changes in bootstrap sample size (Figure 2.5D). However, in our

"DF1, rep2" experiment, we appear to have reached sufficient depth to capture most of the unique barcodes, as the associated bootstrap curve does not change with decreasing bootstrap size (Figure 2.5D). Thus, statistically evaluating the proportions of HFBs in mice and identifying those that are not the result of experimental variability and bias is hindered by these differences between independent experiments and unknowns regarding the diversity of the input library.

Because I wanted to accurately quantify the relative contributions of MuSC lineages offering insight into MuSC population dynamics, I needed to develop a computational method capable of accounting for all potential sources of barcode bias after correcting for differences in experimental depths. To accomplish this, I employed a multi-faceted approach where I integrated assumptions regarding the diversity of the input library and a machine learning algorithm to assign likelihoods of individual barcodes as being true or false positives. Through my analyses, I demonstrate that despite clear and evident bias existing across these lineage tracing experiments, true positive HFBs are detected across most mouse experiments, supporting that high and low expanding MuSC lineages are bona fide features of muscle regeneration.

2.3.5   Bias removal using DF1 controls

In first addressing barcode bias, I considered control experiments that had been conducted where viral library was used to infect DF1 chicken fibroblast cells and the barcodes integrated into these cells were sequenced. Thus, the diversity of barcodes from these experiments are the closest representation of the viral library diversity of which was injected into mice. Importantly, these control DF1 experiments were conducted where 8-fold excess of viral concentrations were used to infect DF1s prior to sequencing to ensure that all barcodes in the library would be represented. Indeed, from my bootstrapping analysis, it is clear that the number of unique barcodes obtained from the second of these two experiments was an accurate representation of the empirical number of unique barcodes, where increasing sequencing depth would lead to only a negligible number of additional unique barcodes detected (Figure 2.5D).

Moreover, the experimental strategy used when infecting DF1s and the sufficient depth is
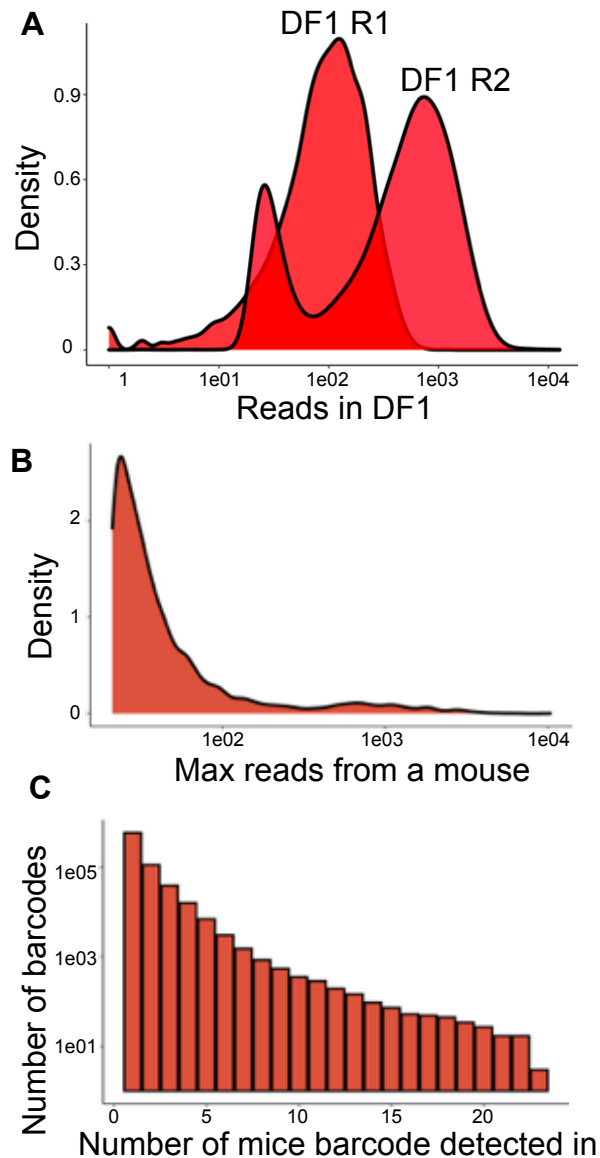
Figure 2.6: **Distribution of barcode for frequencies associated with bias detected from DF1 control experiments.** (A) Frequency distribution of barcodes detected as biased in DF1 experiments. (B) After removing biased barcodes as determined from the DF1 experiments, frequency distributions of barcodes in mice. (C) Distribution of the number of mice barcodes detected as bias from DF1 experiments were detected in.

"DF1, rep2" which also enabled identification of barcodes overrepresented in the initial viral library. Because DF1 cells were infected with 8-fold library concentration (8x MOI), and cells were harvested after 8 hours where no more than a single cell division could have taken place, these parameters confer all barcodes appearing >16x in the DF1s were overrepresented in the viral library.
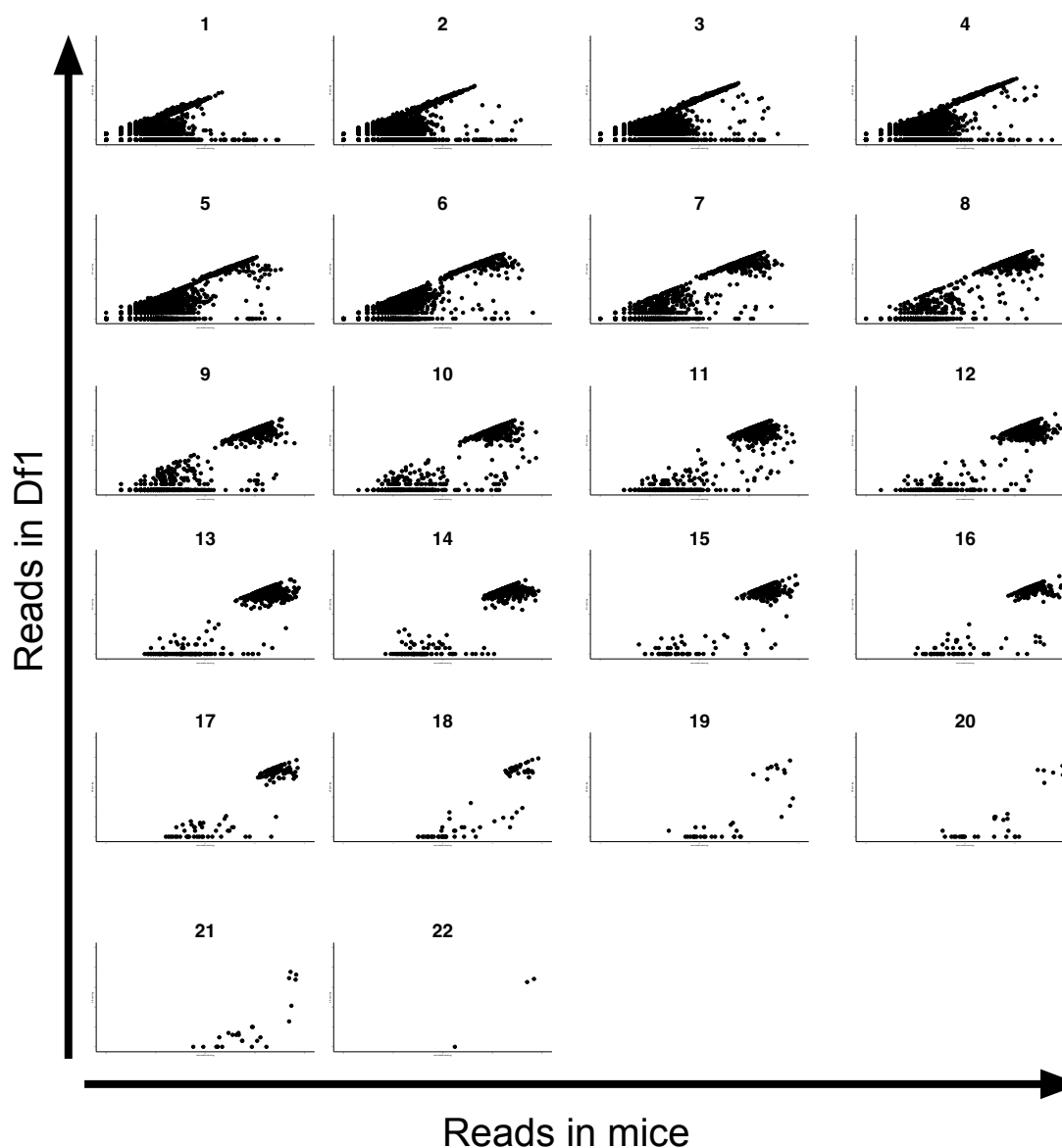
Supplementary Figure 2.1: **Scatterplot matrix of barcode reads in mice and DF1 cells.** Each scatterplot shows barcodes detected in between 1 and 22 mouse experiments. Barcodes in the upper left quadrant of each scatterplot represent barcodes that were detected in high frequency in the mice but were not detected or detected at low frequency in the DF1 experiments.

Altogether, 8,601 barcodes were detected at frequencies >20 indicating overrepresentation in the initial input library. In fact, between the two DF1 control experiments, multiple populations of barcodes are overrepresented, detected at >1,000 in these experiments (Figure 2.6A).

These biased barcodes, appearing >20, were removed from downstream analyses. However,

even after removing this clear bias, there were remaining barcodes detected at high frequency in the mouse experiments (Figure 2.6B). Importantly, a subset of these barcodes were detected, sometimes at high frequency, across several independent mouse experiments (Figure 2.6B-C). This result was problematic for the following reason: if I assume that the overall distribution of barcodes is an accurate depiction of MuSC populations, then the subset of MuSCs that proceed through a large numbers of divisions relative to other MuSCs are inherently rare, and thus the same barcode labeling a rare subset of MuSCs across multiple experiments is highly unlikely.

To further explore this, I plotted the frequency of barcodes detected across multiple mice compared to barcode frequencies in the DF1 experiments, and observed a population of barcodes detected across multiple mice at high frequency that were either not detected, or detected at low frequency, in the DF1 experiments (Figure 2.1). Thus, using the DF1 experiments alone to identify barcode bias is insufficient, as there are sources of bias that are unique to the mouse experiments that requires more nuanced identification.

2.3.6   Hamming distance

Potential sources of barcode bias in mice that would not have been detected from the DF1 control experiments include barcode mutagenesis or the barcode sequence itself having unintended effects on cellular functions. It is possible some HFBs are derivatives of several individual barcodes that mutated and converged into a single sequence. Additionally, it's possible that HFB sequences confer some type of advantage in terms viral infection or increased capacity for cell divisions, resulting in the erroneous occurrence of HFBs. If such scenarios were indeed occurring, they could be revealed by higher sequence similarity among HFBs compared to LFBs. To evaluate this possibility, hamming distances were calculated for different groups of barcodes (Figure 2.7). A hamming distance is a distance measure between two strings, such that their similarity at each individual position is quantified [105]. A hamming distance between two barcodes is calculated by:

$$Hd(b_1, b_2) = \sum b_1[i] \neq b_2[i]$$
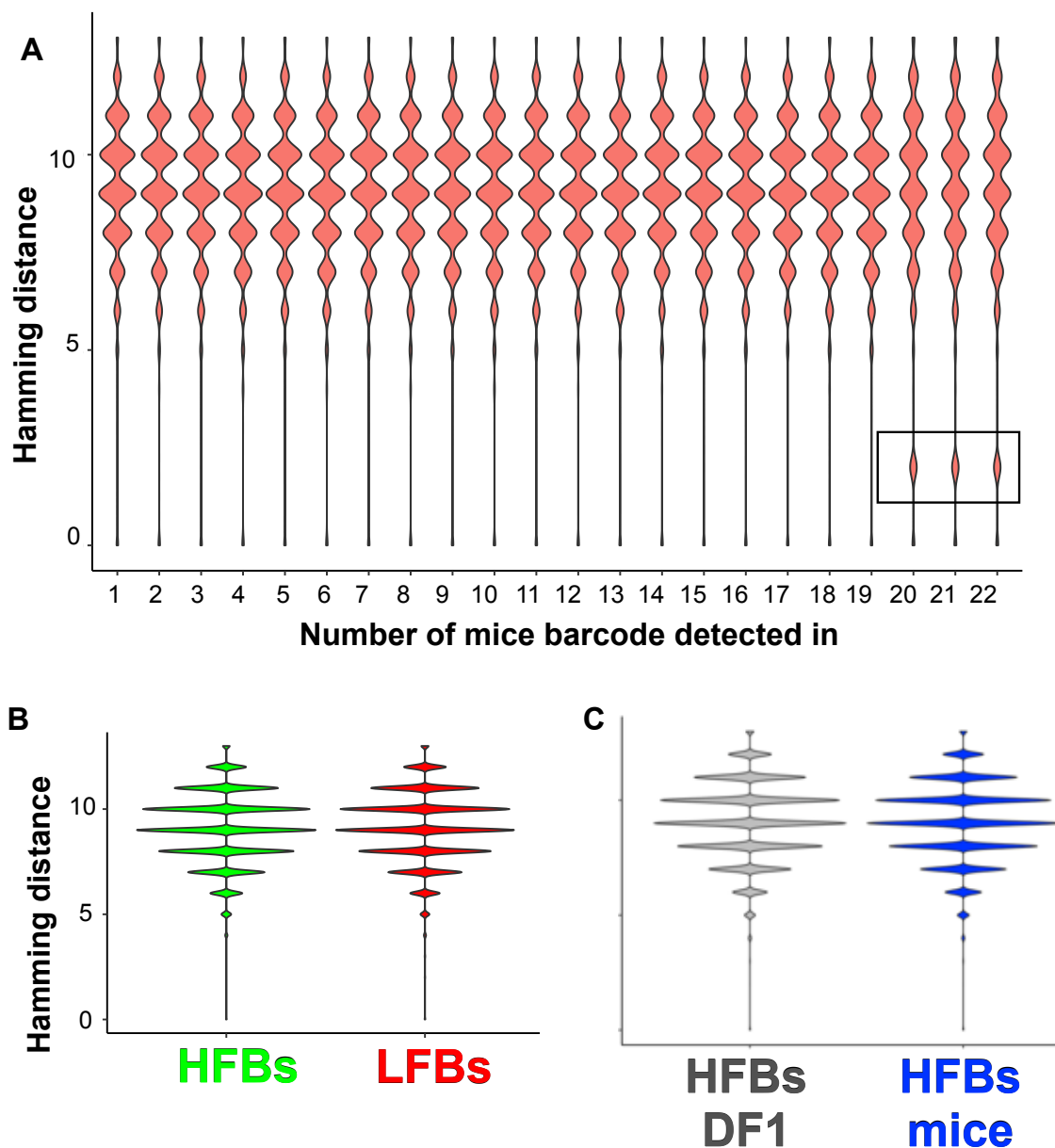
Figure 2.7: **Hamming distance evaluation of barcodes.** (A) Violin plots demonstrating the frequency distribution of hamming distances for top 100 highest frequency HFBs appearing in 1-22 mice. Black box marks slight shift in distribution of hamming distances for barcodes appearing in >20 mice. (B) Comparison of the top 1000 highest HFBs compared to a random sample of 1000 LFBs, or (C) between HFBs from DF1s and HFBs detected in mice.

where b_1 and b_2 are two barcode sequences to compare. The hamming distance (Hd) is the sum of individual positions (i) in each barcode sequence that are different. Thus, sequences with high similarity have low hamming distances, while sequences with low similarity have high hamming

distances.

I calculated hamming distances between the highest frequency HFBs appearing in between 1 and 22 mice. I uncovered that while the affect is moderate, the more mice a set of barcodes were detected in, the more similar in sequence they were. Indeed, a set of HFBs appearing in greater than 20 mice have lower hamming distances compared to the bulk population of HFBs within this subset (Figure 2.7A).

I then calculated hamming distances for random subsamples of HFBs and LFBs and found they were not significantly different between HFBs and LFBs, nor between HFBs in DF1s and from mice (Figure 2.7B-C). Overall, these results suggest that barcode mutations or barcode sequence bias, while potentially present to a small degree, are not a significant source of bias in these experiments. From these results I concluded that there must be sources of bias that are unique to mice, but are unrelated to and cannot be assessed by evaluating sequence-related features and similarities among HFBs.

2.3.7   Using TF-IDF to identify true and false positive HFBs

To further address this issue of mouse-specific bias among HFBs required assignment of likelihood of a given HFB being a true or false positive given whether, and to what extent, it was detected at high frequency in a large number of mice. To accomplish this, I implemented a suggestion made by Zach Mass, a graduate student from Dr. Robin Dowell's lab, to employ an algorithm used developed for information theory known as term frequency inverse document frequency (TF-IDF) [106]. This algorithm was initially developed within a machine learning framework to aid text searching tools by assessing the proportionate power of a given word in distinguishing a document within a series given the prevalence of that word across that series [106]. I applied TF-IDF to barcodes, where I took the product of the frequency of a barcode from a given mouse experiment (tf) by the inverse log of the frequency of that barcode across detected across all mouse experiments (idf):

$$tfidf(f_e, N) = tf(f_e, n) * idf(f_E, N)$$

$$tf(f_e, n) = \frac{f_e}{n}$$

$$idf(f_E, N) = log10(\frac{N}{f_E})$$

In this formula, f_e is the frequency of a barcode in a given experiment, f_E is the frequency of a barcode across all mouse experiments, n is the number of total number of barcodes from a given experiment, and N is 22, the number of independent mouse experiments. This formula assigns a value that represents how proportionate a given barcodes' frequency is in a particular experiment given how proportionate its frequency is across all other 21 mouse experiments. Thus, a barcode appearing at low frequency (<5) in one or many individual experiments will receive a low TF-IDF value, given that its frequency is more or less *average* compared to all other barcodes. Likewise, barcodes appearing at high frequency across multiple mice are also given low TF-IDF values for the same reason. In the former case however, given there is no reason to believe that barcodes appearing at low frequency across all experiments are false, these can be trusted as true positive LFBs. However, in the latter scenario, if a barcode has a low TF-IDF value because it is detected at high frequency across many experiments, this barcode can be considered a false-positive. On the other hand, if a barcode is detected at high frequency in a single or few independent experiments, it will receive a high TF-IDF value because it is disproportionately at high frequency in a single mouse experiment, and is thus likely a true positive barcode. Thus, applying TF-IDF in this way, I assigned the likelihood of an HFB being a true positive and a result of *in vivo* cell expansion, rather than an experimental artifact.

I applied this formula to each barcode in each individual mouse experiment and observed the overall distribution of TF-IDF values. Similar to the frequency distribution of barcodes itself, most barcodes have low frequency and low TF-IDF values, with a long right tail indicative of a minor subpopulation of barcodes with high TF-IDF values (Figure 2.8A-B). I then plotted TF-IDF values against a barcodes' frequency in each individual mouse and observed that while most barcodes
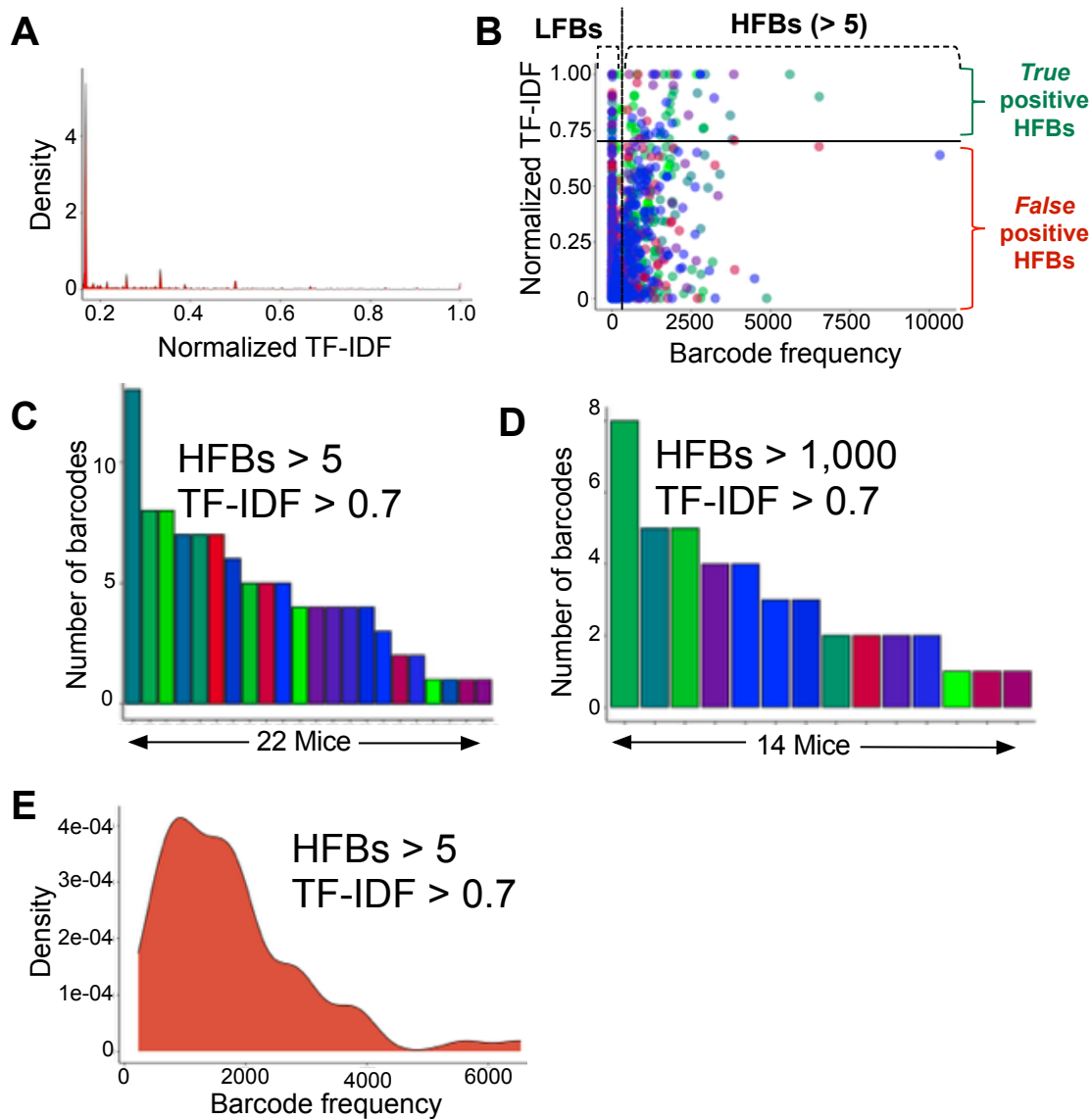
Figure 2.8: **Using TF-IDF to identify true and false positive HFBs.** (A) Probability distribution of normalized TF-IDF values. (B) Individual barcodes plotted by their normalized TF-IDF values and their frequency within individual mouse experiments. Vertical dotted line separates LFBs (barcodes with frequencies <5) and HFBs (barcodes with frequencies >5). Horizontal line distinguishes true positive HFBs (normalized TF-IDF > 0.7, green) from false positive HFBs (normalized TF-IDF<0.7, red). (C) Barplot of total numbers of barcodes sequenced in individual mouse experiments that have TF-IDF > 0.7 and were detected at frequency > 5 (22 mice) (D) or frequency > 1,000 (14 mice). (E) Frequency distribution for barcodes with TF-IDF > 0.7 and with frequencies > 5.

with low or high TF-IDF values are at low frequency, a subset have high TF-IDF values and were detected at high frequency in at least one mouse experiment (Figure 2.8B). These HFBs with high TF-IDF values are thus *high confidence* HFBs (hcHFBs), appearing at disproportionately high frequency in a single or few mouse experiments, yet are detected at average frequencies, if at all, in all other experiments.

I explored these hcHFBs further and found that 22/22 mouse experiments contained at least a single hcHFBs appearing >5, 17/22 with barcodes detected >100, and 14/22 experiments with barcodes >1,000 (Figure 2.8D). Thus, across 22 mouse experiments, we observed an abundance of hcHFBs appearing at high frequency uniquely in a given experiment but not so across other mouse experiments.

I next visualized the frequency distribution of hcHFBs (Figure 2.8E). While the median frequency of hcHFBs was 1,530, a portion were detected at even greater frequencies out to ~6,000 (Figure 2.8E). Altogether, these data suggest that despite bias driving some barcodes to appear to erroneously high frequencies, there are a set of hcHFBs that are specific enough to individual mouse experiments that the most likely explanation is that they are a product of MuSC proliferation into disproportionately large lineages.

2.3.8   MuSC population modeling

A single myofiber in a mouse TA muscle is considered to contain roughly 300-400 myonuclei, and I calculated as many as 200 MuSCs per TA (100k / 5,000 myofibers in single TA) [18,19,33,104]. The observed barcode frequencies among hcHFBs would thus imply that single MuSC clones are generating numbers of progeny greater than total MuSC or myonuclear numbers associated with single myofibers. Given its positioning between the basal lamina and myofiber membrane, it is not believed that single MuSCs can contribute to populating myofibers other than the one it resides on. Thus, either single MuSCs may actually contribute progeny to other myofibers, or total numbers of cells during and post muscle regeneration are significantly greater than in uninjured muscle where much of these cell numbers were observed [18,33,104].

From data published from the Olwin lab, PAX7+ cells expand roughly 20-fold in the first 5 dpi [49]. While PAX7+ cells eventually decrease falling to within range of their initial levels, the fate of the cells from this expansion (other than a lack of detectable PAX7) is not clear. Unless the cells resulting from this expansion are physically removed from the tissue, cells containing a barcode will still be detected through our sequencing experiments. However, whether these progeny of PAX7+ cells fuse and differentiate into myonuclei in the first 5 dpi, or persist as myogenic progenitors only to fuse or give rise to additional *Pax7+* cells a later time, cannot be determined from these experiments. Thus, even after return of PAX7+ cells to basal levels by 14 dpi [49], it's possible that the progeny resulting from their expansion in the first 5 dpi, whether myonuclei or myogenic progenitors, are far greater in regenerated muscle than uninjured muscle, explaining the presence of HFBs.

To help reveal what cell type are represented by HFBs, additional EdU pulse-chase experiments were conducted by a rotation student in the Olwin lab, Rachel Gessner. In prior published data from our group, we have previously demonstrated that central myonuclear production is predominantly complete by 5 dpi, while MuSC self-renewal occurs after this time [49]. In Rachel's experiments (n = 1), mice were given EdU for 3 hours at 3 dpi and then EdU was withdrawn and a chase was conducted out to 14 dpi, revealing that central myonuclei predominantly retained their EdU label (Figure 2.9). However, from a similar pulse-chase conducted at 5 dpi, overall very few nuclei are EdU+ (Figure 2.9). These data support that central myonuclei are derived from only a few cell divisions, while MuSCs and peripheral nuclei have gone through sufficient divisions between 3 dpi and 14 dpi to dilute their EdU label.

Additionally, Rachel conducted pulse experiments (with no chase) where EdU was administered at 3 dpi or 5 dpi, and the tissue was harvested 3 hours after administration. These experiments qualitatively demonstrate there are significantly more EdU+ cells from a 3 dpi pulse compared to a 5 dpi pulse (Figure 2.9). Thus, a greater number of cell divisions are occurring at 3 dpi than 5 dpi, suggesting that after 5 dpi, overall numbers of dividing cells decrease. Altogether, I argue that these experiments provide strong evidence that the bulk of all myogenic cell divisions occur
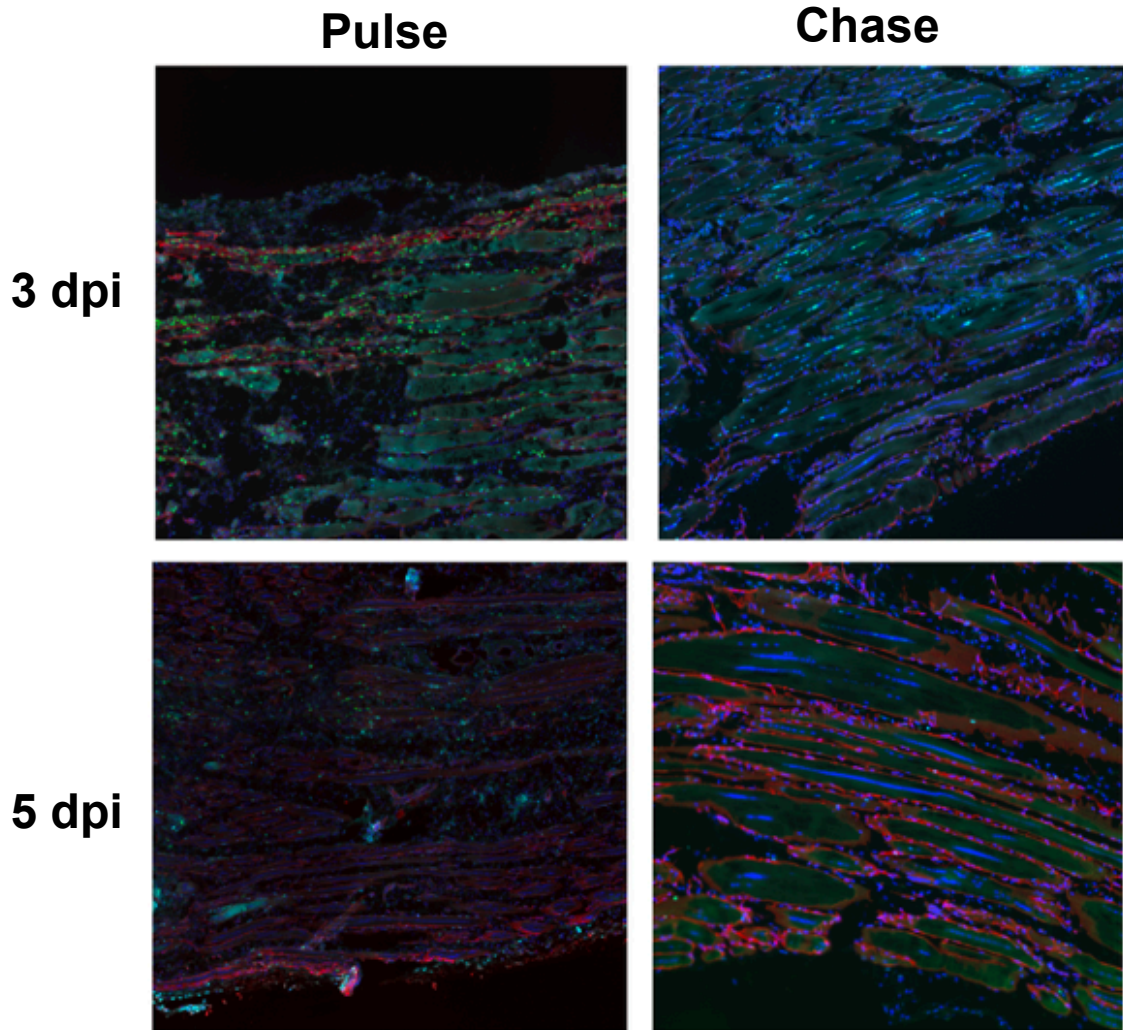
Figure 2.9: **EdU pulse-chase experiments during regeneration.** EdU pulse (left) and EdU pulse-chase (right) experiments done in mice at 3 dpi (top) or 5 dpi (bottom). EdU green, DAPI blue, PAX7 red, laminin magenta.

from 0 dpi – 5 dpi. Some of these divisions result in centrally located myonuclei, some in myogenic progenitors destined to differentiate into peripheral myonuclei at a later time, and some of these divisions likely replenish MuSCs to maintain a sufficiently large pool once regeneration is complete. Whereas divisions still occur after 5 dpi, they are less abundant and are most likely restricted to specific lineages.

By integrating these EdU experiments with results from the barcoding experiments, I can propose a model explaining how asymmetric and symmetric divisions may be balanced by MuSCs

and myogenic progenitors during regeneration. To calculate the number of cells produced by any number of symmetric divisions, one can use this equation:

$$N = N_i * 2^d$$

where a total number of cells N starting from an initial number of cells (N_i) is produced by a given number of divisions d.

Alternatively, the same equation adjusted for a potential of asymmetric divisions, in which one daughter cell, rather than dividing again to produce more cells, differentiates and ceases cell divisions, can be captured by:

$$N = N_i * (1 + r)^2$$

In this adjusted formula, r is ratio of cells that can go on to produce more cells after a subsequent division rather than differentiating. Thus, the r value is the proportion of divisions that are symmetric or asymmetric. A lower r value therefore corresponds to a greater difference between the number of cells produced via symmetric divisions compared to the same number of asymmetric divisions. As r approaches 1, models of asymmetric and symmetric cell expansion converge.

By interpreting the EdU experiments to suggest that most cell divisions are complete by 5 dpi, the question arises as to what balance of asymmetric and symmetric divisions are required for MuSCs to generate thousands of progeny in this time frame. Among hcHFBs, there are several appearing at frequencies >2,000, with a few >4,000, and the highest frequency hcHFB reaching 6,532 (Figure 2.8E). To address whether a single MuSC can produce these numbers of progeny in 5 dpi as is supported by the EdU pulse-chase experiments, I considered what is known about the timing of MuSC divisions after an injury. Published studies have demonstrated that the first MuSC division may occur as soon as 24 hours after an injury, and subsequent divisions may occur as rapidly as every 8 hours after that. These temporal constraints would enable between 10 and 13 divisions to occur within the first 5 dpi (Supplental Figure 2.2).

dpi	Potential divisions per day
1	1
2	2-3
3	3
4	3
5	3
Total Potential cumulative divisions	10-13

Supplementary Figure 2.2: Table describing potential numbers of myogenic progenitor cell divisions occurring in by 5 dpi given temporal constraints.

To address what balance of symmetric or asymmetric divisions are necessary to produce thousands of progeny within 10-13 divisions, I plotted the functions for symmetric and asymmetric expansion with different r values out to 13 divisions (Figure 2.10A). From this analysis of potential different cell expansion dynamics, I find it is indeed possible for a single MuSC to produce up to 8,000 progeny in 5 days, as long as the majority of divisions are symmetric. Moreover, these data suggest it's possible that with predominantly symmetric divisions occurring, even higher numbers of cells can be produced in this time frame.

Given the immense numbers of cells that can be generated through symmetric expansion even within these temporal constraints, it's possible that asymmetric divisions are incorporated in order to reduce overall cell expansion. Or alternatively, it's possible that this period of rapid cell expansion results in a transiently excessive number of cells whereby some are eventually pruned out to reestablish population balance after regeneration is complete. To evaluate these different possibilities, I compared the frequency distributions of hcHFBs in 30 dpi and 90 dpi samples. From looking at these distributions, the numbers of exorbitantly high frequency HFBs (hcHFBs>4,000) are greater at 30 dpi than 90 dpi, while there are increased numbers of more average frequency
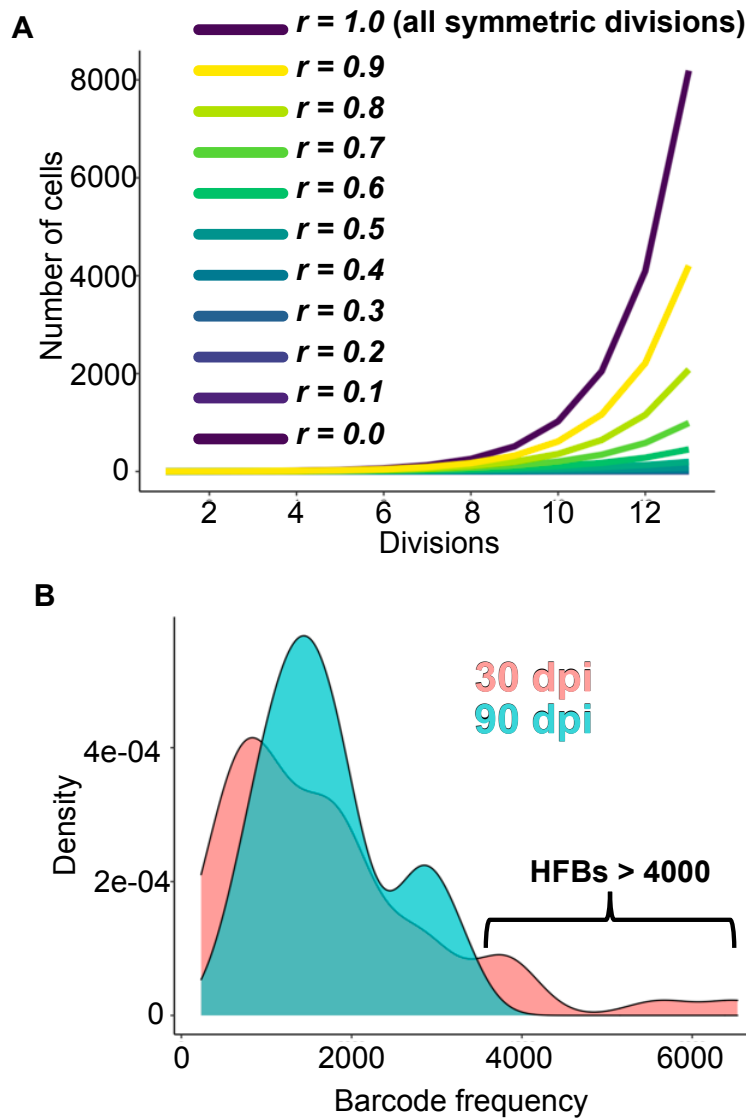
Figure 2.10: **Population modeling of myogenic cell expansion after injury.** (A) Plot of number of cells produced by 13 divisions from either symmetric expansion ($r = 1$), or varying degrees of incorporation of asymmetric divisions ($r < 1$). (B) Frequency distributions of HFBs>100 in 30 dpi and 90 dpi experiments. Bracket marks enrichment of HFBs>4000 in 30 dpi experiments.

hcHFBs (hcHFBs>100 & <4,000) at 90 dpi than at 30 dpi (Figure 2.10B). Altogether, these data suggest that progeny from high expanding lineages proceed through a reduction process between 30 dpi to 90 dpi.

2.3.9   MuSCs population dynamics are different in aged mice

Adult stem cell populations become depleted as organisms age [88], yet whether all populations and functions of MuSCs are affected equally during aging, or whether distinct subsets are preferentially affected is not well understood. Having proposed a model of MuSC expansion after an injury in the previous section, I next wondered how this proposed paradigm may differ in aged mice compared to young mice. HFBs may represent an undesired side effect of regeneration and is a result of some uncontrolled and pathological cell proliferation. This could result in a higher proportion of HFBs detected in aged mice after regeneration, supporting that generation of HFBs is not associated with regeneration in young mice. Alternatively, as proposed by my model, HFBs result from a legitimate biological mechanism needed to ensure appropriate balance of different fate choices and population sizes during and after regeneration. In this latter scenario, less HFBs would be observed in aged mice compared to young mice, indicating improper population balance and depletion of specific MuSC subpopulations that could contribute to regenerative defects during aged mouse regeneration.
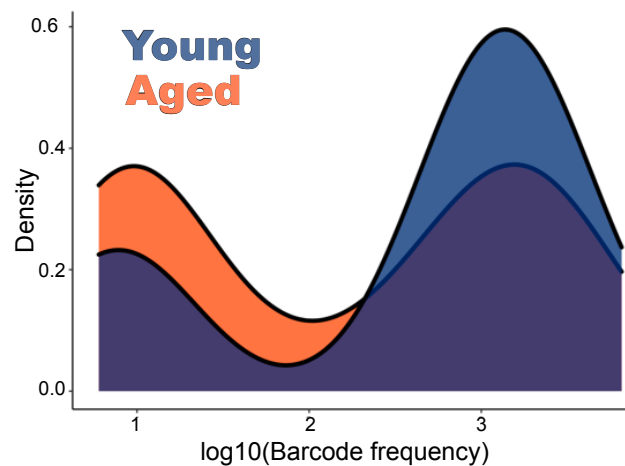
Figure 2.11: **Population dynamics are different in aged compared to young mice after regeneration.** Frequency distribution of HFBs>5 & TF-IDF>0.7 demonstrating an increased density of HFBs in young mice.

When visualizing the frequency distribution of hcHFBs>100 in young and aged mice from

only 30 dpi experiments, I observed more hcHFBs detected in regenerated muscle from young mice compared to aged mice (Figure 2.11). These data support that the capacity for small subsets of MuSCs to generate the disproportionately extensive numbers of progeny is required for appropriate muscle regeneration, and their reduction in aged mice may be a signature of dysregulated myogenic population dynamics accompanying skeletal muscle aging.

2.4   Discussion

My research work described in this chapter contains novel analysis of barcode lineage tracing of MuSCs, the critical myogenic cell type enabling skeletal muscle regeneration [30–32]. Integrating these results with results from EdU labeling and pulse-chase experiments builds on findings from previous studies [8, 52, 54, 62, 70, 107] and improves our understanding of how MuSC fates are regulated to produce sufficient numbers of differentiated myonuclei, while simultaneously not depleting the MuSC pool. Moreover, my results support that population dynamics are disrupted in MuSCs from aged mice during regeneration, suggesting a failure in aged mice to maintain proper population balance among MuSCs.

2.4.1   A small MuSC subpopulation proceeds through disproportionate numbers of cell divisions

After a skeletal muscle injury, MuSCs are the precursors for all myogenic cell types created during regeneration [30–32]. MuSCs balance proliferation rates sufficient to rapidly generate large numbers of myonuclei, while also ensuring that quiescent MuSCs are not depleted by either resisting activation, or through activation and procession through self-renewal divisions [37, 49, 50, 61, 108]. While MuSC progeny can become myonuclei or self-renewed MuSCs, it is not clear whether distinct MuSC subsets are biased towards particular fates.

In order to balance self-renewal and differentiation, adult stem cells regulate their numbers and proliferation rates to ensure appropriate abundances of stem cells and differentiated progeny. These strategies are broadly delineated as one of two models. The first is referred to as invariant

asymmetry, a paradigm in which there is an equipotency of all stem cells to asymmetrically divide, resulting in a self-renewed stem cell and a cell fated to differentiate (Figure 1.2) [53, 108]. The alternative to this model is population asymmetry, where different stem cells have different propensities for either these asymmetric divisions, or symmetric divisions creating two stem cells, or two differentiated progeny 1.3. Thus, in this latter scenario, the balance between self-renewal and differentiation is maintained at the population level, where stem cell fates are heterogeneous and segregate to specific subpopulations, rather than all stem cells dividing asymmetrically [53,108,109]. Nevertheless, sufficient evidence now exists to support that stem cell population paradigms may be more tunable and complex than described these models would imply [56–58, 110].

Because MuSCs are capable of proceeding through both asymmetric self-renewal divisions as well as symmetrically expanding as myogenic progenitors [39, 47, 52, 61, 108], MuSC dynamics most closely resemble a model of population asymmetry. However, how different types of divisions are regulated at a population level, and whether distinct subsets of MuSCs are biased for generating MuSC or myonuclear lineages and where asymmetric and symmetric divisions segregate to different MuSC subpopulations, is not clear. While asymmetric divisions may be critical for maintaining the MuSC pool during homeostasis, symmetric divisions during muscle regeneration may be important for producing sufficient numbers of MuSCs or differentiated myonuclei [39, 48, 61, 108, 109]. This is supported by progressive injuries resulting in reduced clonal complexity, indicating the MuSC pool is maintained by symmetric divisions over time, resulting in neutral clonal drift [52].

We labeled individual MuSCs with inheritable genomic barcodes, determining the proportions of progeny generated by individual MuSCs and their subsequent lineages. My analysis of barcode frequency distributions and the integration of these data with EdU pulse-chase experiments revealed that significant MuSC proliferation appears restricted to rare lineages biased for production of MuSCs. While, strikingly, the bulk of MuSCs proceed through a small number of divisions that primarily generate centrally located myonuclei.

My proposed model of MuSC population dynamics during muscle regeneration describes centrally located myonuclei as most likely derived from the most abundant subpopulation of MuSCs

(MuSCs-A, representing LFBs) (Figure 2.12). Because LFBs represent MuSCs having only pro-
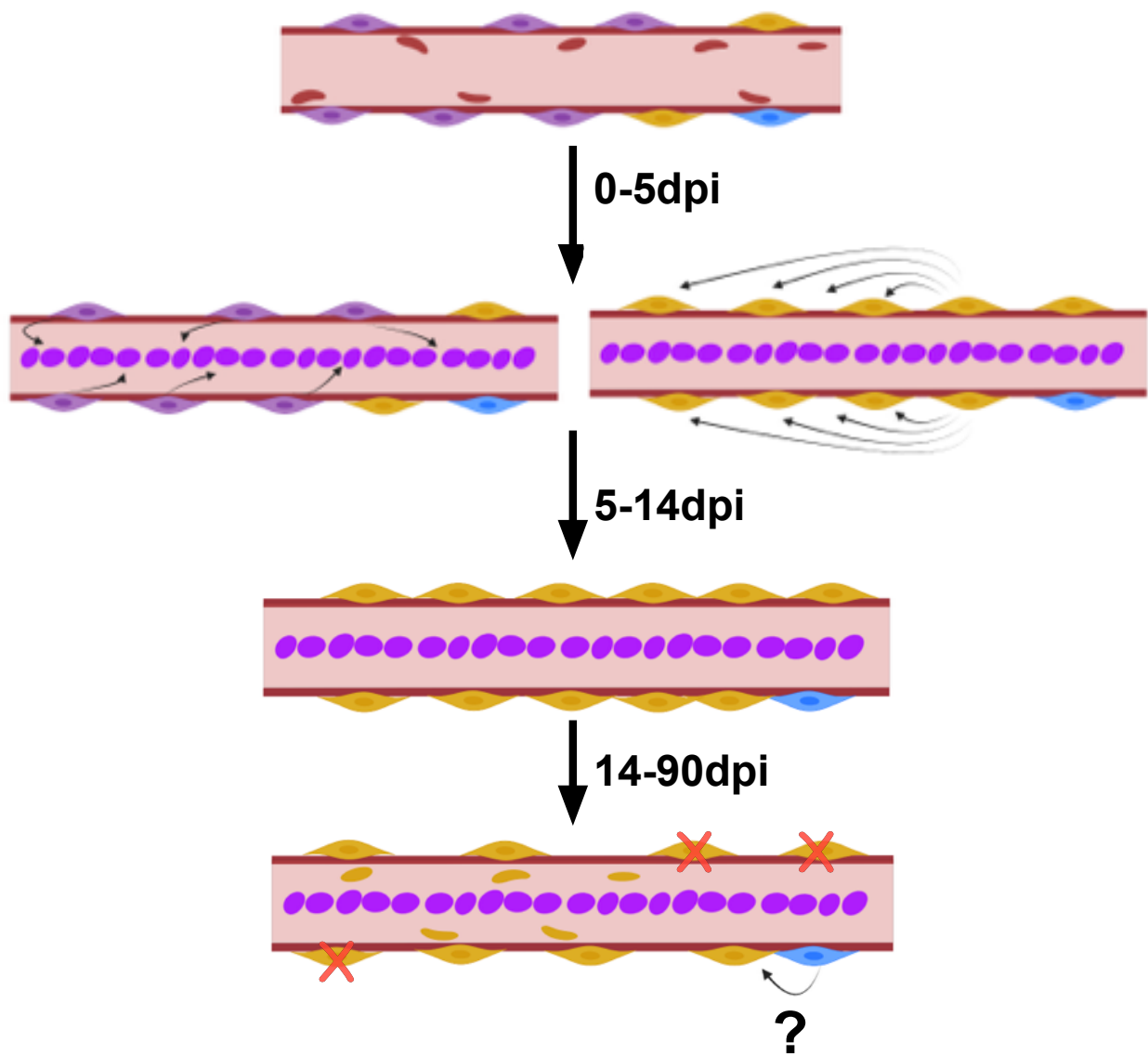
Figure 2.12: **Proposed model of MuSC dynamics after muscle injury.** There are 3x populations of MuSCs; MuSCs-A (purple), MuSCs-B (yellow), MuSCs-C (blue). In the first 5 days following an injury, MuSCs-A and MuSCs-B are activated (top). MuSCs-A divide relatively few times and represent LFBs. Their progeny predominantly differentiate into centrally located myonuclei. MuSCs-B become activated in the same time as MuSCs-A, but they begin dividing and producing more MuSCs or a different class of progenitor. MuSCs-B represent HFBs, and their lineage fate can either be MuSCs, myogenic progenitors, or peripheral myonuclei. Some cells within the MuSCs-B class are pruned out between 14 dpi – 90 dpi (bottom). MuSCs-C also represents LFBs, but these cells may be reserve MuSCs that are only activated after regeneration is complete to reestablish clonal diversity among the MuSC pool.

ceeded through a few cell divisions, these lineages, and the myonuclei derived from them, are likely clonally diverse. These cells, may exist prior to injury in a type of primed state towards production of myonuclei through minimal cell divisions, potentially related to to how levels of *Pax3* and *Pax7* expression confer distinct proliferative and differentiation capacities and the identification of a MuSC "alert" state [9, 66, 111–113] . Whether MuSCs-A divide only asymmetrically, only symmetrically, or a combination of both, cannot be determined from the barcoding and EdU experiments alone. Nevertheless, if symmetric divisions occur, my data support they are minimal given the majority of barcodes were detected at low frequency, and thus is not characteristic of the large number of progeny generated through symmetric cell expansion.

In addition to MuSCs-A, my findings support that a large portion of the replenished MuSC pool, and potentially peripheral myonuclei as well, are generated by another subpopulation of MuSCs dividing at high rate and resulting in HFBs (MuSCs-B, Figure 2.11). While asymmetric divisions occurring within this population cannot be ruled out, my model suggests they are more rare given the time frame in which the EdU data supports it takes for these cells to expand to significant numbers. A reduction in HFBs from 90 dpi to 30 dpi supports the initial process of MuSC expansion results in an overabundant number of cells, whereby some are then pruned to restore population balance once regeneration is complete. Crucially, the reduction of HFBs from 30 dpi to 90 dpi cannot be simply the result of differentiation (as the barcode would still be detected if the cell is still present in the tissue) but rather can only result from physical removal of a given cell containing an HFB from the muscle. It's possible that among the progeny of MuSCs-B containing HFBs, some eventually differentiate generate peripheral myonuclei, or they persist as quiescent MuSCs or as primed progenitors (Figure 2.11). Overall, these pose intriguing questions remaining still to be answered, and evaluating the biological significance of high expanding MuSCs will be critical for understanding population dynamics during and after regeneration in young and aged mice.

I have described two populations of MuSCs (MuSCs-A and MuSCs-B), where each have distinct roles during regeneration and distinct proliferative behaviors to result in the presence of

either LFBs or HFBs. However, this conceptual model as described so far would lead to a complete abatement of MuSC clonal diversity after a single injury, as all quiescent MuSCs remaining after regeneration would be derived from a single expanding lineage (MuSCs-B). Thus, there is likely a third population of MuSCs (MuSCs-C), which may represent a type true "reserve" MuSC, similar to observed in muscle and other tissues (Figure 2.11) [37, 54, 114]. These cells would theoretically only activate under extreme circumstances such as a significant injury, and may be important for maintaining MuSC clonal diversity [37, 54, 115, 116]. MuSCs-C would be indistinguishable from MuSCs-A and other LFBs from our barcoding experiment. However, their role would be distinct and could be the parent cell for both MuSCs-A and MuSCs-B lineages (Figure 2.11).

While this model successfully explains a potential scenario leading to the results obtained from our barcoding experiments, there is admittedly not much explanation for the presence of HFBs reaching frequencies as high as 4,000-6,000. If HFBs do represent predominantly symmetrically expanding MuSC self-renewing lineages, the lineages reaching these sizes would mean that single MuSC clones generate 4-6% of all MuSCs after regeneration. If some of these MuSCs differentiate as peripheral nuclei as explained in my model, this may reduce this percentage some. It is possible that these high expanding lineages are themselves the "reserve" MuSCs responsible for repopulating the MuSC pool, but this seems problematic as this would greatly reduce clonal diversity after a single injury rather than only through successive injuries [52]. A possibility I cannot rule out is that the large MuSC lineage expansions observed from our experiments are pathological, analogous to cancerous growths resulting from uncontrolled cell proliferation. Given the number of MuSCs in the muscle and the severity of chemically induced injuries, it's possible that a small percentage of these cells become dysregulated and expand erroneously. Nevertheless, my proposed model provides a conceptual framework describing the presence of HFBs and the overall observed barcode distributions consistent with experimental data from other groups [29,37,39,52,62,108]. Evaluating the biological significance of HFBs will require hard work from future researchers from our group to further our understanding of MuSC population dynamics.

2.4.2   MuSC population dynamics in aged mice

Skeletal muscle aging is a significant contributor to declining standard of living in elderly individuals. Contributing to this decline are widespread deficits in MuSC function that include altered capacities for self-renewal, proliferation, or differentiation, as well as an overall reduction in numbers [7–10,74,86,89]. However, whether MuSC population dynamics during regeneration differ in aged skeletal muscle is critical to revealing the underlying drivers of muscles reduced regenerative capacity.

Through analysis of our barcode lineage tracing experiment, I reveal that the population balance between HFBs and LFBs observed during young-mouse regeneration is distinct from the balance observed during aged-mouse regeneration. My results support that in aged mice, the presence of high expanding lineages, which may be important for repopulating the MuSC pool, is disrupted. If MuSCs indeed proceed through a predominantly symmetric expansion in order to generate sufficient numbers of self-renewed MuSCs, and this process is awry in aging, it could explain the reductions in MuSC number and clonal diversity among aged mouse MuSCs [52,58,104]. Overall, these findings suggest population and proliferative dynamics driving MuSC expansion and maintenance of quiescent MuSCs is disrupted during aging.

2.5   Methods

This method section provides a brief description of a work in progress. The precise methodologies utilized in this project are subject to change, so the reader is encouraged to refer to the published paper once it is available for a more in depth description of all PCR primer sequences, the barcoding strategy, and all subsequent analyses. The methods provided below were written to be sufficient for the comprehension and interpretation of this thesis.

2.5.1   Mouse genetics and injuries

Mice containing the gene for the TVA receptor were gifted from collaborators outside of the University of Colorado Boulder. In short, the gifted Cre^{TVA^+} mice were bred in-house to generate the $Pax7^{+/Cre^+/TVA^+}$ mice used in this experiment. Upon the addition of Tamoxifen, cre-mediated recombination enables *Pax7*-driven expression of the *TVA* gene. Aged mice were between 22-26 months, young mice were between 4-8 months.

2.5.2   DNA barcode library construction

The barcode library was constructed by annealing oligonucleotides containing randomized sequences interspersed with fixed sequences (——ATC–GAT–AAA–GGT–) flanked by *attb1* and *attb2* sequences for gateway cloning into *E. coli*. This library was then shotgun cloned into an RCAS adaptor plasmid containing an IRES mCherry expression casette. Barcode viruses are produced by transfecting avian DF1 fibroblasts with the viral library, expanding cells, harvesting virus, and purifying by ultracentrifugation yielding $\sim 1x10^8$ ifu/ml of RCAS-BC-mCherry virus.

2.5.3   DF1 experiments

Naive DF1 cells were infected with RCAS viral preparations containing the barcode library at 8-fold representation of library's diversity. DNA was isolated from cells 8 hours after infection using a Qiagen DNAeasy kit, where the protocol was followed according to manufacturers recommendations. Purified DNA was then assessed by gel electrophoresis for size and quality before being subjected to LAM-PCR and prepared for sequencing.

2.5.4   Mouse injuries and DNA isolation

Mice were administered Tamoxifen to induce *TVA* expression in MuSCs 6 hours prior to injuries. For injuries, mice were injected with 1.2% $BaCl_2$ concomitant with injection with RCAS containing barcode libraries. After 30dpi or 90dpi, genomic DNA was isolated from mouse TA muscle using a Qiagen DNAeasy kit, where the protocol was followed according to manufacturers

recommendations. Purified DNA was then assessed by gel electrophoresis for size and quality before being subjected to LAM-PCR and prepared for sequencing.

2.5.5   LAM-PCR

The sequence for the LAM-PCR primer is 5′- GTGACTGGAGTTCAGACGCTCANNNN NNNNCCGCTTTTCGCCTAAACAC where text in red is the degenerate UMI sequence added to each individual barcode, and the text in green represents the portion annealing to the barcode sequence. A single round of LAM-PCR is conducted to generate a sequence to be amplified that has sequencing adapters, degenerate barcode sequence, and a UMI. Universal PCR is then conducted on LAM-PCR products to bulk amplify the library for sequencing.

2.5.6   Sequence processing

Fastq files were assessed for quality using FastQC. Reads containing barcode sequences were aligned and scored for their identity to the consensus region of the barcode using the python package *pairwise2* and the function "align.globalms". The alignment sequence used was "——ATC–GAT–AAA–GGT–ACCCAGCTTTCTTGTACAAAGTGGTTGATCGATGCGATGTACGGGCCAGA TATACGCGTATCTGAGGGGACTAGGGTGTGTTTAGGCGAAAAGCGG——TGAGCGT CTGAACTCCAGTCAC" for each Fastq read. Only sequencing reads with perfect matches to the consensus bases were included for downstream for analyses.

2.5.7   Frequency analysis and further analyses

All barcode analyses was conducted primarily using base packages in R 4.0.1, as well as the *tidyr* and *dplyr* packages for data frame handling. Barcode frequency tables were generated with barcodes and their frequencies merged across individual experiments. Detection of over-represented barcodes from the DF1 experiments, calculation of Hamming distances, and application of the TF-IDF algorithim, were all done *ad hoc*. All code associated with library bias evaluation and frequency distribution analysis will be made publicly available upon time of publication.

<center>

Chapter 3

Aging disrupts gene expression timing during muscle regeneration

</center>

3.1   Chapter Note

The following chapter of this thesis is published work of which I was first author [117]. All supplemental tables can be accessed online. The text comprising this chapter is unchanged apart from those made for organizational purposes. The experiments that generated the data I ultimately processed and analyzed for this study was conducted by Ashleigh Van Deuesen, a talented former undergraduate in the lab, and Dr. Alicia Cutler, a post-doctorate researcher. The EdU experiments were conducted by Dr. Brad Pawlikowski.

Additionally, the publication of this work would have not been possible if not for the significant intellectual and computational guidance provided by Dr. Jacob Stanley, a post-doctoral fellow in the Dr. Robin Dowell's lab. Dr. Stanley's computational expertise, as well as from others from the the lab of Dr. Robin Dowell, was indispensable for the completion and publication of this work.

3.2   Abstract

Skeletal muscle function and regenerative capacity decline during aging, yet factors driving these changes are incompletely understood. Muscle regeneration requires temporally coordinated transcriptional programs to drive myogenic stem cells to activate, proliferate, fuse to form myofibers, and to mature myonuclei, restoring muscle function after injury. We assessed global changes in myogenic transcription programs distinguishing muscle regeneration in aged mice from young mice

by comparing pseudotime trajectories from single-nucleus RNA sequencing of myogenic nuclei. Aging-specific differences in coordinating myogenic transcription programs necessary for restoring muscle function occur following muscle injury, likely contributing to compromised regeneration in aged mice. Differences in pseudotime alignment of myogenic nuclei when comparing aged to young mice via Dynamic Time-Warping revealed pseudotemporal differences becoming progressively more severe as regeneration proceeds. Disruptions in timing of myogenic gene expression programs may contribute to incomplete skeletal muscle regeneration and declines in muscle function as organisms age.

3.3   Introduction

Skeletal muscle is critical for overall health. Deteriorating skeletal muscle function and reduced regeneration occurring during aging negatively impacts mobility and muscle force, contributing to physical and mental decline in elderly individuals [4–6,70,118]. Skeletal muscle is comprised of long syncytial cells (myofibers) formed by fusion of skeletal muscle progenitors during development and during muscle repair and whose nuclei share a common cytoplasm yet are transcriptionally heterogeneous [16, 20–22, 26].

Myofibers are maintained in adult skeletal muscle by a population of quiescent muscle stem cells (MuSCs) that in response to injury, activate, proliferate as mononuclear myogenic progenitors, and then fuse, generating sufficient myonuclear numbers and diversity to repopulate regenerated myofibers [30,31,119]. While most progenitors differentiate and fuse producing myonuclei, a subset undergoes self-renewal, reacquiring quiescence and replenishing the MuSC pool [47,49–51]. Though the transcriptional changes driving MuSC activation and proliferation are well-studied, the mechanisms responsible for maturing and diversifying myonuclei once progenitors have fused are largely unexplored.

Failure to maintain and repair skeletal muscle in aged organisms is attributed in part to deficits in MuSC function that include delays in exiting quiescence, premature differentiation, failure to transplant, and cumulative transcriptional changes [7–10,16,21,74,85,86]. Temporal expression of

myogenic transcription factors (TFs) is disrupted in progenitors isolated from aged mice [74,85,86], eliciting potentially widespread and severe downstream affects in their gene regulatory networks. Aging-associated defects in MuSC transcriptional dynamics are exacerbated upon differentiation [85,86] supporting the idea that disruptions in gene expression timing during regeneration worsen as regeneration proceeds. Yet to what extent these temporal differences drive deficiencies in skeletal muscle repair and function in aged organisms is largely unexplored and cannot be sufficiently recapitulated in culture, as myonuclei fail to organize into the specialized structures found in vivo and never express mature isoforms of skeletal muscle proteins [42, 120, 121].

Evaluating transcriptional changes driving myogenesis *in vivo* is complicated by the multi-nucleated and heterogeneous nature of skeletal muscle cells. Single-cell RNA sequencing provides sufficient resolution of mononuclear progenitors but fails to capture substantial myonuclear numbers [122,123]. RNA-FISH provides spatial and transcriptional information but is low-throughput, while spatial transcriptomics lacks the resolution to examine individual myonuclei [16, 124]. Numerous studies have identified individual genes and pathways through direct experimentation that are disrupted in aged-mouse skeletal muscle, but aging impacts universal properties of transcription [69], thus large-scale transcriptomic interrogations *in vivo* followed by in-depth computational analyses are uniquely situated to further improve our understanding of skeletal muscle aging.

To better understand how the transcriptional changes occurring during muscle regeneration in young-adult and aged mice differ, we constructed a pseudotime trajectory of myogenic differentiation from single-nucleus RNA sequencing (snRNA-seq) of myogenic nuclei isolated from both mononuclear and multinucleated cells prior to and during regeneration in young-adult and aged mice. Ordering nuclei along pseudotime enabled parsing heterogeneous differentiation states present among myogenic nuclei taken at discrete times during regeneration, such that nuclei from young-adult and aged mice could be aligned and compared based on their relative cell fate status. Comparing how the pseudotime ordering of nuclei differs between young-adult or aged mice revealed that genes with aging-associated alterations in pseudotemporal expression are part of myogenic transcriptional programs that are essential for the re-acquisition of muscle function after an injury.

Further analysis of the differences between myogenic nuclei from aged compared to young-adult mice using Dynamic-Time Warping revealed that global transcriptomic differences are larger in post-fusion myogenic nuclei compared to mononuclear progenitors. Collectively, alterations in gene expression timing may amplify as progenitors differentiate into myonuclei and may thus contribute to reduced muscle regeneration and declines in muscle function as mice age.

3.4   Results

3.4.1   MuSC expansion dynamics are disrupted during regeneration of aged mouse TA muscle

MuSCs from aged mice are less proliferative and differentiate prematurely when cultured compared to MuSCs from young mice [8, 74, 80]. To identify differences in MuSC behavior in aged mice *in vivo*, we quantified MuSC number, identified by PAX7 immunoreactivity, in the tibialis anterior (TA) muscle for up to 28 days post-injury (dpi) in aged and young mice. MuSCs exit quiescence and their myogenic progenitor progeny expand rapidly, reaching a peak by 4 dpi in young mouse muscle, and slowly decline to within 2-fold of initial MuSC numbers by 28 dpi (Figure 3.1A). In aged mice, PAX7+ cell expansion is delayed with myoblast numbers peaking at 7 dpi with less than half the peak number in young mice (Figure 3.1A). Nevertheless, at 7 dpi numbers of MuSCs and myoblasts in young and aged mice begin to decline synchronously, such that by completion of regeneration similar numbers of MuSCs are present in both age groups (Figure 3.1A).

Reduced MuSC numbers in aged mice may result from reduced MuSC proliferation, a slower cell cycle, cell death, or from some other cause. To evaluate these possibilities, we used the nucleotide analog ethynul-2'-deoxyuridine (EdU), which is incorporated into DNA during replication, to identify recently divided PAX7+ cells. Young and aged mice were injured and treated with EdU for 6 hours prior to tissue harvest and percentage of EdU+/ PAX7+ cells was quantified at different timepoints (Figure 3.1B). The percentage of EdU+/PAX7+ cells was reduced in aged

mice compared to young mice at all timepoints up to 14 dpi, indicating fewer dividing MuSCs and myogenic progenitors (Figure 3.1B). Although the proportion of dividing PAX7+ cells was diminished in aged mice, the overall proliferative trend is similar in both aged and young mice, as the percentage of EdU+/PAX7+ cells peak at 4 dpi and then decrease (Figure 3.1B).

3.4.2 snRNA-seq of post-injury skeletal muscle in young and aged mice

Temporal differences in the expansion of MuSCs and their progeny between young and aged mice at 4 dpi or 7 dpi suggests temporal coordination of myogenic transcriptional networks driving regeneration may be altered. Probing gene expression changes prior to, during, and following cell fusion is challenging, requiring assessment of transcripts from mononuclear cells as well as myonuclei in syncytial myofibers, rendering use of standard single-cell sequencing ineffective. To evaluate aging-associated transcriptomic differences in myogenic nuclei during muscle regeneration in aged mice, we conducted snRNA-seq on the TA muscles of young and aged mice at 0 dpi (uninjured), at 4 dpi when myonuclear production is largely complete [49], and at 7 dpi when myonuclei are likely maturing (Figure 3.1C; Figure 3.1A-B). Dimensional reduction was conducted on single-nuclear transcriptomes aggregated across all timepoints and combined from both young and aged mice (Figure 3.1A-B). Nuclear clustering revealed the expected cell types including skeletal muscle-associated mononuclear cells (immune cells, FAPs, endothelial cells, etc.), myogenic mononuclear cells (MuSCs and myogenic progenitors), as well as myonuclei within multinucleated myofibers (Figure 3.1C-D; Figure 3.1C).

We subclustered all MuSCs, myogenic progenitors, and myonuclei based on 4 criteria: 1) inclusion in $Ttn+/Neb+$ clusters, 2) expression of the myogenic genes $Pax7$, $Myod1$, $Myog$, Ckm, or $Mylk2$, 3) lack of expression of $Cd74$ or $Pecam1$, and 4) exclusion from the fibroblast, schwann cell, smooth muscle cell, and immune cell clusters (Figure 3.1C) [20, 125–128]. MuSCs, myogenic progenitors, and myonuclei (Figure 3.1E) arrange in unique as well as overlapping clusters when plotted by age (Figure 3.1F) or injury timepoint (Figure 3.1G). This comprehensive myogenic sub-set, comprised of myogenic nuclei from all injury timepoints and young as well as aged-mouse skele-

A Number of PAX7+ cells post-injury

B Percentage EdU+/PAX7+ cells post-injury

C

- Myonuclei
- Progenitors
- MuSCs
- Fibroblast
- Immune
- Endothelial
- Smooth Muscle
- Unidentified

D *Neb*, *Myog*, *Pax7*, *Dcn*, *Cd74*, *Pecam1*, *Rgs5*

E

- Myonuclei
- Progenitors
- MuSCs

F

- Young
- Aged

G

- 0 dpi
- 4 dpi
- 7 dpi
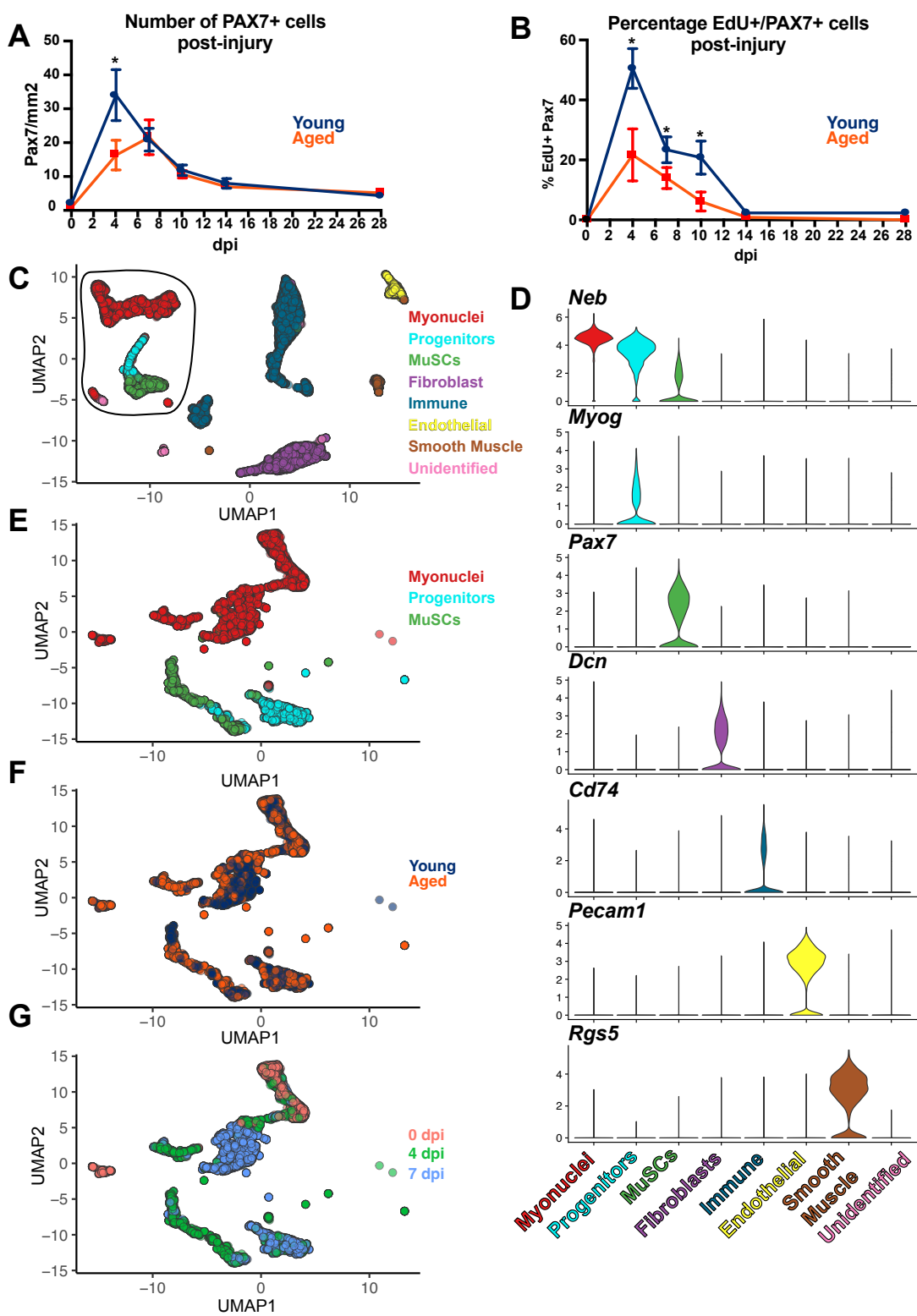
Figure 3.1: **MuSC kinetics and sequencing in regenerating muscle of young and aged mice.** (A) PAX7+ cell quantification from regenerating TA muscles in young and aged mice (n = 3). (B) Percent PAX7+ and EdU+ cells in regenerating young and aged mice. EdU was administered 6 h prior to tissue harvest. *indicates p < 0.05, 1-way ANOVA (n = 3). (C) UMAP clustering of nuclei from sequencing single cells and single nuclei of skeletal muscle from young and aged mouse TA muscles at 0 dpi (n = 4; 2 young, 2 aged), 4 dpi (n = 5; 2 young, 3 aged), and 7 dpi (n = 4; 2 young, 2 aged). Black circle demarks myogenic nuclei used for further analysis. (D) Violin plots of selected genes used to identify cell types from snRNA-seq. (E) Subset of myogenic nuclei used for downstream analyses (F) identified by age, and (G) by dpi. See also Figure 2.1 and Table S1-S2.
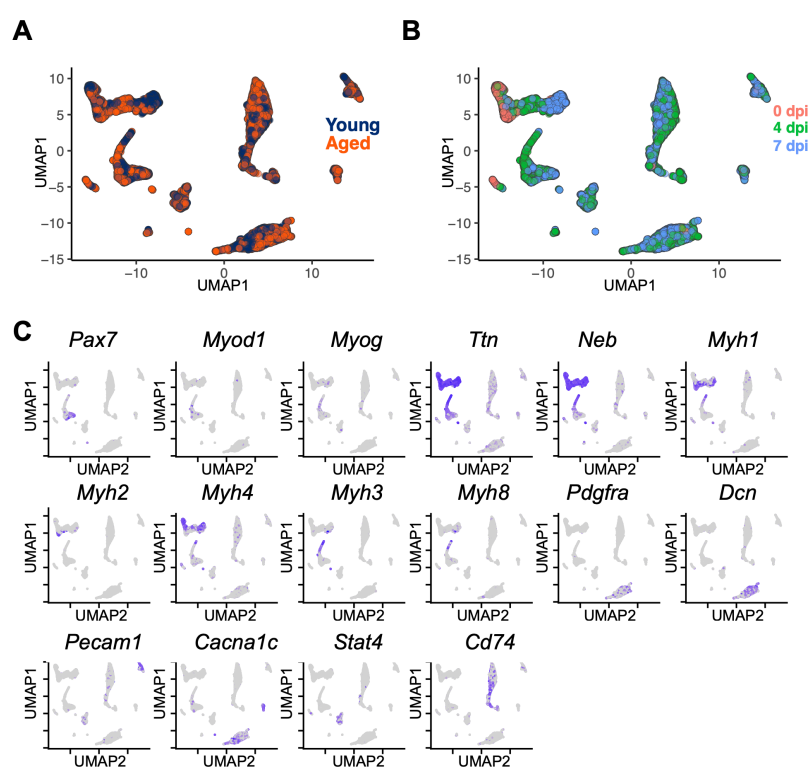
Supplementary Figure 3.1: **Single-nucleus sequencing of TA muscle in young and aged mice 0 dpi, 4 dpi, and 7 dpi.** (A) UMAP clustering of all nuclei identifying those from young mice (blue) and aged mice (orange), and (B) combined nuclei from young and aged mice identifying the contribution from 0 dpi (salmon), 4 dpi (green) and 7 dpi (blue). Black circles represent myogenic population used for additional analysis and described in Figure 3.1C-G. (C) UMAP plots depicting the expression of representative genes for evaluating distinct cell types and representative genes used to identify myogenic sublcusters (*Pax7* = MuSCs, *Myod1/Myog* = myogenic progenitors *Ttn/Neb* = myonuclei, *Myh1* = Type IIa myonuclei, *Myh2* = Type-IIx myonuclei, *Myh4* = Type-IIb myonuclei, *Myh3/Myh8* = regenerating myonuclei, *Pdgfra/Dcn* = FAPs, *Pecam1* = endothelial, *Cacna1c* = smooth muscle, *Stat4/Cd74* = immune). Axis scales are the same as in Figure 3.1C.

tal muscle, was used for further analyses. Comparing GO Processes for myogenic nuclei between young and aged mice at 4 dpi and 7 dpi identified filament assembly and myoblast proliferation as significant at 4 dpi (Figure 3.2A; Table S1), and MuSC differentiation and innervation as significant at 7 dpi (Figure 3.2B; Table S1) [129]. Among the most significantly affected genes within these GO processes are genes encoding receptors *Fgfr1*, *Fgfr4*, and *Notch3* (Figure 3.2C), genes encoding sarcomeric proteins *Ttn* and *Neb* (Figure 3.2D), and transcription factors (TFs) involved in myoblast proliferation, *Six1* and *Runx1* (Figure 3.2E; Table S2) [35, 126, 130–132]. Although the majority of myonuclei are generated by 4 dpi and the majority of MuSCs self-renew between 5 dpi and 7 dpi [49], we observed expression of genes characterizing myogenic progenitors including *Pax7*, *Myod1*, and *Myog* in nuclei from 7 dpi mice (Figure 3.2F). Thus, among nuclei obtained at 4 dpi and 7 dpi there is a diversity of myogenic states present, suggesting heterogeneity in the timing of MuSC activation, proliferation, and differentiation following an induced injury (Figure 3.2G).

3.4.3   Pseudotime trajectory of myogenic nuclei during muscle regeneration

MuSC activation, proliferation, and differentiation appear asynchronous, and therefore correlating nuclear transcriptomes with progression through these cell states using a given injury timepoint is impossible (Figure 3.2G). Thus, we applied Moncole3, a tool for inferring pseudotime trajectories from single-cell sequencing experiments, to better understand how aging-specific transcriptional alterations in MuSCs and their progeny affect myonuclear transcription [133, 134]. The Monocle3-inferred UMAP projection contains two major lobes separated by a hinge region and a continuous branched trajectory representing an average path of pseudotime (Figure 3.2A). Nuclei comprising the initiation of pseudotime are situated in the bottom of the left lobe and express high levels of *Pax7* (Figure 3.2B) among other genes (Figure 3.3A-D) identifying quiescent and activated MuSCs [135]. Nuclei in the hinge region bridging the left and right lobes are enriched for *Mymk* expression, a gene required for fusion of mononuclear progenitors (Figure 3.2C) [136]. Mature myosin isoforms encoded by *Myh4*, and other genes expressed in mature muscle are present in the larger right lobe occupying the end of the pseudotime trajectory (Figure 3.2D; Figure 3.3E-
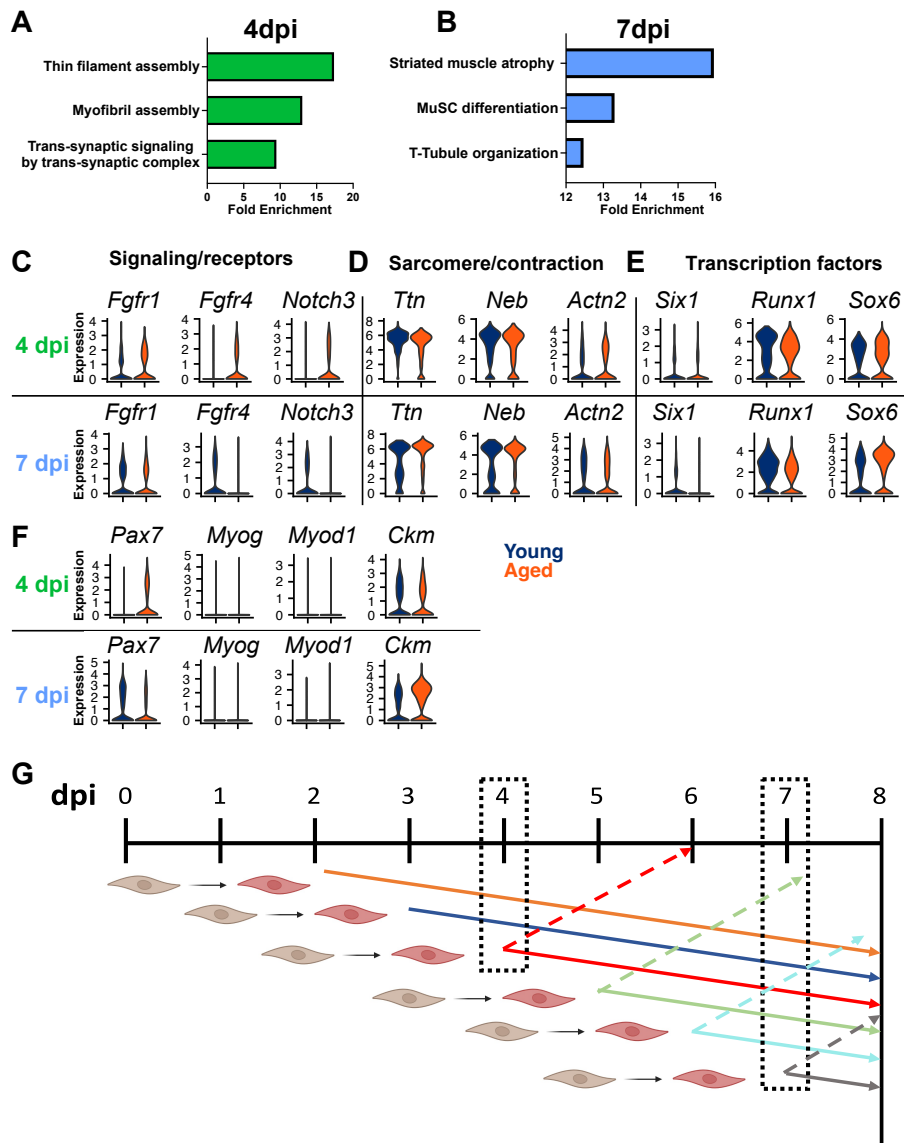
Supplementary Figure 3.2: **GO analysis of nuclei from young and aged mice at 4 dpi and 7 dpi.** (A) Significantly enriched biological pathways identified using the Panther online tool (38, 67) between nuclei from young and aged mice at either 4 dpi and (B) 7 dpi plotted by fold-enrichment. (C) Expression levels of select differentially expressed genes between young (blue) and aged (orange) mouse nuclei at 4 dpi and 7 dpi organized by association with signaling (*Fgfr1*, *Fgfr4*, *Notch3*), (D) genes encoding sarcomeric proteins (*Ttn*, *Neb*, *Actn2*), or (E) transcription factors (*Six1*, *Runx1*, *Sox6*). (F) Relative gene expression levels of *Pax7*, *Myod1*, *Myog* and *Ckm* in myogenic nuclei from 4 dpi and 7 dpi from both young and aged mice. (D) A schematic illustrating asynchronous timing of MuSC activation, proliferation, and differentiation during the first 8 days of muscle regeneration. Vertical axis represents transition of MuSCs from quiescence to differentiation states. See Supplemental Table. S1-S2

G) [20, 42, 126]. Thus, the pseudotime trajectory comprises a comprehensive span of myogenic differentiation beginning with quiescent MuSCs, continuing through progenitor fusion, and ending with myonuclear maturation.

Nuclei from young and aged mice were both included when generating the pseudotime trajectory (Figure 3.2E). Qualitatively, distributions of nuclei from young and aged mice are similar throughout the trajectory, implying the broad transcriptional processes driving myogenic differentiation during skeletal muscle regeneration are largely conserved in aged mice (Figure 3.2E). Nuclei from young mice (Figure 3.2F) and from aged mice (Figure 3.2G) comprising the pseudotime trajectory are derived from uninjured (0 dpi), 4 dpi, and 7 dpi TA muscle (Figure 3.2H). Nuclei from 0 dpi TA muscles occupy the beginning and end of pseudotime, thus relating the transcriptional changes between the initial and final transcriptional states of MuSCs and mature myonuclei, respectively (Figure 3.2I). Indeed, nuclei from 4 dpi mice (Figure 3.2J) and 7 dpi mice (Figure 3.2K) distribute throughout the pseudotime trajectory, bridging populations of quiescent MuSCs to mature myonuclei along a continuous path of myogenic differentiation (Figure 3.2A).

Heterogeneity of 4 dpi and 7 dpi samples is evident from the dispersion of these nuclei across the trajectory, further reinforcing a diversity of myogenic states among nuclei at these timepoints (Figure 3.2G). While the majority of myonuclei are generated within the first 5 dpi, after 5 dpi myonuclear production is reduced [49] and myonuclei are likely undergoing maturation. We identified two distinct groups of 7 dpi myogenic nuclei clustered on either side of the trajectory's hinge region that represents progenitor fusion (Figure 3.2H, K). Expression of *Egfr*, *Mest*, *Itm2a*, *Mgp*, and *Ncoa7*, genes associated with MuSC self-renewal, are enriched in transcriptomes of pre-fusion 7 dpi nuclei from the left lobe when compared to post-fusion 7 dpi nuclei in the right lobe (Figure 3.3H-K; Table S3) [49, 104]. Whereas in the right lobe, myonuclei are enriched for *Myh3* and *Myh8* expression, two myosin isoforms expressed in immature myonuclei during regeneration (Table S3) [40]. Thus, nuclei in the right lobe collected from 7 dpi TA muscles are most likely maturing nascent myonuclei, and the hinge region in the pseudotime trajectory represents commitment of MuSCs to either self-renew or terminally differentiate (Figure 3.2H).
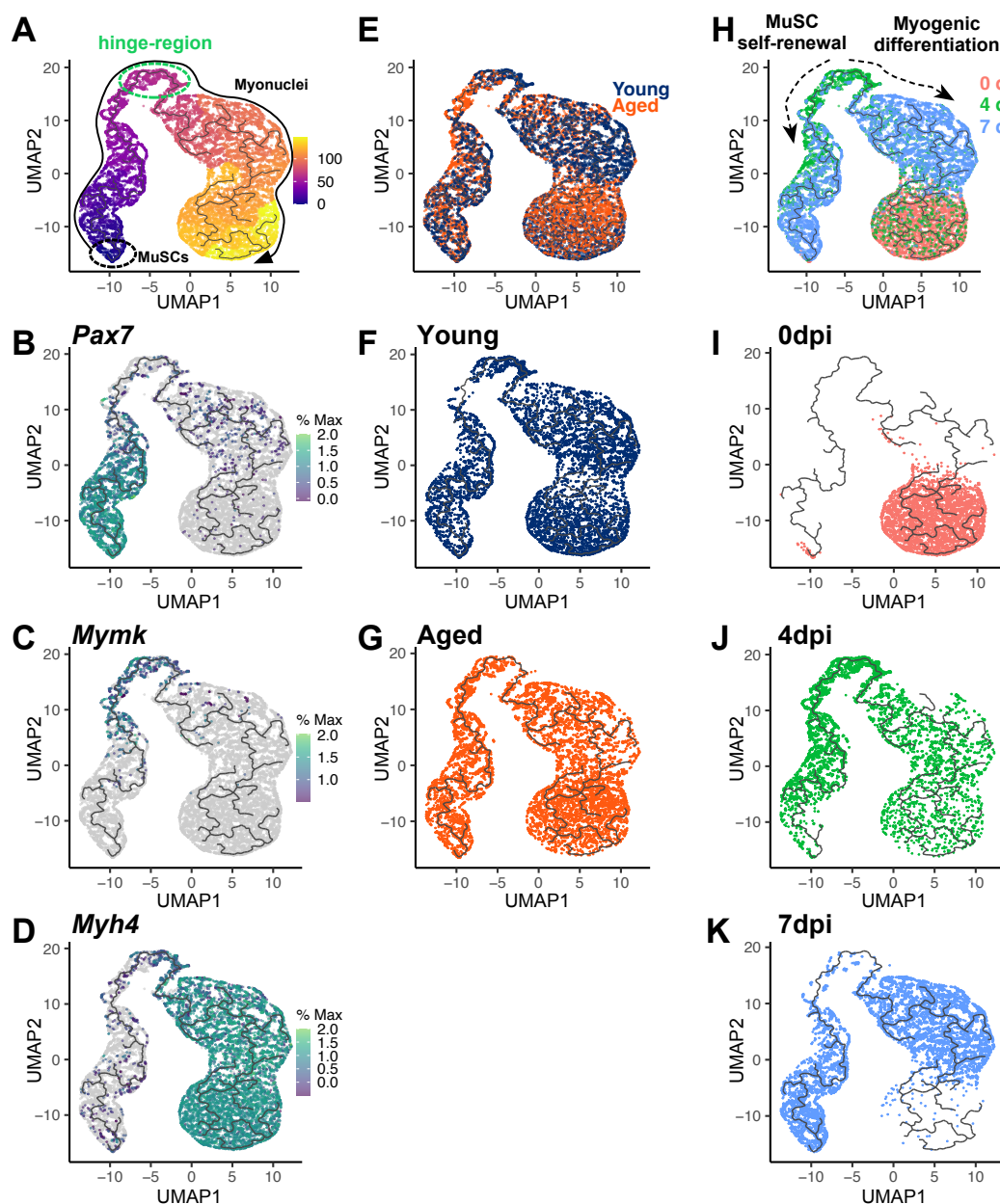
Figure 3.2: **Pseudotime trajectory of myogenic differentiation in young and aged mouse skeletal muscle.** (A) A Monocle-inferred pseudotime trajectory of myogenic nuclei colored by assigned pseudotime value. Arrow represents path of increasing pseudotime. (B-D) Pseudotime trajectory with nuclei colored by gene expression, or (E) by age. Pseudotime trajectory plots comprised of nuclei derived from either (F) young or (G) aged mice. (H) Pseudotime trajectory with nuclei colored by dpi. Two dotted arrows depict an alternative orientation of the trajectory initiating from the hinge region. See Figure 3.1C legend for mouse sample sizes. See also Figure 3.3 and Table S3.
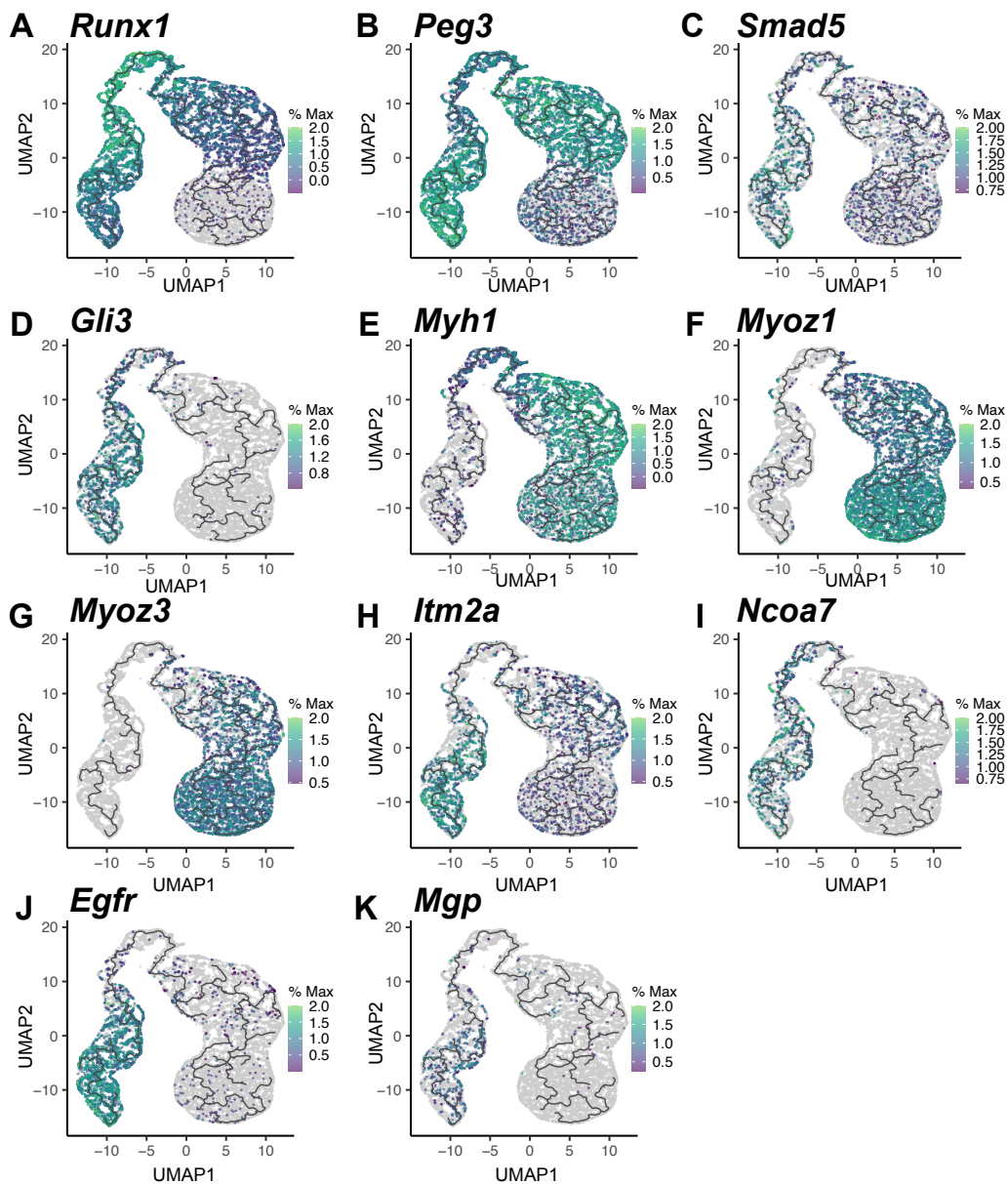
Supplementary Figure 3.3: **Myogenic gene expression plotted within the pseudotime trajectory.** (A) The pseudotime trajectory where nuclei are colored by their expression of transcription factors *Runx*1, (B) *Peg3*, (C) *Smad5*, (D) *Gli3*, (E) mature myonuclear genes *Myh1*, (F) *Myoz1*, (G) *Myoz3*, (H) and genes associated with MuSC self-renewal *Itm2a*, (I) *Ncoa7*, (J) *Egfr*, and (K) *Mgp*. See Figure 3.2 and Supplemental Table. S3.

3.4.4   MuSCs and progenitors have altered gene expression dynamics in aged mice

Dramatic differences in transcriptional states between MuSCs and mature myonuclei may obscure subtle aging-associated differences existing within each population independently. Thus, we partitioned the trajectory into two major branches; Branch 1 (B1), beginning with MuSC nuclei and ending on the distal tip of the hinge region, and Branch 2 (B2), initiating from the hinge region and extending to the end of the myogenic trajectory (Figure 3.4A-E). Nuclei in the hinge region were initially included in both subsets to better anchor each, such that when conducting dimensional reduction, a representative trajectory is inferred for both B1 and B2 (Figure 3.4D-E). An additional subset was generated from B2 nuclei to exclude nuclei in and just after the hinge region, as determined by the point of decreasing *Myh3* and *Myh8* expression and increasing *Myh1* and *Myh4* expression (Figure 3.2D; Figure 3.3E; Figure 3.4F-H). Thus, B1 represents MuSC and myogenic progenitor dynamics through the point of cell fusion, and the B2 myonuclear subset represents post-fusion myonuclei maturing within a syncytial myofiber.

To identify aging-associated changes in transcriptional dynamics, we used Tradeseq, a program for comparing pseudotime trajectories across biological conditions (Figure 3.3A) [137]. Although temporal changes in TF expression between myogenic progenitors isolated from young and aged mice when differentiated in vitro are reported [74, 85, 86], these changes have not been evaluated in vivo. Unlike differential gene expression tests that identify changes in transcript levels, Tradeseq analyses reveal gene expression changes occurring as a function of pseudotime, offering a more relevant strategy to interrogate temporally-resolved transcriptomic data. Tradeseq was used to generate expression trajectories for individual genes expressed within B1 and the B2 myonuclear subset and to conduct statistical tests identifying genes with significantly different pseudotime trajectory patterns between nuclei from young and aged mice (Figure 3.3A). Out of ∼21,000 genes expressed in B1 nuclei, ∼7,000 exhibited differential pseudotime trajectories, while in the B2 subset ∼5,000 genes were detected with differential pseudotime trajectories (Table S4). We selected the 1000 genes with the most significant p-values from B1 as well as the B2 myonuclear subset compar-
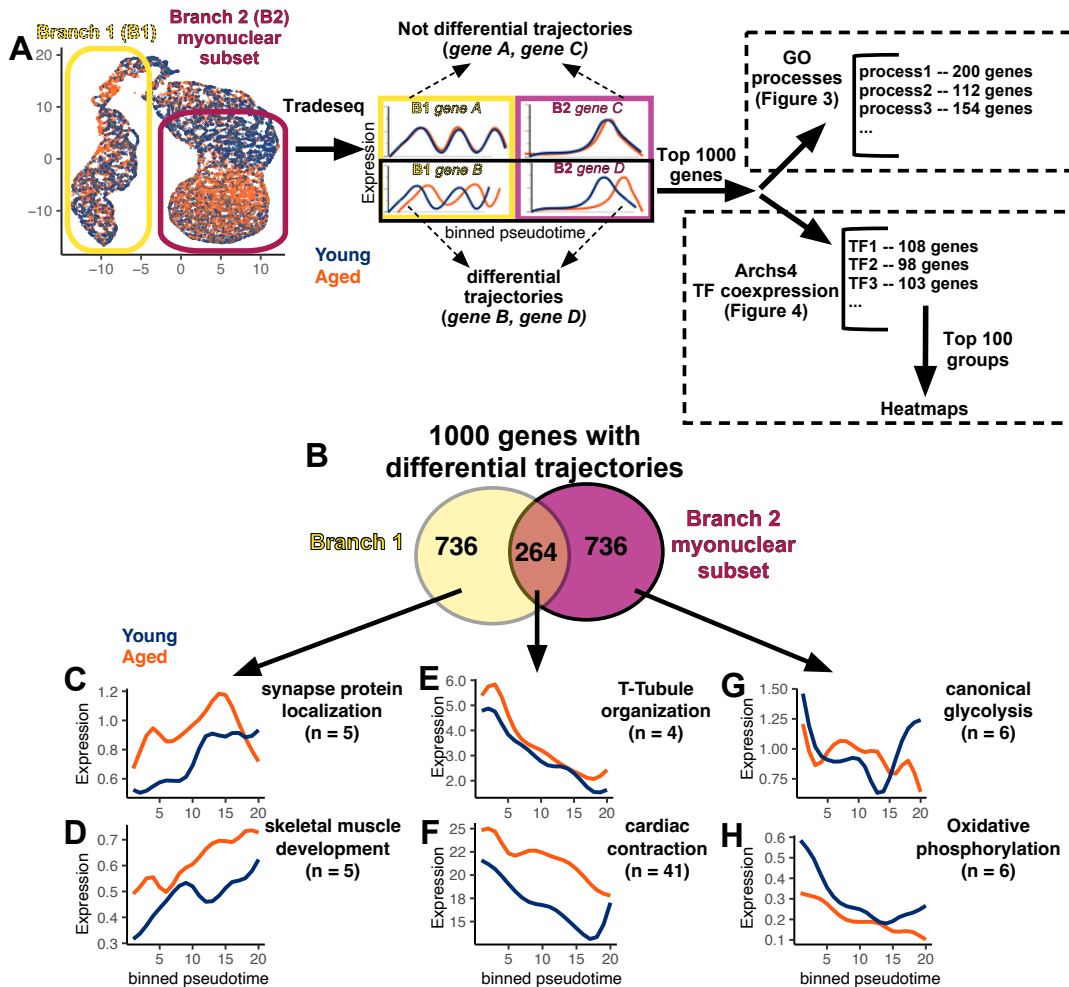
Figure 3.3: **Differences in pseudotime trajectories of genes during early and late myogenesis in regenerating TA muscles.** (A) Analysis pipeline schematic (see Figure 3.4). (B) Venn diagram between top 1000 genes with significantly different pseudotime trajectories from B1 and the B2 myonuclear subset. (C-D) Averaged pseudotime expression plots for genes comprising enriched GO categories from B1-specific genes, (E-F) overlap of B1 and the B2 myonuclear subset genes, and (G-H) B2 myonuclear subset-specific genes. "n" is number of genes averaged in each plot. See also Figure 3.4 and Table S4-S5.
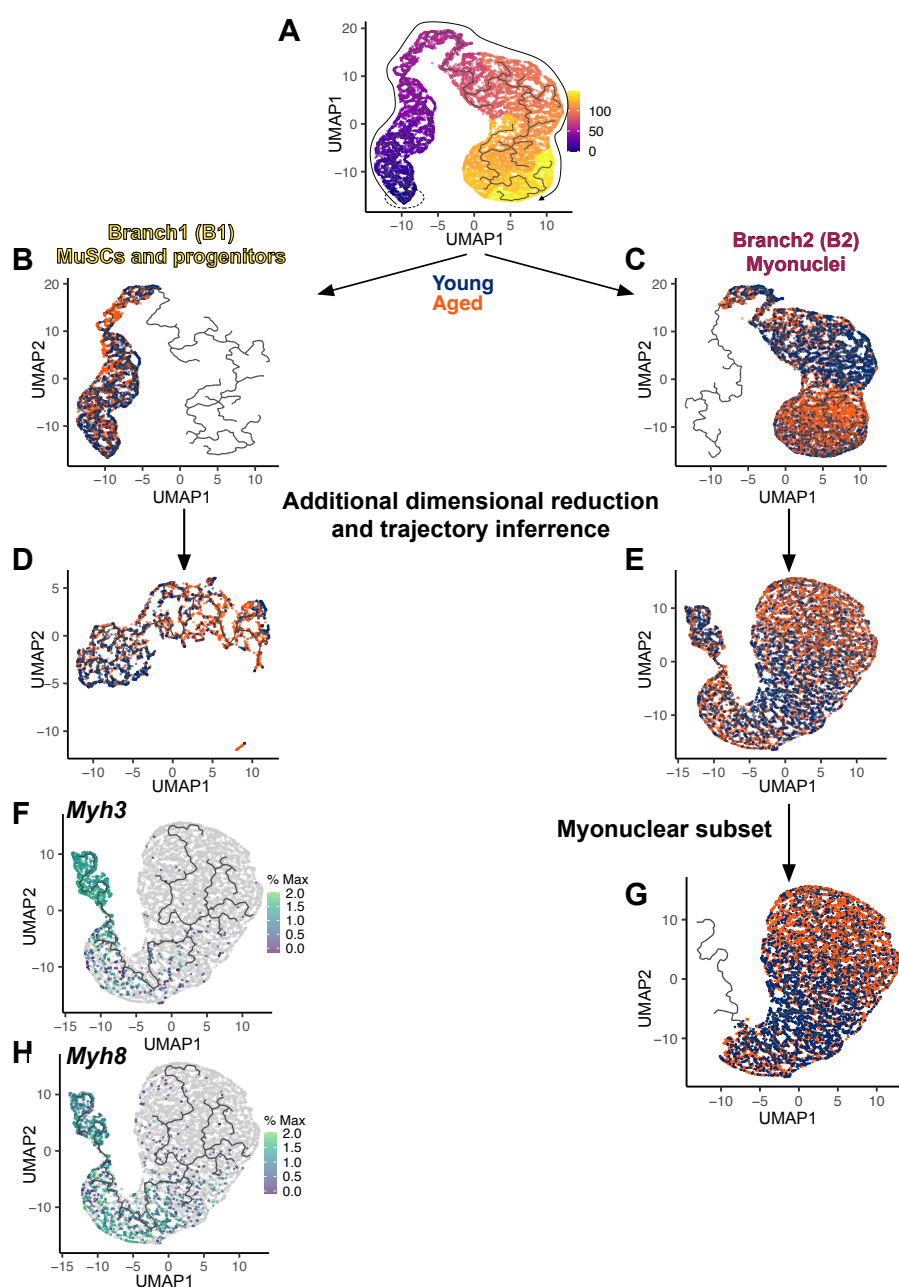
Supplementary Figure 3.4: **Nuclear subsets generated from the complete pseudotime trajectory.** (A) The complete pseudotime trajectory was partitioned into (B) B1 and (C) B2 prior to Tradeseq analysis. (D) B1 and (E) B2 subsets contained nuclei from young (blue) and aged (orange) mice and were re-clustered, and new pseudotime trajectories were inferred separately for each. (G) An additional B2 subset was generated for downstream analyses eliminating the hinge nuclei and containing only maturing myonuclei as judged in part from (F) *Myh3* and (H) *Myh8* expression levels.

isons, restricting our analysis to the most significant aging-associated changes during regeneration. Among these 1000 genes identified from each branch, a group was common to both subsets, surprising considering the disparate processes represented in these respective segments of the myogenic pseudotime trajectory (Figure 3.3B). Among B1-specific genes, GO Processes involving localization of proteins to synapses and myogenic progenitor fusion were detected as exhibiting significantly altered pseudotime in nuclei from aged mice compared to young mice (Figure 3.3C-D; Table S5). Genes with altered pseudotime in nuclei from aged compared to young mice that are common to B1 and B2 are involved in T-tubule organization, myofibril assembly, and NMJ formation (Figure 3.3E-F; Table S5), while metabolic processes including glycolysis and the TCA cycle exhibited the most significant altered pseudotime specific to B2 (Figure 3.3G-H; Table S5). Though the majority of pseudotemporal alterations in gene expression specific to aged mice are unique to either B1 or B2 nuclei, a minority are common to both branches, raising the possibility that alterations in temporal expression of genes in B1 are directly related to the pseudotime changes occurring among nuclei from aged mice in B2.

3.4.5   Genes with altered expression dynamics in aged mice comprise distinct yet overlapping hierarchies between B1 and B2

Cellular transcriptomes organize into distinct gene networks comprised of groups of co-expressed genes involved in common biological processes [138–141]. Ensuring temporally coordinated expression of gene networks during regeneration are myogenic TFs, which in response to specific signals activate or repress gene expression, driving myogenesis. Because of the large number of pathways regulated by myogenic TFs, perturbed gene expression dynamics in MuSCs and progenitors may propagate (by direct and indirect associations) through regulatory hierarchies into later stages of regeneration, affecting transcriptional networks in post-fusion myonuclei. Direct identification of gene networks involved in myogenesis is difficult but can be inferred by genes exhibiting similar temporal- or co-expression patterns with each other and with TFs [138, 141]. If in aged mice temporal regulation of gene networks involved in cell fate transitions and terminal

differentiation of progenitors is altered, myonuclear gene expression and mature muscle function may be impacted.

To identify TFs putatively regulating genes whose expression timing differs in myogenic nuclei between young and aged mice in B1, we mined single-cell RNA-seq datasets using the Archs4_TFs_Coexp database with the 1000 genes exhibiting the most significant aging-associated changes in pseudotime expression dynamics. Querying this database enables the identification of TFs enriched for their co-expression with provided genes [142]. Among the 1000 genes with the most significant aging-associated changes in pseudotime in B1, 334 TFs were enriched, each associated with expression of a gene cohort representing a putative gene network. Predicted co-expressed TFs include critical myogenic regulators *Myf6*, *Myod1*, *Myog*, *Mef2a*, and *Mef2c*, as well as TFs with less well-established roles in myogenesis *Twist1*, *Smad3*, *Snai2*, *Tbx15*, *Nfat5* (Table S6). The 100 most enriched TF-associated gene groups, comprised of ~800 unique genes from the initial 1000 genes used for this analysis, were plotted in a correlation matrix, visualizing the degree of overlap across these TF-associated gene groups (Figure 3.4A). Hierarchical clustering of TF-associated gene groups identified 4 distinct clusters (Figure 3.4A; Table S6). Averaged pseudotime expression patterns of genes comprising the clusters of TF-associated groups were plotted, revealing distinct pseudotime expression patterns associating with each cluster (Figure 3.5A-D). Qualitatively, a total of just 6 trajectory patterns were detected across the 100 TF-associated gene groups comprised of ~800 unique genes represented in the heatmap, suggesting that genes with differential pseudotime trajectories between young and aged mouse nuclei in B1 comprise hierarchical groups associated with myogenesis, each with characteristic pseudotemporal expression patterns (Figure 3.5A-D; Table S6).

Performing TF co-expression analysis on nuclei from B2, we identified 252 TFs enriched as co-expressed (Figure 3.3A; Table S6). The 100 most-enriched TF-associated gene groups predicted from the B2 myonuclear subset were plotted as a heatmap, identifying only a single defined cluster with minimal overlap among most TF-associated gene groups (Figure 3.4B; Table S6). Additionally, a greater diversity of pseudotime expression patterns were observed among the B2 TF-associated
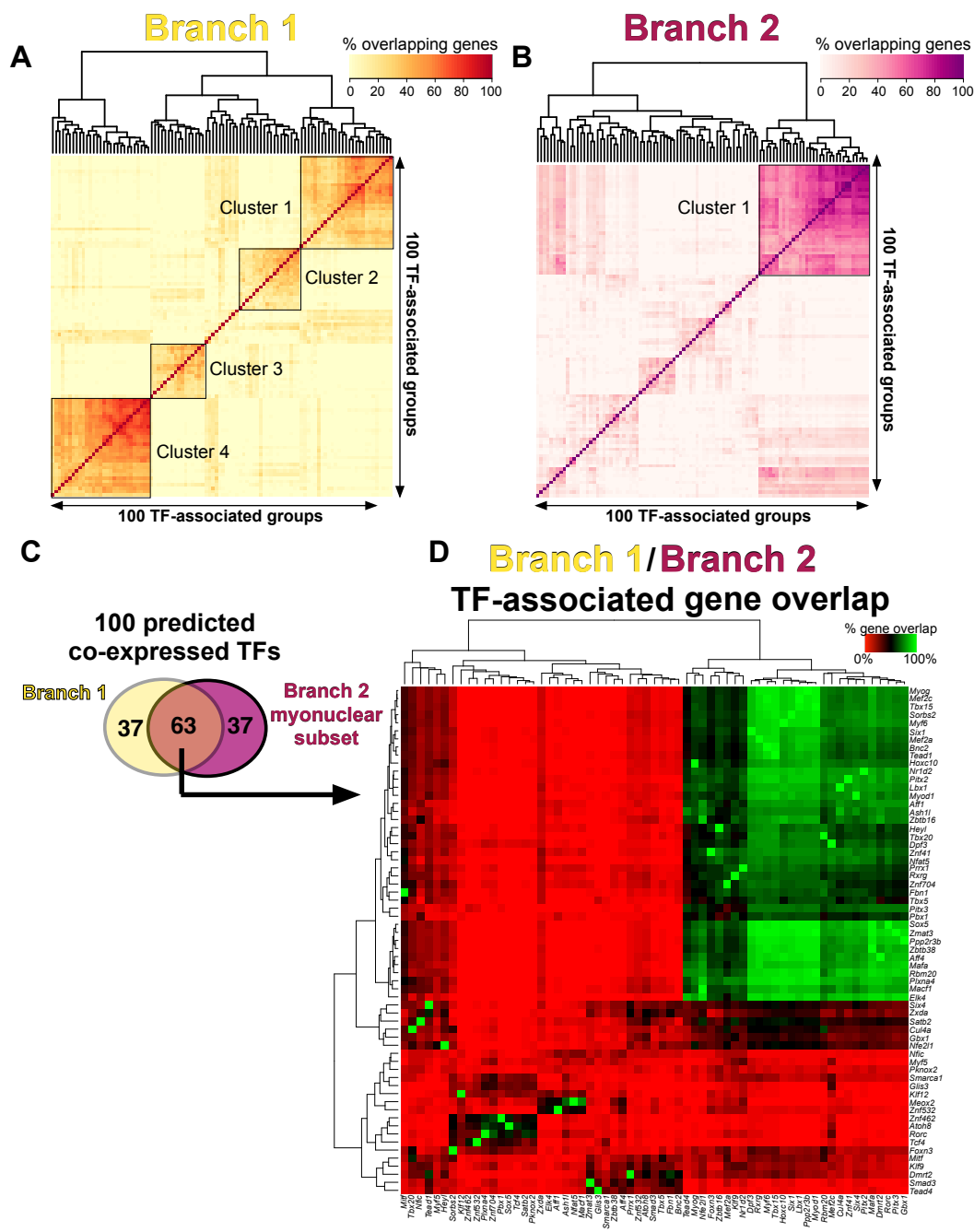
Figure 3.4: **Hierarchical clustering of genes with differential pseudotime between B1 and B2.** (A) Heatmap of 100 most enriched TF-associated groups from B1 genes with differential trajectories in nuclei from aged mice. Rows and columns are TF-associated gene groups, and the heatmap is colored by percent of genes comprising both groups that are shared between them. (B) Analogous heatmap to A, but for TF-associated gene groups identified from the B2 myonuclear subset. (C) Venn diagram depicting overlap of TFs predicted as co-expressed among genes with differential trajectories from either B1 or the B2 myonuclear subset. Overlap was only considered for the 100 groups with the most significant enrichment from each branch. (D) Heatmap of only TF-associated gene groups where the TF was predicted as co-expressed among genes with differential trajectories from both branches. Heatmap is colored by percent of genes overlapping between TF-associated groups from B1 and B2 myonuclear subset predictions. See also Figure 3.5-3.6 and Table S6.
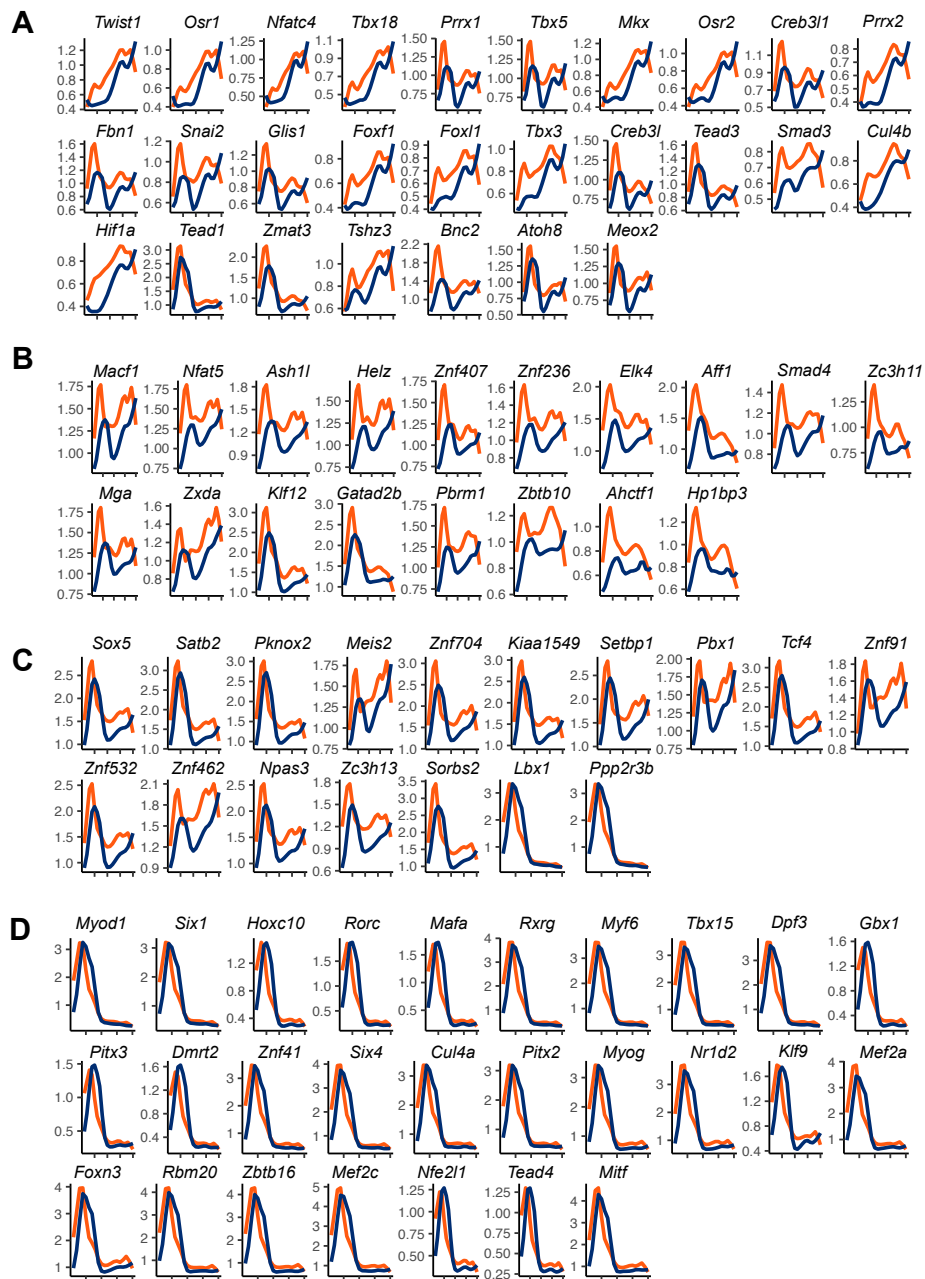
Supplementary Figure 3.5: **Gene expression over pseudotime plots of TF-associated gene groups based on B1 differential trajectory tests.** (A) Expression of genes in young- adult (blue) or aged (orange) mouse nuclei comprising enriched TF-associated gene groups organized by hierarchical order within each cluster from the heatmap in 3.4A; cluster 1, (B) cluster 2, (C) cluster 3, or (D) cluster 4. Each line represents averaged expression over pseudotime of all genes from each group. See Figure 3.4 and Supplemental Table. S6 for TFs represented in each cluster and genes comprising each group.
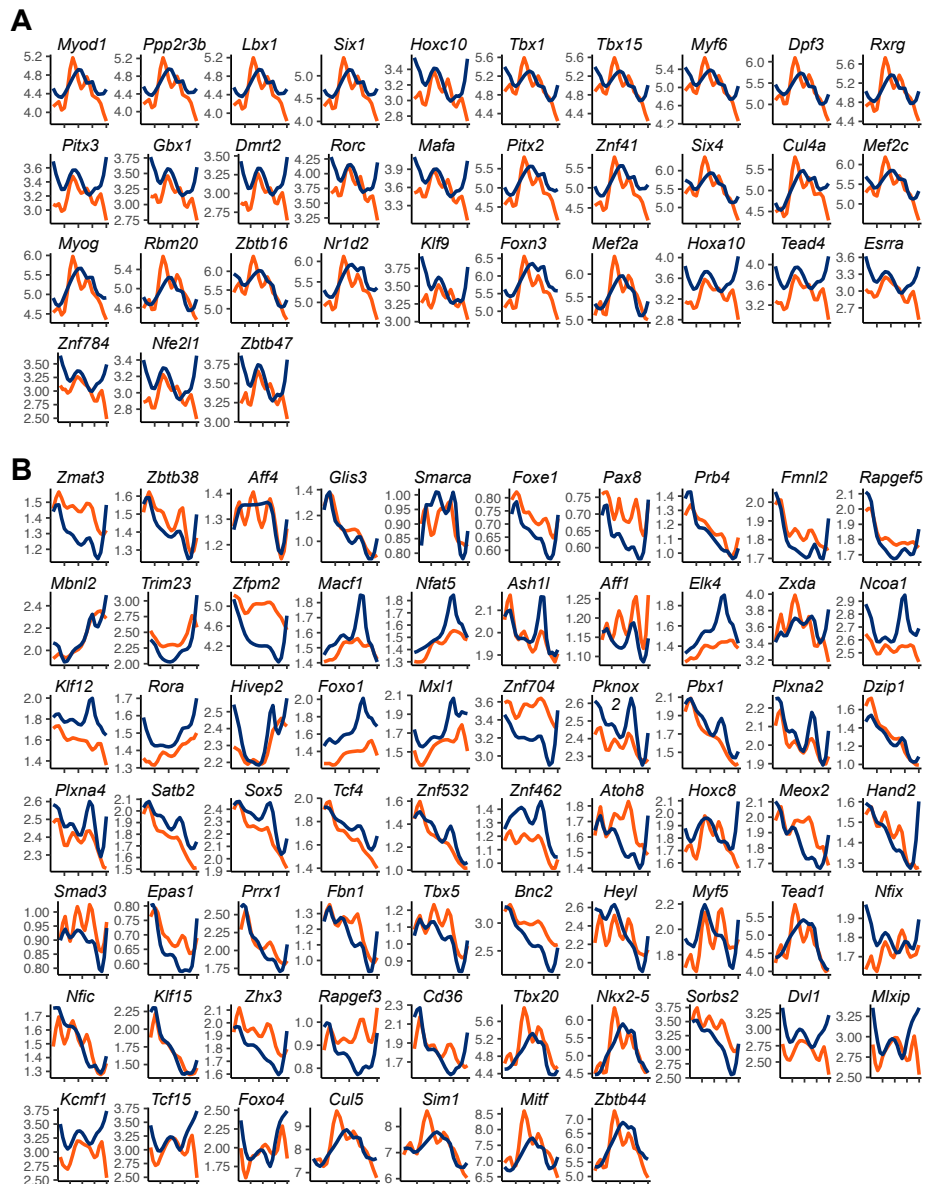
Supplementary Figure 3.6: **Pseudotime expression plots of TF-associated gene groups based on B2 differential trajectory tests.** (A) Expression of genes in young (blue) or aged (orange) mouse nuclei comprising enriched TF-associated gene groups, organized by hierarchical order within each cluster from the heatmap in Figure 3.4B; cluster 1, and (B) all other TF-associated gene groups. Each line represents averaged expression over pseudotime of all genes from each group. See Figure 3.4 and Supplemental Table. S6 for TFs represented in each cluster and genes comprising each group.

gene groups compared to groups identified from B1 (Figure 3.6A-B), suggesting genes with altered pseudotime in B2 myonuclei comprise less defined hierarchies compared to genes expressed in B1. Nevertheless, 63 of the 100 most significant TF predictions from B1 are also present among the 100 most enriched TFs from B2, though the genes comprising these TF-associated gene groups are largely distinct between B1 and B2 (Figure 3.4C-D; Table S6). Common TFs enriched among genes with altered pseudotemporal expression dynamics in both B1 and B2 are thus potential regulators of disrupted gene networks across pre- and post-fusion myogenic nuclei in aged mice. These mutually co-expressed TFs include those critical for myogenesis (*Myf6*, *Myod1*, *Myog*, *Mef2c*, and *Mef2a*), suggesting that though the genes comprising B1 and B2 myogenic gene networks are minimally overlapping, genes with disrupted pseudotemporal expression in aged mice are putatively linked through hierarchical regulatory networks (Figure 3.4D). Thus, during muscle regeneration in aged mice, temporal alterations may propagate from pre-fusion progenitors to post-fusion myonuclei, affecting temporal regulation of interconnected gene networks encoding skeletal muscle structural and metabolic proteins.

3.4.6 Dynamic Time-Warping analysis of myogenic differentiation in young and aged mice

Whether temporal changes in gene expression occurring in aged mice compared to young mice are exacerbated as MuSCs commit to terminal differentiation, fuse, and mature as myonuclei, cannot be inferred from gene network analyses conducted on B1 and B2. To address this question, an integrated analysis that examines aggregate differences between the transcriptomes of nuclei from young and aged mice at different regenerative stages is required. We iteratively subsampled nuclei from the complete pseudotime trajectory (Figure 3.2A), equalizing numbers of nuclei across injury time points, and subjected them to Dynamic Time-Warping (DTW) alignment. DTW is a method that aligns points of two independent time series by locally compressing or expanding time scales for each based on a specified similarity metric, preserving the overall order of each series but not necessarily a one-to-one correspondence of each point along the trajectory [85, 143, 144]

. Euclidean distances based on global nuclear gene expression profiles, rather than on changes to individual gene trajectories, were calculated between nuclei from young and aged mice at different points in pseudotime.
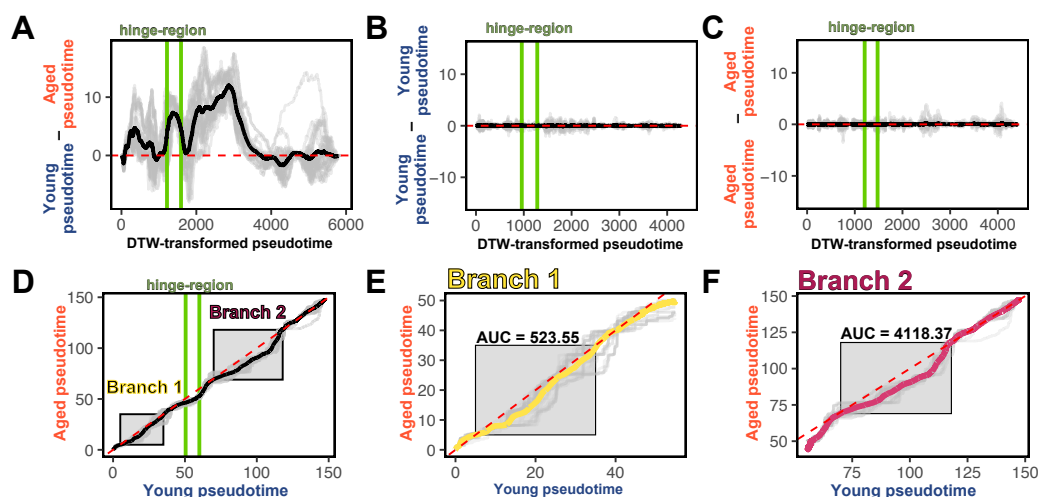
Figure 3.5: **Dynamic Time-Warping analysis of the myogenic trajectory.** (A) Averaged difference of pseudotime values between aligned myogenic nuclei from young and aged mice, and isochronic comparisons between (B) young vs. young and (C) aged vs. aged, along the pseudotime trajectory (See Figure 1C legend for mouse sample sizes). X-axis is the DTW-transformed timescale. Each gray line is a DTW alignment on a single bootstrap (n = 30). Black line is the average of bootstraps. Parallel green lines demarcate the hinge region. Dotted red line depicts theoretical perfect alignment. (D) Pseudotime values for nuclei from young and aged mice plotted by DTW-transformed indices used to generate A-C. Each gray line is a DTW alignment on a single bootstrap. The black line is the average of bootstraps. Red line indicates path of theoretical perfect alignment of the two trajectories. Parallel green lines demarcate the hinge region separating B1 and B2. (E-F) Similar plots to (D) but the B1 and B2 subsets independently. Gray boxes indicate regions with most significant distortions of the aged trajectory used for area under the curve analysis.

We plotted the averaged differences of pseudotime values obtained from subsamples of young and aged-mouse nuclei along each point of the DTW-transformed timescale, revealing predominantly positive deviations of the aged pseudotime trajectory (Figure 3.5A). The magnitude of deviation is smallest in B1 nuclei, larger in the hinge region, and peaks in the middle of B2 (Figure 3.5A). These deviations are specific to comparisons of nuclei from young compared to aged mice,
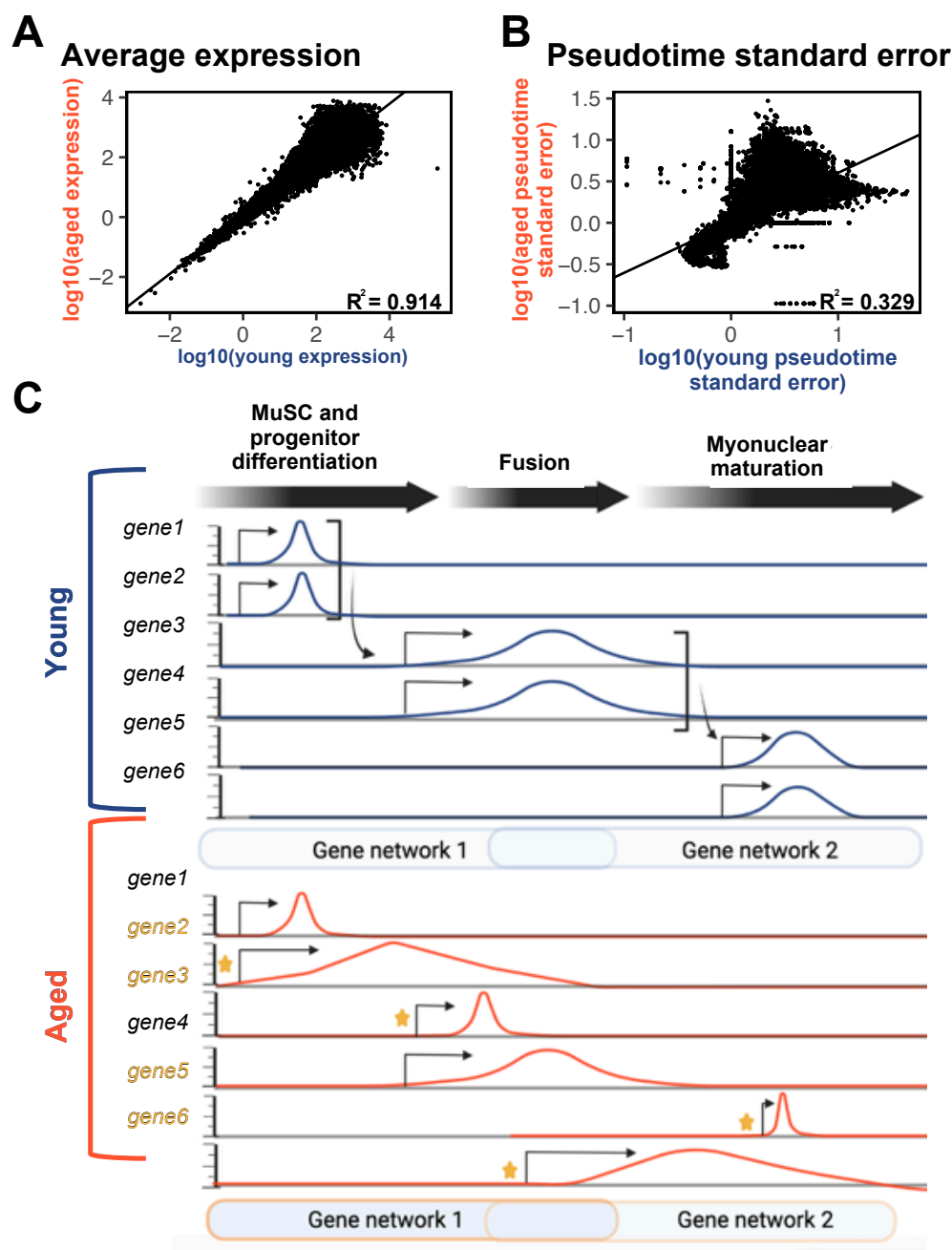
Figure 3.6: **Changes in gene expression pseudotime dynamics are more severe than changes in gene expression levels when comparing myogenic nuclei from aged and young mice.** (A) Scatterplot of average expression values of individual genes with black lines representing perfect correlations and (B) scatterplot of standard error of gene expression across pseudotime of individual genes expressed in myogenic nuclei from either young or aged mice. See Figure 1C legend for mouse sample sizes. (C) A schematic depicting how altered gene expression dynamics propagate through interconnected transcriptional networks during muscle regeneration.

as isochronic (i.e., same-age) comparisons reveal minimal deviations in the pseudotime ordering of nuclei (Figure 3.5B-C).

To quantify the relative magnitudes of aging-associated deviations in pseudotime trajectories associated with B1 and B2, the aligned pseudotime values for young and aged mouse nuclei were plotted against each other and compared to a theoretically perfect alignment of the myogenic trajectories inferred from young and aged mice (Figure 3.5D). Regions of maximal distortion of the trajectory from aged mice within B1 and B2 were identified and a larger area under the curve value was calculated for the B2 segment compared to the B1 segment, demonstrating a distinct increase in magnitude of distortion associated with B2 (Figure 3.5E-F). Thus, independent of sample size differences across injury timepoints, B2, comprised of primarily maturing myonuclei, exhibits more significant aging-associated alterations in the myogenic trajectory compared to the changes occurring in B1 comprised of MuSCs and pre-fusion progenitors.

If temporal processes regulating expression are altered for a given gene, complex downstream effects may ensue that are independent of persistent changes in gene levels. Because differences in both gene expression levels and pseudotime expression dynamics were detected during regeneration when comparing transcriptomes from young and aged mouse nuclei, we asked whether changes in pseudotime were more or less severe compared to changes in gene levels. Plotting the average gene expression levels for all genes expressed in nuclei from young mice against those from aged mice revealed a high correlation ($R^2 = 0.91$) between the two age groups, revealing that the changes occurring in gene expression levels are discriminatory rather than global in aged mice (Figure 3.6A). In contrast, there was poor correlation ($R^2 = 0.329$) when plotting the standard error of gene expression across pseudotime for nuclei from young mice against those from aged mice (Figure 3.6B).

3.4.7   Discussion

Gene networks involved in related biological processes require coordinated temporal control of gene expression [138, 139, 141, 145]. Altering gene expression dynamics regulating these networks

may interfere with complex cell fate transitions required for progenitor cells to differentiate and acquire transcriptional states necessary for organ- and tissue-specific functions. During skeletal muscle regeneration, aging-associated changes in gene expression dynamics are exacerbated during MuSC differentiation *in vitro* [85, 86]. However, differentiation in culture is not representative of regeneration *in vivo* where transcriptional states associated with mature myonuclei are never attained [42, 74, 85, 86, 120].

We compared changes in timing of gene expression *in vivo* through pseudotime analysis of myogenic nuclei sequenced from regenerating skeletal muscle between aged and young mice. This analysis revealed that the genes exhibiting the largest changes in pseudotemporal expression trajectories appear to comprise distinct transcriptional networks involved in progenitor proliferation, innervation, and metabolic pathways conferring myofiber contractile speeds [8, 71, 146]. However, aging effects transcriptomes globally [69], thus we employed DTW analysis, which enabled us to quantify the aggregate differences in global gene expression dynamics rather than focus on specific pathways. We identified that specific segments of the pseudotime trajectory exhibit larger aging-associated differences than others, where peak differences appear in three discrete waves, each associated with a distinct stage of myogenesis. The first wave occurs in the middle of B1, where myogenic progenitors are balancing opposing cell-fate choices to terminally differentiate or self-renew. The second wave of distorted pseudotime, which is larger than the first, occurs in the hinge region where myogenic cells fuse. The final and largest wave of age-distorted pseudotime is observed in myonuclei following fusion, where the transcriptional changes driving myonuclear maturation occur.

During regeneration of skeletal muscle, temporal regulation of gene networks is necessary to repair muscle and re-acquire muscle function. In aged mice the timing for gene networks driving myogenesis and muscle maturation diverges from that in young mice and worsens as regeneration proceeds, potentially propagating through interconnected gene networks associated with expression of mature muscle genes (Figure 3.6C). Although we have not identified mechanistic details, our data support that alterations in temporal coordination of gene expression in myogenic networks

contributes to defects in muscle regeneration and to declining muscle function in aged organisms. Comprehensive analyses of the mechanisms underlying mistimed gene expression during regeneration in aged-mouse skeletal muscle will require future follow-up studies that are currently impractical, requiring temporally altering the expression of large numbers of genes in combination with each other to test the effects on muscle regeneration in young mice. The temporal alterations we observed in gene networks involved in myogenesis provide a novel insight for aging research to base future mechanistic studies where altered temporal coordination of myogenic gene expression as well as changes in the expression levels of specific transcripts contribute to impaired muscle regeneration and declining muscle function in aging organisms.

3.5   Methods

3.5.1   Mice

Mice were bred and housed according to National Institutes of Health (NIH) guidelines for the ethical treatment of animals in a pathogen-free facility at the University of Colorado at Boulder. University of Colorado Institutional Animal Care and Use Committee (IACUC) approved animal protocols and procedures. Young mice were C57B6 mice, (Jackson Labs Stock No. 000664) between 4 and 8 months old and were a mix of male and female. The aged mice used were F1 mice from a C57BL/6J and DBA/2J cross (Jackson Labs No. 100006), collected between 24-28 months old and a mix of male and female. For injuries, mice were anesthetized with 3% isofluorane followed by injection with 50μL of 1.2% BaCl2 into the left TA and EDL muscle.

3.5.2   EdU labeling and injuries

Mice were anesthetized with isofluorane followed by injected with 50μL of 1.2% $BaCl_2$ into the left TA and EDL muscle. To deliver EdU, mice were given IP injections of 10mM EdU (Carbosynth) (Chehrehasa et al., 2009), re-suspended in water, a volume of 100μL per 25g mouse weight.

3.5.3   Immunofluorescence staining of tissue section

The TA muscle was dissected, fixed for 2h on ice cold 4% paraformaldehyde, and then trans-ferred to PBS with 30% sucrose at 4°C overnight. Muscle was mounted in O.C.T. (Tissue- Tek®) and cryo-sectioning was performed on a Leica cryostat to generate 10uM sections. Tissues and sections were stored at -80°C until staining. Tissue sections were post-fixed in 4% paraformalde-hyde for 10 minutes at room temperature and washed three times for 5 min in PBS. To detect Pax7 on muscle sections we employed heat-induced antigen retrieval. Post-fixed sections on slides were placed in a citrate buffer (100mM Sodium citrate containing 0.05% Tween20 at pH 6.0) and subjected to 6 min of high pressure- cooking in a Cuisinart model CPC- 600 pressure cooker. For immunostaining, tissue sections were permeabilized with 0.5% Triton- X100 (Sigma) in PBS con-taining 3% bovine serum albumin (Sigma) for 30 min at room temperature. EdU was visualized following manufacturers guidelines (ThermoFisher Scientific cat#C10337). Primary antibodies in-cluded anti- PAX7 (DSHB) at 2 μg/mL and rabbit anti-laminin (Sigma-Aldrich cat#L9393) at 2.5 μg/mL incubated on muscle sections for 1h at room temperature. Alexa secondary antibodies, donkey anti mouse Alexa Flour 647, donkey anti-rabbit Alexa Flour 555 (ThermoFisher) were used at a 1:750 dilution and incubated with muscle sections for 1 h at room temperature. Prior to mounting, muscle sections were incubated with 1μg/mL DAPI for 10 min at room temperature then mounted in Mowiol supplemented with DABCO (Sigma-Aldrich) as an anti-fade agent.

3.5.4   Microscopy and image analysis

All images were captured on a Nikon inverted spinning disk confocal microscope. Nikon objectives used were: 10x/0.45NA Plan Apo and 20x/0.75NA Plan Apo Images were processed using Fiji ImageJ. Confocal stacks were projected as maximum intensity images for each channel and merged into a single image. Brightness and contrast were adjusted for the entire image as necessary. PAX7 and EdU quantification Statistical tests were performed on PAX7 quantified cells per mm2 for N = 3 young and N = 3 aged mice in Prism (GraphPad). Significance was assessed

using two-tailed unpaired Student's t-test with two-stage step-up method of Benjamini, Krieger, and Yekutieli multiple comparison adjustment with a q < 0.05 considered significant. Each N was generated from an individual mouse.

3.5.5   Nuclear Isolation, 10x genomics, and sequencing

Protocol for nuclear isolation was similar to described previously (Cutler et al., 2017). In short, 2x replicates were done for both young and aged mice at 0 dpi and 7 dpi. We conducted 3x replicates for aged mice at 4 dpi and 2x replicates for young mice at 4 dpi. TA muscles were isolated from uninjured (0 dpi), 4 dpi, and 7 dpi young and aged mice and minced with razor blades prior to mechanical homogenization. Nuclei were filtered (70uM filter), and then separated along a sucrose gradient with differential centrifugation (33,000rpm for 3hrs at 4C), and the interface containing single nuclei (between 2.8M and 2.1M sucrose) were collected by pipette. Nuclei were pelleted (2000g for 10mins at 4C), resuspended in PBS, and stained with DAPI to assess nuclear purity. Homogenization times and intensity, and sucrose gradient concentrations were optimized to maximize nuclear numbers and purity. Nuclear concentrations and purity were further evaluated using the Agilent 2200 TapeStation system (G2964AA) with the High Sensitivity D1000 ScreenTape (5067-5584). We used the Next GEM Single Cell 3' v3.1 system and protocol as described. Between 1,600 and 8,000 nuclei were added to each GEM and each sample was sequenced on either an Illumina Nextseq500 or Novaseq6000 to an estimated depth of 300 million reads.

3.5.6   Software Packages

- Cellranger Software Suite/3.0.1 - FastQC 0.11.8 - R 4.1.1 - Seurat 4.1.1 - monocle3 1.0.0 - DoubletFinder 2.0.3 - SoupX 1.5.2 - Tradeseq 1.7.7 - DTWpython

3.5.7   Quality control, read alignment, and expression quantification

To assess the quality of Fastq files from sequencing, FastQC was used, evaluating depth and quality of each replicate. Cellranger was then used to process Fastq files and aggregate tech-

nical replicates, creating gene-count matrices for each sequencing experiment. For transcriptome alignment, a custom pre-mRNA mm10 reference package was used as previously described [20,147].

3.5.8 Accounting for experimental noise and doublets

Cellranger-aligned feature matrices were then loaded into R using the load10X() function from SoupX. Ambient RNA contamination was predicted using default settings of autoEstCont() and counts were normalized to an estimated noise parameter using adjustcounts(). Doublet contamination was evaluated using the R package DoubletFinder (McGinnis et al., 2019). pK parameter optimization was conducted for each replicate. Doublet threshold was set to 10% and a pN of 0.25. Inferred doublets were removed prior to conducting UMAP dimensional reduction in Seurat.

3.5.9 Normalization, dimensional reduction, and nuclear clustering

The tutorial provided by the Mayaan lab was used to guide data normalization (`satijalab.org/seurat/articles/pbmc3k_tutorial`). Mitochondria and low-quality nuclei were removed. Seurat objects were then passed through NormalizeData(), FindVariableFeatures(), ScaleData() to scale and log normalize gene counts within each sample. Data were then integrated using the FindIntegrationAnchors() and IntegrateData() functions in Seurat using the reciprocal PCA (rPCA) algorithim. The integrated Seurat object was then transformed using SCTransform() and the "glmGamPoi" method, before conducting

dimensional reduction using UMAP and clustering using the shared nearest neighbor (SNN) modularity optimization based clustering algorithm, adjusting the minimum number of neighbors, minimum distance, and resolution parameters to achieve adequate separation of nuclear clusters [148]. Identification of nuclear clusters was done manually, using differential gene expression from the FindMarkers() function between clusters combined with manual literature curation. The Myoatlas database and webtool (research.cchmc.org/myoatlas/) was of particular help in identifying clusters of nuclei [20].

3.5.10   Pseudotime trajectory inference

For trajectory inference, a tutorial to generate pseudotime trajectories from Seurat objects was used as a guide (cole-trapnell-lab.github.io/monocle3/docs/trajectories/). Briefly, inputting only myogenic subset of nuclei, gene matrices were first scaled and normalized using preprocess_cds() and batch corrected across individual mice using align_cds() to account for technical variability across experiments. (Haghverdi et al., 2018; Qiu et al., 2017; Trapnell et al., 2014). For UMAP projection, the minimum number of neighbors and minimum distance parameters were adjusted to achieve optimal reduction. For clustering with cluster_cells(), the k parameter was modulated, preventing over- or under-fitting trajectory tree inference using learn_graph().

3.5.11   Differential expression tests

Differential gene expression was assessed by the Wilcoxon Rank Sum Test in the Seurat FindMarkers() function. Genes were assessed as significant with an adjusted p-value < 0.05.

3.5.12   Tradeseq analysis and differential trajectory tests

Tradeseq was installed directly from the github repository "statOmics/tradeseq". The tutorial associated with this repository (statomics.github.io/tradeSeq/articles/tradeSeq) was used as a guide. In short, smoothed gene expression curves were calculated for individual genes using the fitGAM() function, which fits each genes' expression over pseudotime to a negative binomial distribution. The knots parameter was set to 10. For each nuclear subset analyzed (B1 or the B2 myonuclear subset), curves were inferred for genes normalized to only nuclei within the same subset, ensuring accurate representations of a genes' pseudotime expression distribution specific to each subset. The Tradeseq package offers multiple tests for evaluating differences in pseudotime trajectories between two groups. Based on their descriptions, the PatternTest() was chosen as the test most relevant for our analyses. The PatternTest() function ranks genes with a p-value and a Wald statistic. The top 1000 genes with the largest Wald statistic were selected for GO analyses (see next section).

3.5.13 GO analyses and TF-associated group identification using a coexpression database

GO analyses identifying differentially expressed genes were conducted using Panther [129, 149]. A background gene set was used comprising all genes expressed in myogenic nuclei detected from sequencing. GO Biological Processes Complete hierarchy was used to organize results. Example categories in figures were chosen as contained within ranked clusters. Json files were then downloaded, and individual Tradeseq-generated smoothed expression curves for genes comprising each category group were used for plotted. The Archs4_TF_coexpression database was queried using the Enrichr webtool [142, 150]. This tool enables querying existing single-cell sequencing experiments to detect whether inputted genes are enriched for their co-expression with TFs across a collection of single-cell experiments.

3.5.14 Hierarchical clustering of TF-associated gene groups (correlation matrix)

From the top 100 most enriched TF-associated gene groups, a matrix was constructed where the overlap was determined as the percent of unique genes comprising both groups that are shared between each group. Hierarchical clustering of this matrix was conducted using the default settings for heatmap.2() function in R, using Euclidean distances and the complete agglomeration method for clustering. Dynamic Time-Warping (DTW) analysis DTW is a method for aligning the data points of two independent time series by locally compressing or expanding the scales for both time series based on the comparison between the time series of some relevant metric. This process preserves the order of each time series, but not necessarily a one-to-one correspondence of the data points between them. In our case the independent time series for young and aged myogenic nuclear populations was derived from the pseudotime analysis. The metric for comparison was the Euclidean distance between the global gene expression profiles for each individual nuclei. To generate each young and aged mouse time series to which we would apply DTW, we first needed to subsample the nuclei of each injury timepoint to equal number, across all dpi. This was done to

account for the technical bias that would result from unequal tissue sample sizes from each animal, which would result in an over/under representation of nuclei for that timepoint based on the size of the tissue sample. Instead, the relevant comparison to make is between the distributions of nuclei across the injury timepoints that comprise the transcription trajectory, which could be achieved by equally subsampling the nuclei to equal number, prior to applying DTW. One key assumption inherent to DTW that also needed to be accounted for is that the starting and ending points of each time series correspond to one another. In our case, we conformed to this assumption by constructing our pseudotime series from cell populations that start from MuSCs and end in mature myonuclei for both young and aged mice. This way we can assume, that nuclear populations from both young and aged mice are in the same transcriptional states at the start and end of the trajectories, which conforms with the assumed alignment of the first and last points of the two trajectories by the DTW algorithm. We used the fastdtw (v0.3.4) Python package implementation of the DTW algorithm to perform our analysis (see supplemental for code) and used Euclidean distance as our metric for the cell comparison. We also tried the common cosine distance metric to check the robustness of our alignments, which showed comparable results. Also results reported herein are computed using the Euclidean metric. In order to estimate the variation in the alignment of our trajectories, we performed DTW on 30 independent random subsamples (with replacement). For each subsampled trajectory, $\sim$1,500 nuclei were sampled from each of the 0 dpi, 4 dpi, and 7 dpi timepoints. We calculated an average trajectory from the 30 trajectories. Both the average trajectory and the distribution of the individual trajectories can be seen in Figure. 3.5A-D.

<center>Chapter 4</center>

<center>Reversing cell-intrinsic MuSC aging defects does not improve skeletal muscle aging</center>

4.1   Chapter note

This project was developed by a post-doctorate researcher in the Olwin lab, Dr. Alicia Cutler. Dr. Cutler conducted all wet-lab experiments, including generation of scRNA-seq and snRNA-seq datasets. My contribution to this project was the analysis and interpretation of single-cell sequencing experiment conducted by Dr. Cutler that comprise Figure 4.2 and Supplemental Figure 4.2 in this chapter.

4.2   Abstract

With an increasingly elderly world population, understanding and reducing aging associated frailty derived from reduced muscle function is necessary to increase healthspan. Cell intrinsic defects in muscle stem cells, or satellite cells, make them less able to maintain and repair skeletal muscle in aged individuals. Reversing the cell intrinsic aging phenotype of muscle stem cells could potentially ameliorate decreased muscle function in muscle of aged individuals. A drug inducible FGF receptor 1 (FGFR1) rescues muscle stem cell aging deficits in vitro. We bred mice to express a constitutively active FGFR1 (caFGFR1) specifically in muscle stem cells to test whether caFGFR1 expression improved muscle stem cells and skeletal muscle in vivo. While caFGFR1 expression was sufficient to rescue cell intrinsic aging defects, the rejuvenated muscle stem cells did not affect a broader improvement of skeletal muscle morphology or regeneration. Our findings emphasize the

need to approach skeletal muscle aging as a complex multifactorial process in need of multifaceted interventions.

4.3   Introduction

Skeletal muscle mass, function, and regenerative capacity decline with age, which in elderly individuals increases frailty, decreases ambulation, and increases morbidity [151–154]. By 2050 20% of the world population will be over the age of 60 [146] costing an enormous amount in associated health care. Increasing health span and quality of life for the elderly by ameliorating or slowing aging related muscle declines will dramatically decrease societal burden and health costs associated with our increasingly aging population.

Skeletal muscle in elderly individuals is less capable of regeneration at least in part due to cell intrinsic aging defects in the resident muscle stem cells (MuSC) or satellite cells. Muscle from old individuals contains fewer MuSCs than that from in younger individuals and the MuSCs that are present have inherently reduced regenerative capacity [155, 156], undergo a lower percentage of self-renewing asymmetric divisions [74, 156], and undergo increased in spontaneous premature differentiation [8,74]. Although exposing aged muscle to a young environment improves regeneration [76, 157], transplantation of MuSC from aged muscle into a young environment does not rescue MuSC function, indicating cell intrinsic aging defects [74]. These cell intrinsic MuSCs compromise myofiber maintenance and regeneration, reversing these deficiencies in MuSCs could allow them to repair myofibers improving muscle aging phenotypes.

These aging- associated MuSC defects coincide with reduced MuSC reactivity to extracellular signaling, including Fibroblast Growth Factor (FGF) signaling [8, 52, 74–80, 82]. MuSCs express predominantly FGF receptor 1 (FGFR1) with moderate levels of FGFR4 and low levels of FGFR2 and FGFR3 [107, 158]. A drug inducible FGF receptor 1 (FGFR1) in MuSCs partially rescues self-renewal in MuSCs from aged mice and rescues engraftment of MuSCs transplanted from aged mice to young mouse [74].Similarly, activating ß1-integrin, a cell surface protein which cooperates with FGF ligands in FGF signaling, improves FGF signaling in muscle of aged mice and rescues

myofiber size and strength in a mouse model of Duchenne's muscular dystrophy [79]. Together these findings suggest that activating FGF signaling in MuSC *in vivo* will rescue muscle aging phenotypes.

4.4 Results

4.4.1 Generation of inducible caFGFR1 mice

Mice were bred to temporally and spatially express a constitutively active FGFR1 (caFGFR1) [159] (Figure 4.1A) where the caFGFR1 transgene is a chimeric receptor consisting of the mutant FGFR3c(R248C) extracellular and transmembrane domains [160] fused to the intracellular FGFR1 tyrosine kinase domain with a C-terminal MYC epitope tag [31, 161]. To determine the efficiency of the genetic system including three transgenes, Pax7CreERT2; LSL-rtTA; tetO:caFGFR+ (caFGFR1+) mice and $Pax7^{CreERT2}$; LSL-rtTA; tetO:caFGFR1- (caFGFR1-) mice were treated with tamoxifen and fed doxycycline-containing chow for 5 days, myoblasts isolated and cultured in the presence or absence of doxycycline. The myoblasts were fixed, stained for DAPI and scored for immunoreactivity for PAX7, MYC, and FGFR3, which is not expressed in SCs or their progeny [20] (Figure. 4.11B). In caFGFR1+ cultures with doxycycline, 58% of the PAX7+ cells are immunoreactive for MYC or FGFR3 (Figure 4.1C). We further tested whether caFGFR1 expression was temporally responsive by treating caFGFR1+ mice with tamoxifen and then a combination of doxycycline or vehicle *in vivo* and *in vitro*. While *Gapdh* transcripts were detectable by RTPCR under all conditions MuSCs maintain transgene expression only in the presence of doxycycline as SCs isolated and cultured from mice fed doxycycline chow express caFGFR1 only if doxycycline is provided in the culture media (Figure 4.1D). Thus, caFGFR1 transgene expression is reversible and changes observed upon expression of the receptor are the result of the activated receptor.

If intracellular signaling in myoblasts isolated from caFGFR+ mice1 signaling replace smimics effects of FGF-2 addition to the media, then the recombined MuSCs should be less unresponsive to added FGF-2. MuSCs explanted from recombined caFGFR1+ and caFGFR1- mice were cul-

tured in the presence and absence of doxycycline and with or without FGF-2, followed by EdU addition 2 hours prior to fixing and staining for immunoreactivity to PAX7 and ClickIT chemistry for EdU (Figure 4.1E). Addition of FGF-2 to either caFGFR1+ or caFGFR1- cultures yields ~75% PAX7+/EdU+ cells and addition of FGF-2 and doxycycline to caFGFR1+ cultures does not increase the percent of PAX7+/EdU+ cells compared to FGF-2 addition alone (Figure 4.1E). Activation of FGFR1 signaling replaces mimics FGF-2 addition in recombined cells and thus, we asked if activated caFGFR1 would partially restore age-related losses of FGF signaling.

MuSCs isolated from aged mice are less proliferative and differentiate prematurely compared to MuSCs isolated from young mice, in part due to loss of FGF responsiveness [74, 79]. Similarly, MuSCs from aged mice are less resilient in response to stress. Primary myoblasts isolated from 24-month-old caFGFR1+ mice were cultured in high serum growth media with or without doxycycline, followed by a 2hr pulse of EdU (Figure 4.1F). Proliferating MuSCs were increased 3-fold by doxycycline addition, which also reduced differentiation by 4-fold compared to MuSCs cultured with with vehicle only demonstrating caFGFR1 expression rescues age-associated proliferation deficits and prevents age-associated premature differentiation (Figure 4.1G-H). In low serum FGF-2 maintains explanted SCs from young mice in a quiescent, undifferentiated state and re-introducing serum promotes cell cycle re-entry, while explanted SCs from aged mice prematurely differentiate [74]. We induced a reserve/quiescent state by reducing serum and then assessed the ability of the reserve cells to re-enter the cell cycle upon reintroduction of high serum growth media (Figure 4.1I) [74, 162]. Less than 3% of the SCs from caFGFR1- mice were reentered the cell cycle upon serum restoration, while 8-fold more caFGFR1+ SCs reentered the cell cycle 24h after reintroducing serum (Figure 4.1J). SCs expressing caFGFR1 cultured in low serum differentiation media with doxycycline or vehicle (Figure 4.1K) were equally capable of differentiating as the percent of myonuclei in myosin positive cells were statistically indistinguishable (Figure 4.1L). Thus, signaling from caFGFR1, which rescues cell intrinsic MuSC aging phenotypes does not prevent MuSCs from differentiating.
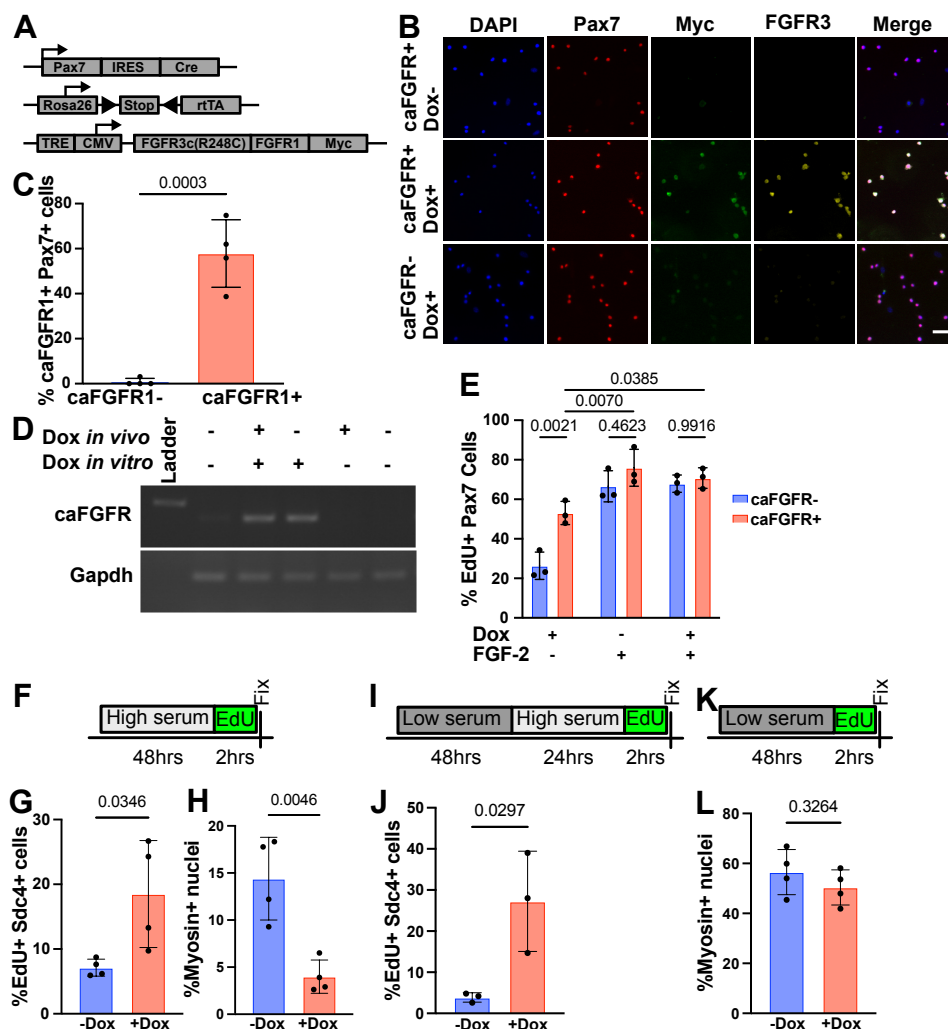
Figure 4.1: **caFGFR1 expression.** (A) Schematic of caFGFR1 mouse genetics (B) Immunofluorescence images of MuSCs isolated from caFGFR1+ and caFGFR1- mice treated with doxycycline or vehicle and tested for immunoreactivity to Pax7 (MuSC marker), Myc, and FGFR3. Bar=50 um C) Quantification of percentage of *Pax7+* cells positive for FGFR3 (n=4 primary myoblast isolates from young mice) comparison by t-test. D) RTPCR gels of transcripts isolated from caFGFR1+ cells treated with doxycycline in vivo and/or in vitro. Primers to the chimeric caFGFR1 transcript or GAPDH were provided. E) Quantification of precent EdU positive Pax7 cells treated with doxycycline (Dox) FGF-2 or both. n=3 primary myoblast isolates from young mice comparison by one-way ANOVA. (F) Schematic proliferation and premature differentiation experimental approach for primary myoblasts isolated from old (20-24 month old) mice. (G) Quantification of EdU+ myoblasts, identified by syndecan4 immunoreactivity, under growth conditions. H) Quantification of nuclei in myosin+ cells under growth conditions. (I) Schematic of differentiation experimental design (J) Quantification of nuclei in myosin+ cells under differentiation conditions. (K) Schematic of stress recover experimental design. (L) Quantification of EdU+ myoblasts, identified by syndecan4 immunoreactivity, under growth conditions following stress from serum withdrawal. For G-L n=4 primary myoblast isolates comparisons by t-test.

4.4.2 caFGFR1 expression increases MuSC number and asymmetric division in aged mice

Ectopically activating FGFR1 signaling in SCs from aged mice restores asymmetric division and presumably SC self-renewal, the loss of which is a hallmark of SCs from aged mice [74]. Expressing a constitutively active FGFR1 in cultured SCs from aged mice enhances the proliferative capacity and prohibits SCs from prematurely differentiating restoring them to a more youthful behavior. Since aged mice possess half of the youthful complement of SCs we asked if caFGFR1 signaling *in vivo* could restore MuSCs numbers in aged mice. Aged (20-26 month old) caFGFR+ and caFGFR1- mice treated with tamoxifen and maintained on doxycycline chow for 30 days prior to collection (Figure 4.2A) were assayed for SC numbers in the tibialis anterior (TA) muscles. When scored for immunoreactivity to PAX7, cross sections of TA muscles from aged caFGFR1+ mice possessed 1.7-fold more SCs than comparably aged caFGFR1- mice (Figure 4.2B, 4.1A). Concomitant with the increase in SC numbers, we observed a >2-fold increase in asymmetrically dividing SCs in myofibers explanted from aged caFGFR1+ mice compared to aged caFGFR1- mice (Figure 4.2C-D). The increase in asymmetrically dividing caFGFR1+ SCs restores 75% of the asymmetrically dividing population of SCs from young mice indicating that caFGFR1 expression rescues the majority of age-related declines in asymmetric division [74].

Expressing ectopic caFGFR1 in SCs from aged mice rescues cell intrinsic aging phenotypes *in vitro* and *in vivo*, suggesting caFGFR1 expression rejuvenates MuSCs in aged mice to a youthful state. If SCs from aged mice are rejuvenated by caFGFR1 expression then caFGFR1+ transcriptomes would appear more youthful than caFGFR1- transcriptomes. To assess the transcriptomes of mononuclear cells and myonuclei in skeletal muscle we employed three distinct sequencing strategies: 1) single cell RNA-sequencing (scRNA-seqs) of all mononuclear cells isolated from muscle, 2) scRNA-seq of enriched SCs, and 3) single nuclear RNA sequencing (snRNA-seqs) optimized to capture myonuclei from myofibers (Figure 4.2E, 4.2A) [117]. Clustering single-cells and single-nuclei together revealed cell types expected from skeletal muscle identified by cell-type specific markers
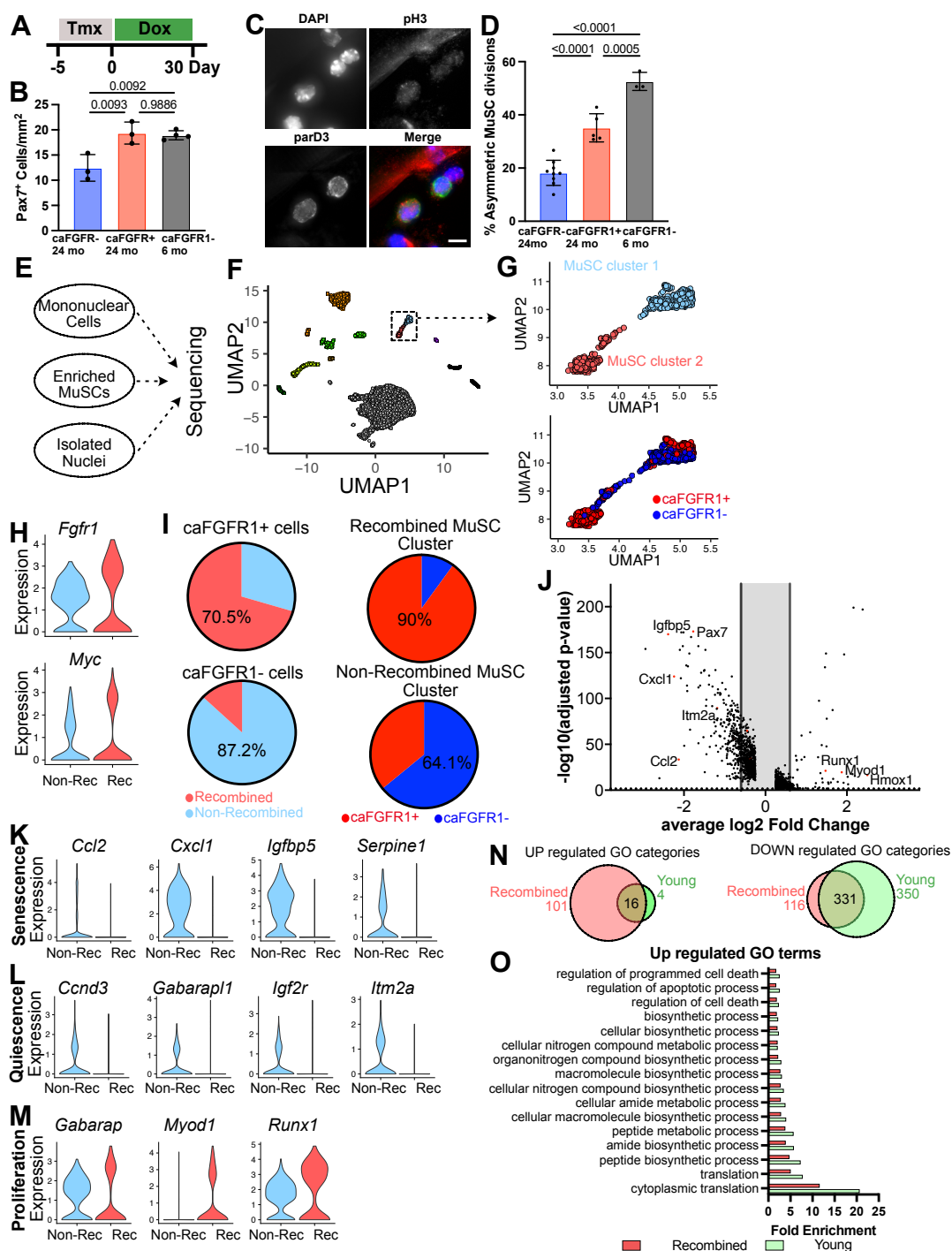
Figure 4.2: **caFGFR1 expression partially rejuvenates MuSCs in old mice** (A) Treatment of old mice (20-24 month) with tamoxifen and 30 days of doxycycline. (B) Quantification of *Pax7+* cells/mm2. n=3-4 mice per genotype comparisons by one way ANOVA. (C) Immunofluorescence images of MuSC on isolated myofibers isolated from aged mice. Bar= 10 um.

Figure 4.2: ***continued*** (D) Quantification of the percentage of asymmetric MuSC divisions on isolated myofibers n=3-9 mice with >100 MuSC quantified per mouse, comparisons by one way ANOVA. E) Schematic of single cell and single nuclear sequencing experiments from old caFGFR1+ and caFGFR1- mice. (F) UMAP of all cells and nuclei pooled from the 3 sequencing experiments. (G) Inset of the two MuSC clusters colored by cluster and by genotype. (H) Violin plots of *Fgfr1* and *Myc* transcript levels in the putative recombined and non-recombined clusters. G) Quantification of the percent of MuSCs isolated from caFGFR1+ mice in the recombined and non-recombined clusters and of the percent of the recombined and non-recombined clusters composed of each genotype. (J) Volcano plot comparing transcripts between the recombined and non-recombined MuSC clusters. Transcripts of special note with greater than 1.5 fold change compared to control are marked in red and labeled. Violin plots of transcript levels between recombined and non-recombined MuSC clusters for transcripts associated with (K) senescence, (L) proliferation, and (M) quiescence. (N) Venn diagrams of GO terms of the upregulated transcripts and down regulated transcripts for the comparison of recombined and non-recombined clusters (pink) and comparison of MuSCs isolated from young and old mice (green). (O) Quantification of the fold enrichment relative to background of the concordant GO categories of up regulated transcripts.

(Figure 4.2F, 4.2B-D). Two distinct MuSC clusters were identified, one enriched in cells isolated from caFGFR1+ mice and one enriched in cells from caFGFR1- mice (Figure 4.2G). As expected, MuSCs in the predominantly caFGFR1+ cluster were enriched for *Fgfr1* and *Myc* transcripts relative to the predominantly caFGFR1- cluster (Figure 4.2H), indicating that the predominant MuSC cluster from caFGFR1+ mice represented recombined MuSCs and the other myogenic cluster, non-recombined SCs. When quantified, 71% of MuSCs isolated from caFGFR1+ segregate into the recombined cluster (Figure 4.2I), consistent with the recombination frequencies determined for caFGFR1+ cultured myoblasts (Figure 4.1D). We compared the recombined SCs and non-recombined MuSCs identifying 127 differentially regulated transcripts (Figure 4.2J, Table S1). Transcripts associated with senescence [163, 164] (Figure 4.2K) and quiescence [165] (Figure 4.2M) were downregulated while transcripts associated with SC activation [35, 49, 162] (Figure 4.2L) were up regulated.

To further examine whether caFGFR1+ MuSCs were rejuvenated, we compared the gene ontology (GO) terms of the differentially expressed transcripts between the recombined and non-recombined MuSC clusters from old caFGFR1+ mice and and old caFGFR1- mice to the GO terms obtained from differentially expressed transcripts between young (3-6 month old) and aged
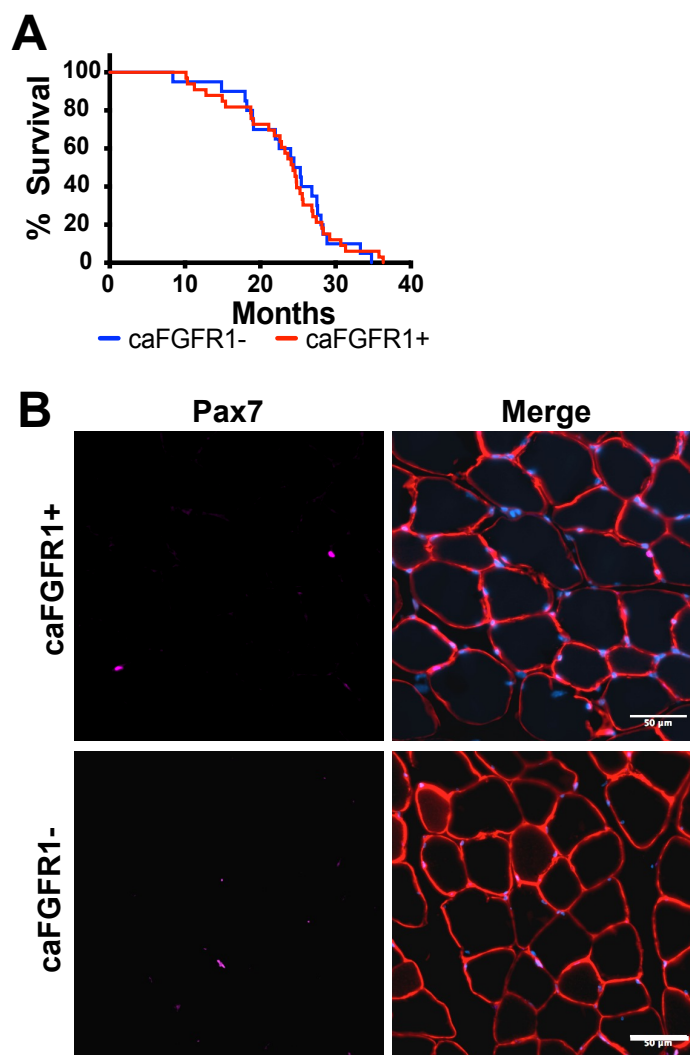
Supplementary Figure 4.1: **Related to Figure 1 and Figure 2** (A) Kaplan Myers survival curve of caFGFR1+ and caFGFR1- mice. B) Immunohistochemistry images of the tibialis anterior of old caFGFR1+ and caFGFR1- mice treated with doxycycline for 30days Bar=50 um. PAX7 pink, laminin Red, dapi blue.

(24 month old) mice [166–168] revealing 16 GO terms upregulated in caFGFR1+ recombined SCs and SCs from young mice (Figure 4.2N). These shared processes between caFGFR1+ recombined and young mouse SCs were associated with protein translation, altered metabolism, and negative regulation of apoptosis (Figure 4.2O). An overlap of 331 depleted GO terms were detected in caFGFR1+ recombined MuSCs and MuSCs from young mice (Figure 4.2N) associated with ATP

Supplementary Figure 4.2: **Related to Figure 2** (A) UMAP of pooled results from single cell and single nuclear sequencing experiments with events colored by isolation method, (B) genotype, or (C) cell type. D) Violin plots of transcript levels of cell type specific transcripts to identify the cell type of each cluster. E) Additional violin plots of quiescence associated transcripts. F) Quantification of the fold enrichment relative to background of the concordant GO categories of down regulated transcripts.

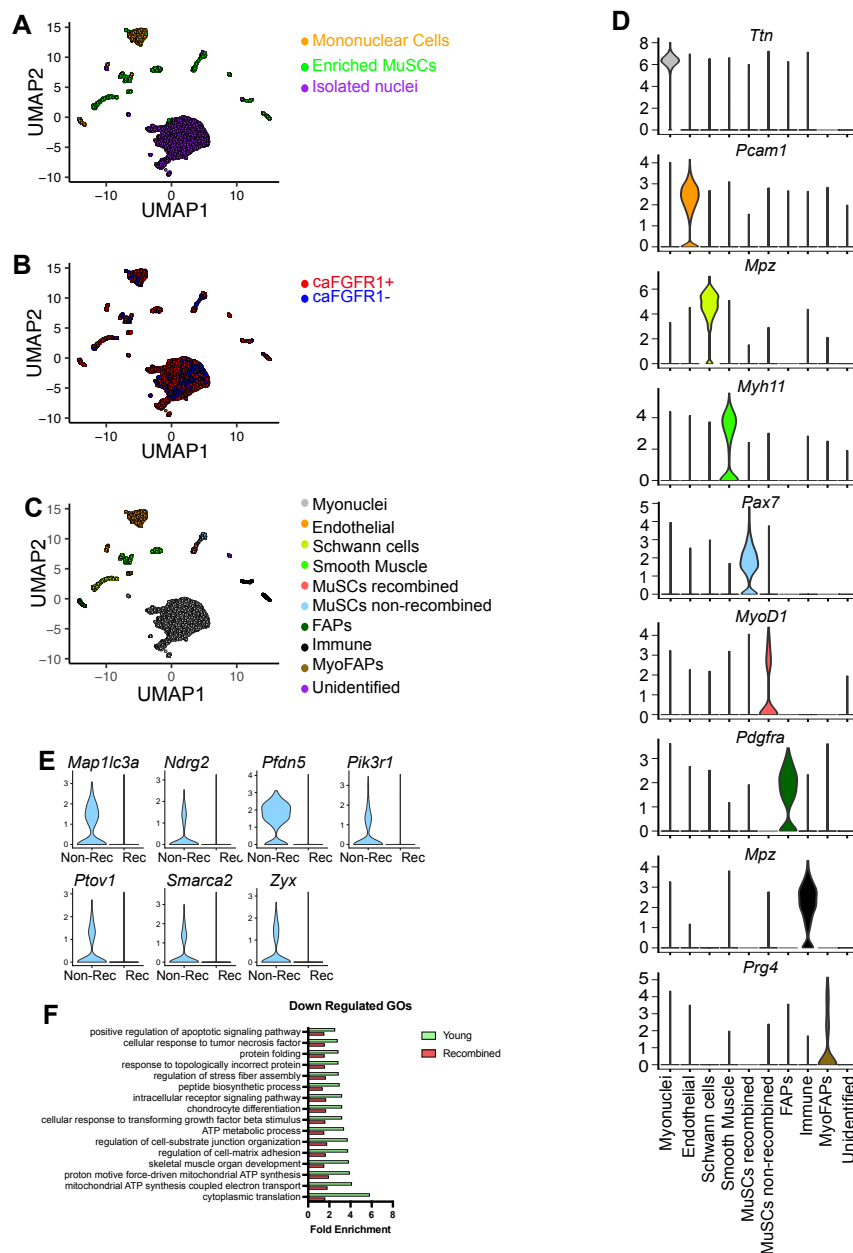production, response to growth factors, and positive regulation of apoptosis (Figure 4.2O). The similar overlap in regulated GO processes detected when comparing recombined and non-recombined MuSCs with those in MuSCs isolated from young and aged mice suggests that the processes altered by caFGFR1 expression are processes affected by aging. Thus, caFGFR1 expression is altering MuSC transcriptomes to be more similar to MuSCs from young mice.

4.4.3   caFGFR1 expression does not improve skeletal muscle

Having determined that caFGFR1 expression rescues cell intrinsic aging in MuSCs, we next asked whether rejuvenating MuSCs could restore skeletal muscle in aged mice to a more youthful state. Despite random insertion, the caFGFR1 transgene did not decrease mouse lifespan (Figure 4.1A). We returned to our sc/snSeq data set comparing caFGFR1+ and caFGFR1- mice that were maintained on doxycycline chow for 30 days (Figure 4.3A), and focused on comparing myonuclei nuclei isolated from aged caFGFR1+ and caFGFR1- mice (Figure 4.3F, 4.2A,D). Among 730 differentially expressed transcripts between myonuclei isolated from caFGFR1+ and caFGFR1- mice (Figure 4.3B, Table S2) the 310 enriched in caFGFR1+ myonuclei belonged to GO processes largely associated with proteostasis and denervation response (Figure 4.3A). Transcripts depleted from caFGFR1+ myonuclei were associated with GO processes linked to metabolism (Figure 4.3B). Altered levels of proteostasis linked transcripts led us to ask whether caFGFR1 expression in MuSC caused muscle hypertrophy. However, TA muscle wet weight (Figure 4.3C), myofiber number (Figure 4.3D), and myofiber diameter (Figure 4.3E-F) in aged caFGFR1+ mice were unchanged compared to caFGFR1- controls. Prompted by the changes in metabolic transcript levels we asked whether caFGFR1 expression affected myofiber type, but myofiber type distribution (Figure 4.3G) was not significantly different between caFGFR1+ and caFGFR1- TA muscles.

While the myofibers were not detectably altered by MuSC caFGFR1 differentially expressed myonuclear transcripts suggested that the interactions between MuSCs, the myofiber, and other cell types may change in response to caFGFR1 expression. MuSCs reside in a niche nestled against the myofiber, close to capillaries [169] and are enriched at the neuromuscular junction (NMJ) [73].
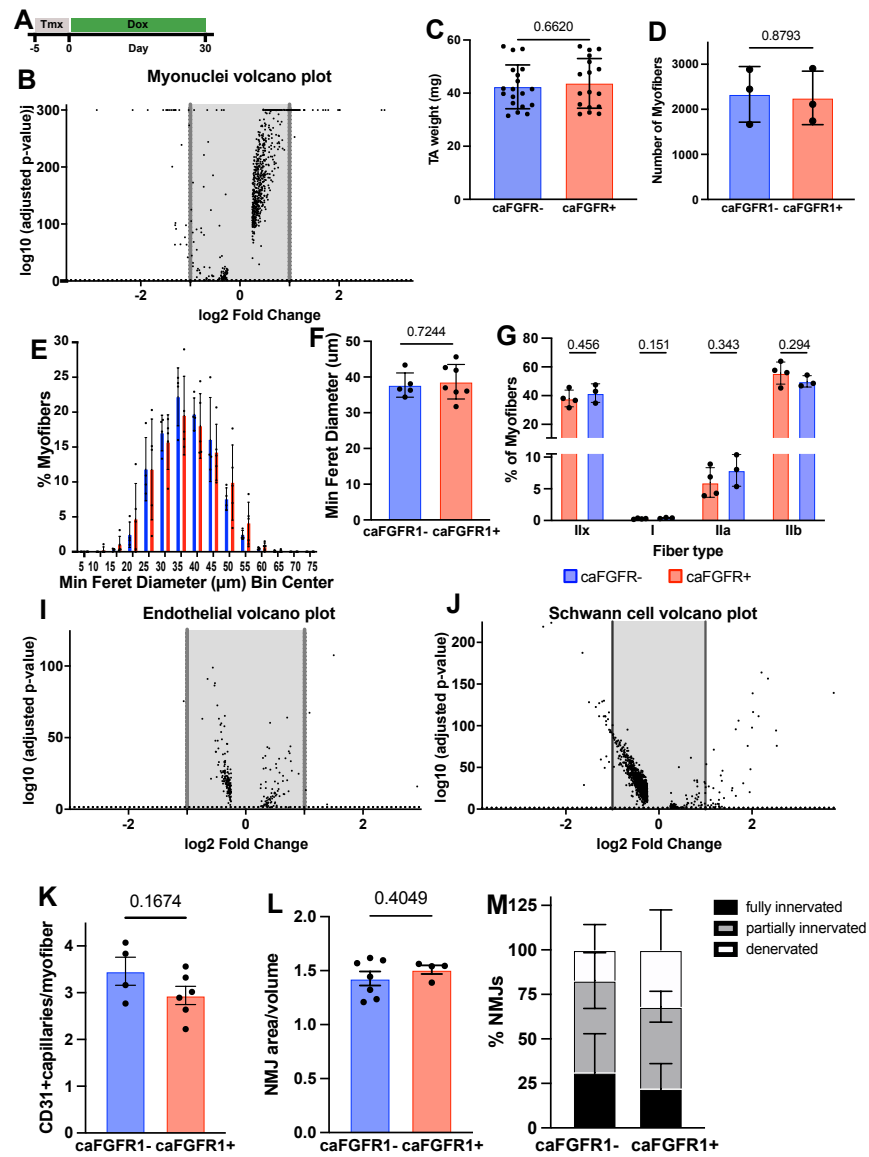
Figure 4.3: **MuSC caFGFR1 expression does not affect muscle in aged mice.** A) Treatment of old mice with tamoxifen and 30 days of doxycycline. B) Volcano plot comparing myonuclear transcripts from caFGFR1+ and caFGFR1- mice. C) Quantification of TA muscle wet weight from old caFGFR1+ and caFGFR1- mice n=17-20 mice, comparison by t-test. D) Quantification of the number of myofibers in a full TA muscle section from caFGFR1+ and caFGFR1- old mice n=3 mice with 3 full TA sections quantified per mouse comparison by t-test. E) Distribution of myofiber minimum Feret diameters in the TA n=4 mice with >500 myofibers quantified per mouse F) Median minimum Feret diameter for TA muscles from caFGFR1+ and caFGFR1- old mice n=5-7 mice comparison by t-test.

Figure 4.3: *continued* G) Quantification of the percentage of each fiber type in TA muscle sections from old caFGFR1+ and caFGFR1- mice n=3-4 mice with 3 full TA sections quantified per mouse comparisons by one way ANOVA. H) Volcano plot comparing endothelial transcripts from caFGFR1+ and caFGFR1- mice. J) Volcano plot comparing Schwann cell transcripts from caFGFR1+ and caFGFR1- mice. K) Quantification of number of CD31+ capillaries/myofiber in TA muscles from old caFGFR1+ and caFGFR1- mice n=4-6 mice comparison by t-test. L) Quantification of neuromuscular junction complexity (represented as Bungarotoxin+ area/endplate volume) on individual myofibers isolated from the extensor digitorum longus of caFGFR1+ and caFGFR1- mice n=4-7 mice with ¿100 NMJs quantified per mouse comparison by t-test. L) Quantification of NMJ innervation on individual myofibers n=4-7 mice with ¿100 NMJs quantified per mouse comparison by one way ANOVA no values were significantly different.

caFGFR1+ myonuclei expression of of transcripts associated with glycogen processing and the electron transport chain was depleted, suggesting a shift in the balance of oxidative and glycolytic metabolism (Figure 4.3B). Additionally, the endothelial cell population was underrepresented in the caFGFR1+ derived samples compared to the caFGFR1- samples but few transcripts were differentially regulated between caFGFR1+ and caFGFR1- endothelial cells, suggesting an overall shift in cell abundance (Figure 4.3I). We asked if vascularization was altered in caFGFR1+ muscle. We quantified the number of capillaries per myofiber by PECAM1 immunoreactivity but detected no difference in vascularization between caFGFR1+ and caFGFR1- TA muscles (Figure 4.3K, Figure 4.3C). Similarly, caFGFR1+ myonuclei were enriched in transcripts associated with denervation response and a large numbers of transcripts (1141) were differentially regulated in Schwann cells isolated from caFGFR1+ mice compared to caFGFR1- mice (Figure 4.3J) suggesting that the NMJ in caFGFR1+ mice may be altered. Increased MuSC contribution to NMJs improves innervation in old mice, thus the increased MuSC content of caFGFR1+ muscles may improve myofiber innervation. To evaluate whether caFGFR1 expression reduced denervation myofibers in aged mice [73], we isolated myofibers and evaluated NMJ complexity (Figure 4.3L, Figure 4.3D) and innervation (Figure 4.3L-M, Figure 4.3E). Neither measure was significantly different between caFGFR1+ and caFGFR1- muscles. These data indicate that rejuvenating MuSCs is insufficient to broadly improve skeletal muscle in aged mice and restore more youthful muscle phenotypes.
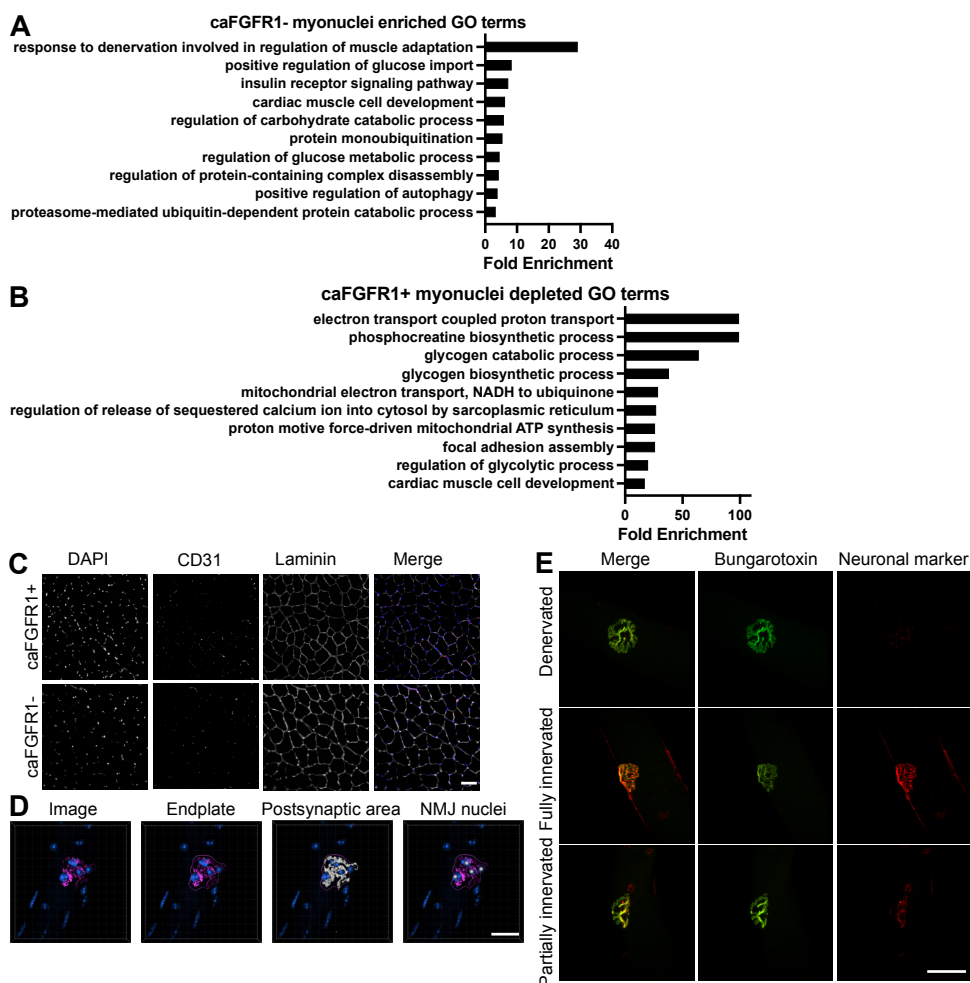
Supplementary Figure 4.3: **The top ten biological process GO terms by fold change of transcripts** (A) significantly enriched in and (B) significantly depleted from caFGFR1+ myonuclei relative to background are presented. C) Representative images immunohistochemistry for capillaries in TA muscle cross sections. D) Representative images of NMJ staining on isolated myofibers and quantification of NMJ complexity. E) Representative images of immunofluorescence for NMJ innervation.

4.4.4   caFGFR1 MuSC do not improve skeletal muscle regeneration

While skeletal muscle does not appear rejuvenated by expressing caFGFR1 in MuSCs for 30 days, perhaps longer exposure is required to alter muscle phenotypes in aged mice. As a proxy for this, we tested whether caFGFR1 expression MuSCs rescues age-associated deficits in skeletal muscle regeneration and thus, may contribute to long-term improvement of the muscle. Upon injury, caFGFR1+ and caFGFR1- aged mice were maintained on doxycycline chow for 30 days, the muscle collected, and myofiber diameter and MuSC content quantified (Figure 4.4A). Myofibers were significantly smaller in regenerated caFGFR1+ muscles than caFGFR1- TA muscles (Figure 4.4B-C; Figure 4.4A). Following regeneration, MuSC number was increased in both caFGFR1+ and caFGFR1- muscles to the same level, similar to that observed in young mice (Figure 4.4D).

Because caFGFR1+ mice fed doxycycline for 30 days have nearly two-fold more MuSCs in the TA muscle than caFGFR1- mice, mice pretreated with doxycycline could rescue age related muscle regeneration deficits. Recombined caFGFR1+ and caFGFR1- mice were fed doxycycline chow for 30 days prior to TA muscle injury and then maintained on standard chow for 30 days of regeneration (Figure 4.4E). Despite entering regeneration with more MuSCs, caFGFR1+ myofiber diameter was significantly smaller than the myofiber diameter in caFGFR1- mice, (Figure 4.4F-G; Figure 4.4B). Doxycycline pretreated caFGFR1+ and caFGFR1- muscles contained comparable numbers of MuSCs post regeneration (Figure 4.4H). Together these results establish that neither partially rejuvenating MuSCs nor increasing MuSC number by ectopically expressing caFGFR1 rescue age-related deficiencies in regenerating muscles of aged mice.

4.4.5   Discussion

Because a drug inducible FGFR1 rescued aging associated defects in cultured MuSC and in transplantation, we tested whether FGFR1 activation would rescue muscle aging *in vivo*. caFGFR1 expression rescued MuSC cell intrinsic defects: cell number, resistance to stress and premature differentiation, and asymmetric differentiation rates. The transcriptomic differences between caFGFR1+
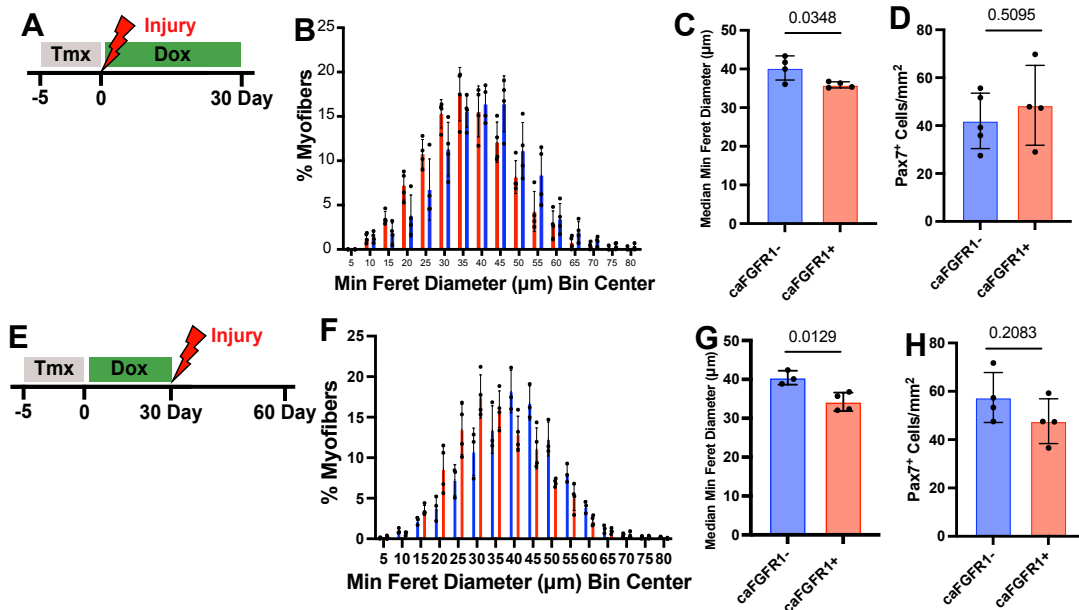
Figure 4.4: **caFGFR1 expression does not rescue muscle regeneration in aged mice.** A) Schematic of muscle injury and regeneration in the presence of doxycycline. B) Distribution of minimum Feret diameters of regenerated myofibers in TA muscle of old caFGFR1+ and caFGFR1- mice. n=4 mice with ¿500 myofibers quantified per mouse. C) Quantification of median minimum Feret diameter of regenerated myofibers from caFGFR1+ and caFGFR1- mice n=4 mice comparison by t-test. D) Quantification of number of PAX7+ MuSC per mm2 in regenerated TA muscle from caFGFR1+ and caFGFR1- mice n=4-5 mice comparison by t-test. E) Schematic of muscle injury following 30 days of doxycycline treatment with regeneration in the absence of doxycycline. F) Distribution of minimum Feret diameters of regenerated myofibers. G) Quantification of median minimum Feret diameter of regenerated myofibers n=3-4 mice with >500 myofibers quantified per mouse comparison by t-test. H) Quantification of number of PAX7+ MuSC per mm2 in regenerated TA muscle n=4 mice comparison by t-test.

Figure S4
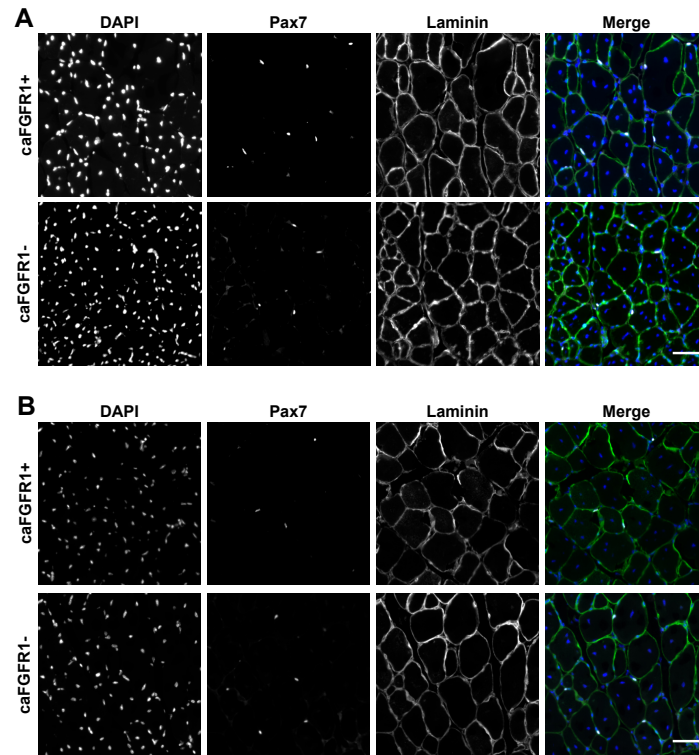
Supplementary Figure 4.4: (A) Representative images of regenerated TA muscles from old caFGFR1+ and caFGFR1- mice with regeneration in the presence of doxycycline. (B) Representative images of regenerated TA muscles from old caFGFR1+ and caFGFR1- mice pretreated with doxycycline and then with regeneration in the absence of doxycycline. Bar=50uM.

and caFGFR1- MuSCs isolated from old mice were similar to the differences between MuSCs isolated from young adult and old mice, supporting a broader rejuvenation of the MuSC transcriptome. However, despite rescuing age associated deficiencies in MuSC, caFGFR1 expression did not improve skeletal muscle morphology.

Recently, Wang et al reported that increasing EGF signaling in MuSCs of x-linked muscular dystrophy model (mdx) not only rescues disease phenotypes in the MuSCs but also muscle histology and function [104]. Because EGF was identified in a screen for promoters of MuSC asymmetric division, the proposed mechanism of improving muscle was increased MuSC asymmetric division. That stimulating EGF signaling broadly rescues muscle phenotypes in mdx mice but stimulating FGF signaling in MuSC of old mice rescued only MuSC intrinsic phenotypes, including asymmetric division, could reflect a combination of three differences. First, we expressed caFGFR1 specifically in MuSC via transgene while EGF signaling was stimulated by introducing an EGF expression plasmid into the skeletal muscle resulting in EGF ligand available to all cell types. Second, while some mdx phenotypes are similar to aging phenotypes these two states are fundamentally different. Third, although both EGF and FGF signaling promote MuSC asymmetric division, they may do so through distinct biochemical pathways. EGF signaling may stimulate a pathway separate from asymmetric division that promotes improved muscle health.

Similarly, the recombined caFGFR1+ MuSC had lower levels of senescence associated transcripts; however, reduced MuSC senescence did not improve overall muscle health. Eliminating senescent cells either, genetically or pharmacologically, improves muscle phenotypes in both aging and disease [170–172]. This surprising discordance could arise from either the need to remove senescent cells of many different lineages to positively affect the muscle or that recombined caFGFR1+ MuSCs expressed reduced levels of senescence associated transcripts but were not ablated. In either case, it is clear that simply reducing MuSC senescence is insufficient to ameliorate the effects of aging.

Together our findings that caFGFR1+ expression in MuSCs rescues cell-intrinsic age associated defects but does not improve the muscle holistically offer further support that approaches

to tackle the effects of aging will require multifactorial interventions that target multiple cell types and processes. Because MuSCs maintain muscle throughout life repairing damage and supporting exercise mediated benefits, MuSCs are an attractive target for gene or cell-based therapies intended to improve muscle health in aging and disease. However, MuSCs make up only 2-7% of nuclei in adult skeletal muscle [33], and basal rates of MuSC activation and fusion in old mice are notably low [173]. Experimental interventions that have had the greatest effect on reducing muscle aging phenotypes have involved broad systemic treatments like ablating all senescent cells, caloric restriction, exercise, or heterochronic parabiosis. So, while correcting cell intrinsic aging defects in MuSCs will likely be necessary to tackle some aging phenotypes, simply focusing on the MuSCs is insufficient to reverse the negative effects of aging.

4.5   Methods

4.5.1   Mice

Mice were bred and housed according to National Institutes of Health (NIH) guidelines for the ethical treatment of animals in a pathogen-free facility at the University of Colorado at Boulder. The University of Colorado Institutional Animal Care and Use Committee (IACUC) approved all animal protocols and procedures. Pax7iresCre; ROSA26LSLrtTA; caFGFR1 mice were generated by crossing C57Bl/6 (Jackson Labs, ME, USA), Pax7iresCre mice [31], ROSA26-rtTA mice [161] (Jackson Labs), and conditional caFGFR1 transgenic mice [159]. Mice from 20-24 month old mice were considered old. Initial observations in a small cohort of aged mice suggested a sex difference, consequently, unless otherwise noted experiments were restricted to male mice.

4.5.2   Tibialis anterior injuries and tamoxifen injections

Mice were anesthetized with isoflurane, received sustained release Buprenorphine (ZooPahrm) and meloxicam as analgesics, and supportive warmed saline, and the left TA muscle was injected with 50uL of 1.2% $BaCl_2$. TA muscles were harvested at the indicated time points post injury.

4.5.3   Primary muscle stem cell isolation

Hindlimb muscles were dissected, minced, and digested in Hams F12 (Gibco) containing 400U/ml collagenase (Worthington) for 60 minutes at 37°C. Digest was quenched with serum containing media and cells filtered through 100um, 70um and 40um Cells were maintained in Hams F12 media supplemented with Myocult (StemCell Technologies) and 0.8 mM CaCl at 37°C in 5% CO2. Doxycycline was included at 1 ug/ml as experimentally indicated. If required, cells were incubated with 10uM 5-ethynyl-2'-deoxyuridine (EdU – Life Technologies) for two hours prior to fixation. Cells were fixed in 4% paraformaldehyde for 10 minutes and then processed for immunocytochemistry.

4.5.4   Primary myofiber isolation

Individual extensor digitorum longus myofibers were isolated cultured and immunostained according to [174]. Extensor digitorum longus muscles were dissected and digested in Hams F12 containing 400-U/mL collagenase at 37 °C for 1.5 h. Collagenase was inactivated by the addition serum containing media. Individual myofibers were gently isolated by trituration maintained in Ham's F-12 supplemented with 15% horse serum, 0.8mM CaCl, and 50nM FGF-2 at 37°C in 5% CO2. Doxycycline was included at 1 ug/ml as indicated. Myofibers were fixed in 4% paraformaldehyde for 10 minutes and then processed for immunocytochemistry.

4.5.5   Immunohistochemistry

TA muscles were dissected and either immediately embedded in O.C.T. (Tissue-Tek) and flash frozen in liquid nitrogen (for fiber type staining) or fixed on ice for 2hrs with 4% paraformaldehyde, and then transferred to PBS with 30% sucrose at 4C overnight. Muscle was mounted in O.C.T. (Tissue-Tek) and cryo-sectioning was performed on a Leica cryostat to generate 10um thick sections. Tissue sections were post-fixed in 4% paraformaldehyde for 10 minutes at room temperature (RT) and washed three times for 5 min in PBS. Immunostaining with anti-*Pax7*, anti-Laminin antibodies required heat-induced epitope retrieval where post-fixed slides were placed in citrate buffer, pH 6.0,

and subjected to 6 min of high pressure-cooking in a Cuisinart model CPC-600 pressure cooker. All other antibodies did not require antigen retrieval and so proceeded directly to immunostaining. For immunostaining, tissue sections were permeabilized with 0.25% Triton-X100 (Sigma) in PBS containing 2% bovine serum albumin (Sigma) for 60 min at RT. Incubation with primary antibody occurred at 4°C overnight followed by incubation with secondary antibody at room temperature (RT) for 1hr. Primary antibodies included mouse anti-Pax7 (Developmental Studies Hybridoma Bank, University of Iowa, USA) at 1:750, rabbit anti-laminin (Sigma-Aldrich) at 1:250, rabbit anti-myc-tag (CellSignaling) at 1:200 and a mouse anti-eMHC (Developmental Studies Hybridoma Bank, University of Iowa, USA) at 1:5. Alexa secondary antibodies (Molecular Probes) were used at a 1:1000 dilution. For analysis that included EdU detection, EdU staining was completed prior to antibody staining using the Click-iT EdU Alexa fluor 488 detection kit (Molecular Probes) following manufacturer protocols. Sections were incubated with 1 ug/mL DAPI for 10 min at room temperature then mounted in Mowiol supplemented with DABCO (Sigma-Aldrich) or ProLong Gold (Thermo) as an anti-fade agent.

4.5.6 Immunocytochemistry

Fixed cells or fibers were then permeabilized with 0.25% Triton-X100 (Sigma) in PBS containing 2% bovine serum albumin (Sigma) for 60 min at RT. Incubation with primary antibody occurred at 4°C overnight followed by incubation with secondary antibody at room temperature (RT) for 1hr. Primary antibodies included mouse anti-Pax7 (Developmental Studies Hybridoma Bank, University of Iowa, USA) at 1:750, rabbit anti-myc-tag (CellSignaling) at 1:400, chicken anti-syndecan4 (Developmental Studies Hybridoma Bank, University of Iowa, USA) at 1:1000 and a mouse anti-phosphoFGFR1 (CellSignaling) at 1:100, phospho H3 (Millipore Sigma) at 1:500, myog F5D (abcam) 1:1, emhc F1.652 (DSHB) at 1:5. Alexa secondary antibodies (Molecular Probes) were used at a 1:1000 dilution. For analysis that included EdU detection, EdU staining was completed prior to antibody staining using the Click-iT EdU Alexa fluor 488 detection kit (Molecular Probes) following manufacturer protocols. Cells were incubated with 1 ug/mL DAPI for 10 min

at room temperature then mounted in Mowiol supplemented with DABCO (Sigma-Aldrich) or ProLong Gold (Thermo) as an anti-fade agent.

4.5.7   Microscopy and image analyses

Images were captured on a Nikon inverted spinning disk confocal microscope or an invereted fluorescence scanner microscope (Olympus IX83). Objectives used on the Nikon were: 10x/o.45NA Plan Apo, 20x/0.75NA Plan Apo and 40x/0.95 Plan Apo. Confocal stacks were projected as maximum intensity images for each channel and merged into a single image. Brightness and contrast were adjusted for the entire image as necessary. Both muscle stem cell numbers and average myofiber diameter were counted manually using Fiji ImageJ. Images were processed using Fiji ImageJ and the analysis package myosoft [175]. Primers for caFGFR1 detection by PCR FGFR3 TMD – FGFR1 TKD spanning primers: FR3-FR1-FW: AGCTACGGGGTGGTCTTCTT FR3-FR1-RV: AACCAGGAGAACCCCAGAGT

4.5.8   Software Packages

- Cellranger Software Suite/3.0.1 - FastQC 0.11.8 - R 4.1.1 - Seurat 4.1.1 - SoupX 1.5.2

4.5.9   Quality control, read alignment, and expression quantification

To assess the quality of Fastq files from sequencing, FastQC was used, evaluating depth and quality of each replicate. Cellranger was then used to process Fastq files and aggregate technical replicates, creating gene-count matrices for each sequencing experiment. For transcriptome alignment of the snRNA-seq datasets, a custom pre-mRNA mm10 reference package was used as previously described for nuclei [20, 147]. For the scRNA-seq experiments, the recommended reference package was used [16].

4.5.10   Accounting for experimental noise and doublets

Cellranger-aligned feature matrices were then loaded into R using the load10X() function from SoupX. Ambient RNA contamination was predicted using default settings of autoEstCont() and counts were normalized to an estimated noise parameter using adjustcounts(). In Seurat, doublets and debris were removed as per their recommended metrics. Cells or nuclei expressing greater than 2,500 or less than 200 features were removed.

4.5.11   Normalization, dimensional reduction, and nuclear clustering

The tutorial provided by the Mayaan lab was used to guide data normalization (`satijalab.org/seurat/articles/pbmc3k_tutorial`). Mitochondria and low-quality nuclei were removed. Seurat objects were then passed through NormalizeData(), FindVariableFeatures(), ScaleData() to scale and log normalize gene counts within each sample. Data were then integrated using the FindIntegrationAnchors() and IntegrateData() functions in Seurat using the reciprocal PCA (rPCA) algorithim.

While performing dimensional reduction of the integrated Seurat object using UMAP and clustering using the shared nearest neighbor (SNN) modularity optimization based clustering algorithm, adjusting the minimum number of neighbors, minimum distance, and resolution parameters to achieve adequate separation of nuclear clusters [148]. Identification of nuclear clusters was done manually, using differential gene expression from the FindMarkers() function between clusters combined with manual literature curation. The Myoatlas database and webtool (research.cchmc.org/myoatlas/) was of particular help in identifying clusters of nuclei [20].

4.5.12   Comparison to Kimmel, et. al 2021

To compare the recombined and non-recombined clusters of MuSCs to existing data, data from [85] were downloaded from GEO_number and processed identically as described above.

4.5.13   Differential expression tests

Differential gene expression was assessed by the Wilcoxon Rank Sum Test in the Seurat FindMarkers() function. Genes were assessed as significant with an adjusted p-value ¡ 0.05. GO analyses identifying differentially expressed genes were conducted using Panther [129, 149]. A background gene set was used comprising all genes expressed in myogenic nuclei detected from sequencing. GO Biological Processes Complete hierarchy was used to organize results. Example categories in figures were chosen as contained within ranked clusters.

Chapter 5

Discussion

Skeletal muscle health is critical for human well-being. As individuals age, skeletal muscle function and regenerative capacity deteriorates, disrupting the lives of elderly individuals [4–6,70]. Disruptions to MuSC function are considered a fundamental driver of aging-associated skeletal muscle decline [8,76,80,104], yet the precise mechanisms for how MuSC dysfunctions contribute to changes in mature muscle function in aging is not fully understood [176,177]. Additionally, while MuSC populations exist within functionally-defined subsets with distinct proliferative behaviors, how these subpopulations are impacted by aging is not clear. Contributing to this incomplete understanding of the relationship between MuSC biology and age-associated skeletal muscle decline is the complex nature of aging, where fundamental cellular processes, such as transcription and cell fate determination, are disrupted globally and impact each other in complex and synergistic ways, such that unraveling the causes versus the effects of aging is exceedingly difficult [6,67–69,89,178, 179]. Because the changes that occur with aging are so pervasive, only systematically assessing changes to myogenic processes will reveal underlying drivers of skeletal muscle aging. Thus, I applied transcriptomic and other population-level analyses to expose various fundamental elements of aging-associated changes to MuSC biology and reduced regenerative capacity, and how these changes may contribute to the overall decline of skeletal muscle during aging.

To thoroughly explore the fundamental drivers of aging requires strategies capable of assessing biological processes holistically, rather than on the level of individual genes or pathways. One of the most effective ways to accomplish this is single-cell transcriptomics, which captures global

transcriptional states of single cells [180,181]. To compare the transcriptional states of regenerating myogenic nuclei from young and aged mice, they must first be oriented so that nuclei that at comparable stages of myogeneis are being directly compared. To accomplish this, I integrated single-nuclear transcriptomic with in-depth pseudotime analysis to identify temporal changes to gene expression during myogenesis in aged mice. Through this analysis, I revealed that coordination of myogenic gene expression networks is disrupted during regeneration in aged mice. While previous studies support straightforward delays in the activation of myogenic transcriptional networks [74,85, 86], my findings support much more complex and nuanced aging-associated temporal disruptions to myogenic gene expression. I uncovered that genes with disrupted pseudotime expression dynamics comprised distinct transcriptional networks identified by enriched co-expression of TFs and shared pseudotime expression patterns. Additionally, I reveal through a novel application of the Dynamic Time-Warping algorithm that mis-coordination of gene expression networks in aged mice worsens as MuSCs and progenitors proliferate, fuse, and mature as myonuclei, similar to a propagating wave of temporally disrupted gene expression during regeneration in aged mice. My work adds to a growing body of evidence that temporal disruption of gene expression dynamics is a critical driver of aging phenotypes in skeletal muscle, as well as possibly within other tissues and diseases [6,85,86]. While further studies are required to unravel the mechanisms of altered gene expression dynamics in skeletal muscle, my work builds on an important perspective that will help guide future research into the phenomenon of temporally disrupted gene expression in aging.

The extent of cell fate heterogeneity among MuSCs is not well understood, and the functional consequences of different distinct MuSC behaviors, and how they are affected in aging, has not been sufficiently explored. In aging, skeletal muscle is more easily injured, and thus is chronically existing within a regenerative state [182,183]. Clonal diversity and maintenance of MuSC subpopulations may be critical for myonuclear maturation and reestablishment of critical anatomical structures after muscle regeneration is complete, which if lost or disrupted in aging could help explain associated muscle decline. I analyzed single-cell frequency distributions of MuSCs and their progeny generated from a novel barcode lineage tracing conducted in young and aged mice during regener-

ation. I uncovered evidence supporting at least two types of MuSC lineages exhibiting strikingly distinct proliferative dynamics, where one type is exceedingly rare, the other is associated with a significant majority of MuSCs. I detected that this extremely minor subpopulation of MuSCs proceeds through significantly more divisions than the bulk population, producing thousands of progeny compared to the average MuSC lineage size of ∼1-2. When I asked how these population dynamics differ during regeneration in aged mice, I uncovered a reduction of these high expanding MuSCs compared to young mice, suggesting either the processes of cell expansion is awry in aged mice, or the necessary pruning down of these large lineages once regeneration is complete in order to reestablish population balance, is dysregulated in aging. This work is preliminary in many regards, leaving significant holes in our understanding of sources of experimental bias and the biological significance of high dividing MuSCs. Nevertheless, my findings provide a previously unattainable glimpse into MuSC population dynamics during regeneration in aged mice. Moving forward, the novel barcoding technique developed by the our group can be extended to other adult stem cell populations to identify potentially similar aging and disease-associated changes in stem cell population dynamics.

Chapter 4 of my dissertation includes a study where a genetic perturbation to MuSCs in aged mice recovers aspects of their function relative to young mice, however, unexpectedly this was insufficient to detectably affect muscle function. This finding is critical for contextualizing the broader significance of my dissertation work. While I describe complex defects in MuSC transcriptional trajectories and population dynamics during regeneration in Chapter 2 and Chapter 3, it is important to consider the deeply intertwined physiological systems that govern skeletal muscle function and decline in aging. In fact, the findings provided in Chapter 4 suggest that, at least to some degree, the changes to MuSCs described in Chapter 2 and Chapter 3 are downstream effects of more widespread disruptions to organismal and tissue functions in aging. Thus, the results comprising Chapter 4 reinforce the need for holistic approaches when studying the underlying drivers of aging, ensuring anything less than such methodologies will provide only a fragmented picture of the complex changes that occur as organisms age. Thus, while my work offers significant insights

into the fundamental drivers of skeletal muscle aging, future studies are required to unravel the specific mechanisms that when disrupted lead to the observed changes.

Future Directions

Throughout this thesis, I've described previously unresolved features of skeletal muscle regeneration in aged mice including propagation of mis-timed gene expression, defects in proliferative dynamics, and the role of extrinsic factors in affecting MuSC function. However, in doing so, my work has simultaneously generated new questions regarding the mechanisms of these observed disruptions. Rather than an exhaustive exploration of these mechanisms, my work offers perspectives that align with established paradigms of MuSC biology and aging, as well as those that will be considered more controversial by researchers in the field. To delve deeper and comprehensively evaluate the full extent and implications of these perspectives in terms of muscle biology, as well as the process of aging more broadly, warrants further investigations.

My analysis of barcode lineage tracing revealed a small subset of MuSCs proceed through a strikingly disproportionate number of cell divisions, yet the role and consequences of this minor subpopulation is not clear. The consideration that some MuSCs proceed through significantly more divisions than the average MuSC challenges many of the fields' assumptions about how generation of myonuclei and MuSCs during and after regeneration is accomplished. Moving forward, experiments to further explore the cell fates of high dividing MuSCs (whether they are predominantly myonuclei or MuSCs) are critical. This will be accomplished through additional barcoding experiments currently being conducted by our group where mice at earlier time points after muscle injury (3 dpi, 5 dpi, 7 dpi, 10 dpi, 14 dpi, 20 dpi) are evaluated. Including additional time points, combined with EdU labeling revealing the time windows when different classes of myogenic progeny are being produced, will be instrumental in helping narrow down the specific myogenic fates, and biological significance, of high dividing MuSCs.

Additionally, modifying this barcoding strategy to acquire transcriptomic information as well as cell division quantification, a long-term goal of our group, will be significant for unraveling the

features of high dividing MuSCs that distinguish them from the bulk population. Are high dividing MuSCs intrinsically distinct from other MuSCs, or do they acquire the specialized transcriptional states conferring their capacity to expand disproportionately only upon injury and environmental stimuli? What are the transcriptional landscapes that drive some MuSCs to go through large numbers of divisions, while others do not? These are all questions that can be answered through these lines of experimentation.

While identification of high dividing MuSCs was surprising given current understandings of MuSC biology, muscle regeneration, aging, and stem cell biology broadly, instead my results obtained from analysis of pseudotime trajectories of myogenic differentiation in young and aged mice builds on previous studies identifying temporal changes to gene expression during differentiation of MuSCs isolated from aged mice. Expanding on these previous studies [74, 85, 86], my research highlights the pervasive nature of mis-timed gene expression during muscle regeneration in aged mice, as well as provides potent evidence that temporal aberrations propagate from MuSCs and progenitors into mature myonuclei, contributing to regenerative and functional decline in aged skeletal muscle.

Nevertheless, open questions still remain regarding the underlying causes of these temporal aberrations. What are the fundamental drivers of mis-timed gene expression during muscle regeneration in aged mice? Could a sequence of stochastic changes in the transcriptional landscapes and chromatin organization in aged mouse myogenic progenitors result in promiscuous transcription that disrupts gene expression timing broadly? Alternatively, do specific mutations in transcriptional regulators impede their function and their ability to maintain appropriate temporal regulation of transcription? Or maybe the transcriptional mechanisms in MuSCs themselves remain relatively unperturbed, while aging-specific changes to the intricate extracellular signals generated from non-myogenic cells types orchestrating MuSC and myogenic progenitor transitions during regeneration are what drive mis-timed myogenic gene network expression? To explore these questions further requires explicitly interrogating the mechanisms of mis-timed gene expression in aged mice. Firstly, experiments such as ChIP-seq of TFs identified as enriched among genes with

disrupted pseudotime expression would be critical to identifying downstream regulatory networks more directly. These experiments combined with ATAC-seq, where global chromatin organization of MuSCs and progenitors from aged mice are evaluated, would begin to unravel the transcriptional mechanisms associated with mis-timed gene expression. Additionally, further experiments where TF and chromatin modifying proteins are genetically perturbed and conditionally expressed during regeneration would help illuminate the complex mechanisms of how mis-timed gene expression propagates through myogenic transcriptional networks. If the timing of expression, rather than transcript levels, of TF expression is modulated in young mouse regeneration, does this elicit an phenotype similar to regeneration in aged mice? And vise versa, if TF expression is activated at times in aged mice that they are activated in young mice, is this sufficient to rescue regenerative phenotypes in aged mice? These last experiments also can potentially help explain the findings that recovery of myogenic signaling is insufficient to rejuvenate aged skeletal muscle, by revealing the, to at least some degree, extrinsic factors that may drive mis-timed gene expression in aged mice.

Thus, as with all research in molecular biology, my findings have both advanced the fields' knowledge, as well as sparked the need for future exploration. It is only through the pursuit of these unresolved questions and the continuous efforts of the scientific community that we can deepen our understanding of the intricate processes governing organismal aging and the associated regenerative and functional decline of skeletal muscle.

Bibliography

[1] Walter R. Frontera and Julien Ochala. Skeletal muscle: A brief review of structure and function. Calcified Tissue International, 96(3):183–195, 2015.

[2] Koichiro Matsuo and Jeffrey B. Palmer. Anatomy and physiology of feeding and swallowing: Normal and abnormal. Physical Medicine and Rehabilitation Clinics of North America, 19(4):691–707, 2008.

[3] Christopher McCuller, Rishita Jessu, and Avery L Callahan. Physiology, skeletal muscle. In StatPearls [Internet]. StatPearls Publishing, 2022.

[4] Hiroshi Akima, Yutaka Kano, Yoshitaka Enomoto, Masao Ishizu, Morihiko Okada, Yoshie Oishi, Shigeru Katsuta, and Shin-Ya Kuno. Muscle function in 164 men and women aged 20–84 yr. Medicine and Science in Sports and Exercise, pages 220–226, 2 2001.

[5] Salah Gariballa and Awad Alessa. Association between muscle function, cognitive state, depression symptoms and quality of life of older people: evidence from clinical practice. Aging Clinical and Experimental Research, 30(4):351–357, 2018.

[6] Carlos López-Otín, Maria A Blasco, Linda Partridge, Manuel Serrano, and Guido Kroemer. The hallmarks of aging. Cell, 153(6):1194–1217, 2013.

[7] Helen M. Blau, Benjamin D. Cosgrove, and Andrew T. V. Ho. The central role of muscle stem cells in regenerative failure with aging. Nature Medicine, 21(8):854–862, 8 2015. PMID: 26248268 PMCID: PMC4731230.

[8] Joe V Chakkalakal, Kieran M Jones, M Albert Basson, and Andrew S Brack. The aged niche disrupts muscle stem cell quiescence. Nature, 9 2012.

[9] William Chen, David Datzkiw, and Michael A. Rudnicki. Satellite cells in ageing: use it or lose it. Open Biology, 10(5):200048, 2020.

[10] Kenneth Day, Gabi Shefer, Andrew Shearer, and Zipora Yablonka-Reuveni. The depletion of skeletal muscle satellite cells with age is concomitant with reduced capacity of single progenitors to produce reserve progeny. Dev Biol, 340(2):330–43, 4 2010.

[11] Kavitha Mukund and Shankar Subramaniam. Skeletal muscle: A review of molecular structure and function, in health and disease. WIREs Systems Biology and Medicine, 12(1), 2020.

[12] N. Amy Yewdall, Alexander F. Mason, and Jan C. M. Van Hest. The hallmarks of living systems: towards creating artificial cells. Interface Focus, 8(5):20180023, 2018.

[13] Arul Subramanian and Thomas F. Schilling. Tendon development and musculoskeletal assembly: emerging roles for the extracellular matrix. Development, 142(24):4191–4204, 2015.

[14] James G. Tidball and S. Armando Villalta. Regulatory interactions between muscle and the immune system during muscle regeneration. American Journal of Physiology-Regulatory, Integrative and Comparative Physiology, 298(5):R1173–R1187, 2010.

[15] Beatrice Biferali, Daisy Proietti, Chiara Mozzetta, and Luca Madaro. Fibro–adipogenic progenitors cross-talk in skeletal muscle: The social network. Frontiers in Physiology, 10:1074, 2019.

[16] Minchul Kim, Vedran Franke, Bettina Brandt, Elijah D. Lowenstein, Verena Schöwel, Simone Spuler, Altuna Akalin, and Carmen Birchmeier. Single-nucleus transcriptomics reveals functional compartmentalization in syncytial skeletal muscle cells. Nature Communications, 11(1):6375, 12 2020.

[17] Aliza B Rubenstein, Gregory R Smith, Ulrika Raue, Gwénaëlle Begue, Kiril Minchev, Frederique Ruf-Zamojski, Venugopalan D Nair, Xingyu Wang, Lan Zhou, Elena Zaslavsky, et al. Single-cell transcriptional profiles in human skeletal muscle. Scientific reports, 10(1):229, 2020.

[18] Qingnian Goh, Taejeong Song, Michael J Petrany, Alyssa AW Cramer, Chengyi Sun, Sakthivel Sadayappan, Se-Jin Lee, and Douglas P Millay. Myonuclear accretion is a determinant of exercise-induced remodeling in skeletal muscle. eLife, 8:e44876, 2019. Publisher: eLife Sciences Publications, Ltd.

[19] Alyssa AW Cramer, Vikram Prasad, Einar Eftestøl, Taejeong Song, Kenth-Arne Hansson, Hannah F Dugdale, Sakthivel Sadayappan, Julien Ochala, Kristian Gundersen, and Douglas P Millay. Nuclear numbers in syncytial muscle fibers promote size but limit the development of larger myonuclear domains. Nature communications, 11(1):6287, 2020.

[20] Michael J. Petrany, Casey O. Swoboda, Chengyi Sun, Kashish Chetal, Xiaoting Chen, Matthew T. Weirauch, Nathan Salomonis, and Douglas P. Millay. Single-nucleus rna-seq identifies transcriptional heterogeneity in multinucleated skeletal myofibers. Nature Communications, 11(1):6374, 12 2020.

[21] Matthieu Dos Santos, Stéphanie Backer, Benjamin Saintpierre, Brigitte Izac, Muriel Andrieu, Franck Letourneur, Frederic Relaix, Athanassia Sotiropoulos, and Pascal Maire. Single-nucleus RNA-seq and FISH identify coordinated transcriptional activity in mammalian myofibers. Nature Communications, 11(1):5102, 12 2020.

[22] Yuan Wen, Davis A. Englund, Bailey D. Peck, Kevin A. Murach, John J. McCarthy, and Charlotte A. Peterson. Myonuclear transcriptional dynamics in response to exercise following satellite cell depletion. iScience, 24(8):102838, 8 2021.

[23] AB Knudsen, M Larsen, AL Mackey, M Hjort, KK Hansen, K Qvortrup, M Kjaer, and MR Krogsgaard. The human myotendinous junction: An ultrastructural and 3 d analysis study. Scandinavian journal of medicine & science in sports, 25(1):e116–e123, 2015.

[24] Marta Gonzalez-Freire, Rafael de Cabo, Stephanie A Studenski, and Luigi Ferrucci. The neuromuscular junction: aging at the crossroad between nerves and muscle. Frontiers in aging neuroscience, 6:208, 2014.

[25] Steven J Burden, Maartje G Huijbers, and Leonor Remedio. Fundamental molecules and mechanisms for forming and maintaining neuromuscular synapses. International journal of molecular sciences, 19(2):490, 2018.

[26] Caroline Ketterer, Ulrike Zeiger, Murat T. Budak, Neal A. Rubinstein, and Tejvir S. Khurana. Identification of the neuromuscular junction transcriptome of extraocular muscle by laser capture microdissection. Investigative Opthalmology & Visual Science, 51(9):4589, 2010.

[27] B. Charvet, A. Guiraud, M. Malbouyres, D. Zwolanek, E. Guillon, S. Bretaud, C. Monnot, J. Schulze, H. L. Bader, B. Allard, M. Koch, and F. Ruggiero. Knockdown of col22a1 gene in zebrafish induces a muscular dystrophy by disruption of the myotendinous junction. Development, 140(22):4602–4613, 2013.

[28] Markus A Ruegg. Organization of synaptic myonuclei by syne proteins and their role during the formation of the nerve–muscle synapse. Proceedings of the National Academy of Sciences, 102(16):5643–5644, 2005.

[29] Emilie Barruet, Steven M Garcia, Katharine Striedinger, Jake Wu, Solomon Lee, Lauren Byrnes, Alvin Wong, Sun Xuefeng, Stanley Tamaki, Andrew S Brack, et al. Functionally heterogeneous human satellite cells identified by single cell rna sequencing. Elife, 9:e51576, 2020.

[30] Christoph Lepper, Terence A Partridge, and Chen-Ming Fan. An absolute requirement for Pax7-positive satellite cells in acute injury-induced skeletal muscle regeneration. Development, 138(17):3639–46, 9 2011.

[31] Malea M Murphy, Jennifer A Lawson, Sam J Mathew, David A Hutcheson, and Gabrielle Kardon. Satellite cells, connective tissue fibroblasts and their interactions are crucial for muscle regeneration. Development, 138(17):3625–37, 9 2011.

[32] A. Mauro. Satellite cell of skeletal muscle fibers. J Biophys Biochem Cytol, 9:493–5, 1961.

[33] Hang Yin, Feodor Price, and Michael A Rudnicki. Satellite cells and the muscle stem cell niche. Physiological reviews, 93(1):23–67, 2013.

[34] Karin C Lilja, Nan Zhang, Alessandro Magli, Volkan Gunduz, Christopher J Bowman, Robert W Arpke, Radbod Darabi, Michael Kyba, Rita Perlingeiro, and Brian D Dynlacht. Pax7 remodels the chromatin landscape in skeletal muscle stem cells. PLoS One, 12(4):e0176190, 2017.

[35] Kfir Baruch Umansky, Yael Gruenbaum-Cohen, Michael Tsoory, Ester Feldmesser, Dalia Goldenberg, Ori Brenner, and Yoram Groner. Runx1 transcription factor is required for myoblasts proliferation during muscle regeneration. PLoS Genetics, 11(8), 8 2015. PMID: 26275053 PMCID: PMC4537234.

[36] M. Buckingham and S. Tajbakhsh. Expression of myogenic factors in the mouse: myf-5, the first member of the MyoD gene family to be transcribed during skeletal myogenesis. C R Acad Sci III, 316(9):1032–46, 1993.

[37] Annarita Scaramozza, Dongsu Park, Swapna Kollu, Isabel Beerman, Xuefeng Sun, Derrick J Rossi, Charles P Lin, David T Scadden, Colin Crist, and Andrew S Brack. Lineage tracing

reveals a subset of reserve muscle stem cells capable of clonal expansion under stress. Cell stem cell, 24(6):944–957, 2019.

[38] Laura Forcina, Marianna Cosentino, and Antonio Musarò. Mechanisms regulating muscle regeneration: insights into the interrelated and time-dependent phases of tissue healing. Cells, 9(5):1297, 2020.

[39] Micah T. Webster, Uri Manor, Jennifer Lippincott-Schwartz, and Chen-Ming Fan. Intravital imaging reveals ghost fibers as architectural units guiding myogenic progenitors during regeneration. Cell Stem Cell, 18(2), 2016.

[40] Stefano Schiaffino, Alberto C. Rossi, Vika Smerdu, Leslie A. Leinwand, and Carlo Reggiani. Developmental myosins: expression patterns and functional significance. Skeletal Muscle, 5(1):22, 2015.

[41] Francesco Chemello, Camilla Bean, Pasqua Cancellara, Paolo Laveder, Carlo Reggiani, and Gerolamo Lanfranchi. Microgenomic analysis in skeletal muscle: Expression signatures of individual fast and slow myofibers. PLoS ONE, 6(2):e16807, 2011.

[42] Yuki Yoshimoto, Madoka Ikemoto-Uezumi, Keisuke Hitachi, So-ichiro Fukada, and Akiyoshi Uezumi. Methods for accurate assessment of myofiber maturity during skeletal muscle regeneration. Frontiers in Cell and Developmental Biology, 8:267, 4 2020.

[43] Eric S. Folker and Mary K. Baylies. Nuclear positioning in muscle development and disease. Frontiers in Physiology, 4, 2013.

[44] William Roman and Edgar R. Gomes. Nuclear positioning in skeletal muscle. Seminars in Cell & Developmental Biology, 82:51–56, 2018.

[45] James R Bagley, Lance T Denes, John J McCarthy, Eric T Wang, and Kevin A Murach. The myonuclear domain in adult skeletal muscle fibres: Past, present, and future. The Journal of Physiology, 2023.

[46] Jianming Liu, Zhan-Peng Huang, Mao Nie, Gang Wang, William J Silva, Qiumei Yang, Paula P Freire, Xiaoyun Hu, Huaqun Chen, Zhongliang Deng, et al. Regulation of myonuclear positioning and muscle function by the skeletal muscle-specific cip protein. Proceedings of the National Academy of Sciences, 117(32):19254–19265, 2020.

[47] Charlotte A Collins and Terence A Partridge. Self-renewal of the adult skeletal muscle satellite cell. Cell Cycle, 4(10):1338–41, 10 2005.

[48] Peter Feige, Caroline E. Brun, Morten Ritso, and Michael A. Rudnicki. Orienting muscle stem cells for regeneration in homeostasis, aging, and disease. Cell Stem Cell, 23(5):653–664, 2018.

[49] Alicia A. Cutler, Bradley Pawlikowski, Joshua R. Wheeler, Nicole Dalla Betta, Tiffany Elston, Rebecca O'Rourke, Kenneth Jones, and Bradley B. Olwin. The regenerating skeletal muscle niche drives satellite cell return to quiescence. iScience, 25(6):104444, 6 2022.

[50] Shihuan Kuang, Kazuki Kuroda, Fabien Le Grand, and Michael A Rudnicki. Asymmetric self-renewal and commitment of satellite stem cells in muscle. Cell, 129(5):999–1010, 6 2007.

[51] H. C. Olguin and B. B. Olwin. Pax-7 up-regulation inhibits myogenesis and cell cycle progression in satellite cells: a potential mechanism for self-renewal. Dev Biol, 275(2):375–88, 11 2004.

[52] Matthew T. Tierney, Michael J. Stec, Steffen Rulands, Benjamin D. Simons, and Alessandra Sacco. Muscle stem cells exhibit distinct clonal dynamics in response to tissue repair and homeostatic aging. Cell Stem Cell, 22(1):119–127.e3, 2018.

[53] Cédric Blanpain and Benjamin D. Simons. Unravelling stem cell dynamics by lineage tracing. Nature Reviews Molecular Cell Biology, 14(8):489–502, 2013.

[54] Eric D Bankaitis, Andrew Ha, Calvin J Kuo, and Scott T Magness. Reserve stem cells in intestinal homeostasis and injury. Gastroenterology, 155(5):1348–1361, 2018.

[55] Alicia L Connor, Philip M Kelley, and Richard M Tempero. Invariant asymmetry renews the lymphatic vasculature during homeostasis. Journal of Translational Medicine, 14:1–11, 2016.

[56] Yoshitatsu Sei, Jianying Feng, Carson C Chow, and Stephen A Wank. Asymmetric cell division-dominant neutral drift model for normal intestinal stem cell homeostasis. American Journal of Physiology-Gastrointestinal and Liver Physiology, 316(1):G64–G74, 2019.

[57] Carlos Lopez-Garcia, Allon M Klein, Benjamin D Simons, and Douglas J Winton. Intestinal stem cell replacement follows a pattern of neutral drift. Science, 330(6005):822–825, 2010.

[58] Sahand Hormoz. Stem cell population asymmetry can reduce rate of replicative aging. Journal of theoretical biology, 331:19–27, 2013.

[59] Daniel Kalderon. Investigating adult stem cells through lineage analyses. Stem cell reviews and reports, pages 1–21, 2022.

[60] Richard Bischoff and Catherine Heintz. Enhancement of skeletal muscle regeneration. Developmental Dynamics, 201(1):41–54, 1994.

[61] Norio Motohashi and Atsushi Asakura. Muscle satellite cell heterogeneity and self-renewal. Frontiers in cell and developmental biology, 2:1, 2014.

[62] Joe V. Chakkalakal, Josef Christensen, Wanyi Xiang, Mathew T. Tierney, Francesca S. Boscolo, Alessandra Sacco, and Andrew S. Brack. Early forming label-retaining muscle stem cells require p27kip1 for maintenance of the primitive state. Development, 141(8):1649–1659, 2014.

[63] John Saber, Alexander Y.T. Lin, and Michael A. Rudnicki. Single-cell analyses uncover granularity of muscle stem cells. F1000Research, 9:31, 2020.

[64] Pierre Rocheteau, Barbara Gayraud-Morel, Irene Siegl-Cachedenier, Maria A. Blasco, and Shahragim Tajbakhsh. A subpopulation of adult skeletal muscle stem cells retains all template DNA strands after cell division. Cell, 148(1):112–125, 2012.

[65] Matthew T Tierney and Alessandra Sacco. Satellite cell heterogeneity in skeletal muscle homeostasis. Trends in cell biology, 26(6):434–444, 2016.

[66] F. Relaix, M. Bencze, M. J. Borok, A. Der Vartanian, F. Gattazzo, D. Mademtzoglou, S. Perez-Diaz, A. Prola, P. C. Reyes-Fernandez, A. Rotini, and Taglietti. Perspectives on skeletal muscle stem cells. Nature Communications, 12(1):692, 2021.

[67] Alessandro Cellerino and Alessandro Ori. What have we learned on aging from omics studies? Seminars in Cell & Developmental Biology, 70:177–189, 2017.

[68] João Pedro De Magalhães, João Curado, and George M. Church. Meta-analysis of age-related gene expression profiles identifies common signatures of aging. Bioinformatics, 25(7):875–881, 2009.

[69] Thomas Stoeger, Rogan A. Grant, Alexandra C. McQuattie-Pimentel, Kishore R. Anekalla, Sophia S. Liu, Heliodoro Tejedor-Navarro, Benjamin D. Singer, Hiam Abdala-Valencia, Michael Schwake, Marie-Pier Tetreault, Harris Perlman, William E. Balch, Navdeep S. Chandel, Karen M. Ridge, Jacob I. Sznajder, Richard I. Morimoto, Alexander V. Misharin, G. R. Scott Budinger, and Luis A. Nunes Amaral. Aging is associated with a systemic length-associated transcriptome imbalance. Nature Aging, 2022.

[70] Rachel McCormick and Aphrodite Vasilaki. Age-related changes in skeletal muscle: changes to life-style as a therapy. Biogerontology, 19(6):519–536, 2018.

[71] Youngmok C. Jang and Holly Van Remmen. Age-associated alterations of the neuromuscular junction. Experimental Gerontology, 46(2):193–198, 2011.

[72] Kathrine B Nielsen, Navneet N Lal, and Philip W Sheard. Age-related remodelling of the myotendinous junction in the mouse soleus muscle. Experimental Gerontology, 104:52–59, 2018.

[73] Wenxuan Liu, Alanna Klose, Sophie Forman, Nicole D. Paris, Lan Wei-LaPierre, Mariela Cortés-Lopéz, Aidi Tan, Morgan Flaherty, Pedro Miura, Robert T. Dirksen, and Joe V. Chakkalakal. Loss of adult skeletal muscle stem cells drives age-related neuromuscular junction degeneration. eLife, 6:e26464, 6 2017.

[74] J. D. Bernet, J. D. Doles, J. K. Hall, K. Kelly Tanaka, T. A. Carter, and B. B. Olwin. p38 MAPK signaling underlies a cell-autonomous loss of stem cell self-renewal in skeletal muscle of aged mice. Nat Med, 20(3):265–71, 3 2014.

[75] A S Brack and T A Rando. Intrinsic changes and extrinsic influences of myogenic stem cell function during aging. Stem Cell Reviews and Reports, 3(3):226–237, 2007.

[76] Irina M Conboy, Michael J Conboy, Gayle M Smythe, and Thomas A Rando. Notch-mediated restoration of regenerative potential to aged muscle. Science, 302(5650):1575–7, 11 2003.

[77] Ju Li, Suhyoun Han, Wendy Cousin, and Irina M Conboy. Age-specific functional epigenetic changes in p21 and p16 in injury-activated satellite cells. Stem Cells, 33(3):951–61, 3 2015.

[78] Feodor D Price, Julia von Maltzahn, C Florian Bentzinger, Nicolas A Dumont, Hang Yin, Natasha C Chang, David H Wilson, Jérôme Frenette, and Michael A Rudnicki. Inhibition of jak-stat signaling stimulates adult satellite cell function. Nat Med, 20(10):1174–81, 10 2014.

[79] Michelle Rozo, Liangji Li, and Chen-Ming Fan. Targeting β1-integrin signaling enhances regeneration in aged and dystrophic muscle in mice. Nat Med, 22(8):889–96, 8 2016.

[80] Gabi Shefer, Daniel P Van de Mark, Joshua B Richardson, and Zipora Yablonka-Reuveni. Satellite-cell pool size does matter: defining the myogenic potency of aging skeletal muscle. Dev Biol, 294(1):50–66, 6 2006.

[81] Matthew Timothy Tierney, Tufan Aydogdu, David Sala, Barbora Malecova, Sole Gatto, Pier Lorenzo Puri, Lucia Latella, and Alessandra Sacco. Stat3 signaling controls satellite cell expansion and skeletal muscle repair. Nature Medicine, 20(10):1182–1186, 10 2014.

[82] Z. Yablonka-Reuveni, R. Seger, and A J Rivera. Fibroblast growth factor promotes recruitment of skeletal muscle satellite cells in young and old rats. J Histochem Cytochem, 47(1):23–42, 1 1999.

[83] Korin Sahinyan, Felicia Lazure, Darren M Blackburn, and Vahab D Soleimani. Decline of regenerative potential of old muscle stem cells: contribution to muscle aging. The FEBS Journal, 290(5):1267–1289, 2023.

[84] Hiroyuki Yamakawa, Dai Kusumoto, Hisayuki Hashimoto, and Shinsuke Yuasa. Stem cell aging in skeletal muscle regeneration and disease. International Journal of Molecular Sciences, 21(5):1830, 2020.

[85] Jacob C. Kimmel, Nelda Yi, Margaret Roy, David G. Hendrickson, and David R. Kelley. Differentiation reveals latent features of aging and an energy barrier in murine myogenesis. Cell Reports, 35(4):109046, 2021.

[86] Jacob C. Kimmel, Ara B. Hwang, Annarita Scaramozza, Wallace F. Marshall, and Andrew S. Brack. Aging induces aberrant state transition kinetics in murine muscle stem cells. Development, page dev.183855, 2020.

[87] Antoine De Morree and Thomas A. Rando. Regulation of adult stem cell quiescence and its functions in the maintenance of tissue integrity. Nature Reviews Molecular Cell Biology, 24(5):334–354, 2023.

[88] Liangyu Mi, Junping Hu, Na Li, Jinfang Gao, Rongxiu Huo, Xinyue Peng, Na Zhang, Ying Liu, Hanxi Zhao, Ruiling Liu, Liyun Zhang, and Ke Xu. The mechanism of stem cell aging. Stem Cell Reviews and Reports, 18(4):1281–1293, 2022.

[89] Anne Brunet, Margaret A Goodell, and Thomas A Rando. Ageing and rejuvenation of tissue stem cells and their niches. Nature Reviews Molecular Cell Biology, pages 1–18, 2022.

[90] Justus M Kebschull and Anthony M Zador. Cellular barcoding: lineage tracing, screening and beyond. Nature methods, 15(11):871–879, 2018.

[91] Cheng Chen, Yuanxin Liao, and Guangdun Peng. Connecting past and present: single-cell lineage tracing. Protein & Cell, 13(11):790–807, 2022.

[92] Vijay G. Sankaran, Jonathan S. Weissman, and Leonard I. Zon. Cellular barcoding to decipher clonal dynamics in disease. Science, 378(6616):eabm5874, 2022.

[93] Tamar Tak, Almut S Eisele, and Leïla Perié. In vivo tracking of hematopoietic stem and progenitor cell ontogeny by cellular barcoding. In Bone Marrow Environment: Methods and Protocols, pages 281–300. Springer, 2021.

[94] Lars Thielecke, Tim Aranyossy, Andreas Dahl, Rajiv Tiwari, Ingo Roeder, Hartmut Geiger, Boris Fehse, Ingmar Glauche, and Kerstin Cornils. Limitations and challenges of genetic barcode quantification. Scientific Reports, 7(1):43249, 2017.

[95] Cristina Parigini and Philip Greulich. Universality of clonal dynamics poses fundamental limits to identify stem cell self-renewal strategies. eLife, 9:e56532, 2020.

[96] Fatemah Chehrehasa, Adrian CB Meedeniya, Patrick Dwyer, Greger Abrahamsen, and Alan Mackay-Sim. Edu, a new thymidine analogue for labelling proliferating cells in the nervous system. Journal of neuroscience methods, 177(1):122–130, 2009.

[97] Vasily Shinin, Barbara Gayraud-Morel, Danielle Gomès, and Shahragim Tajbakhsh. Asymmetric division and cosegregation of template dna strands in adult muscle satellite cells. Nature cell biology, 8(7):677–682, 2006.

[98] Charles Bramlett, Du Jiang, Anna Nogalska, Jiya Eerdeng, Jorge Contreras, and Rong Lu. Clonal tracking using embedded viral barcoding and high-throughput sequencing. Nature protocols, 15(4):1436–1458, 2020.

[99] Frauke Gotzhein, Tim Aranyossy, Lars Thielecke, Tanja Sonntag, Vanessa Thaden, Boris Fehse, Ingo Müller, Ingmar Glauche, and Kerstin Cornils. The reconstitution dynamics of cultivated hematopoietic stem cells and progenitors is independent of age. International Journal of Molecular Sciences, 23(6):3160, 2022.

[100] Leanne G Ahronian and Brian C Lewis. Using the rcas-tva system to model human cancer in mice. Cold Spring Harbor Protocols, 2014(11):pdb–top069831, 2014.

[101] Janet Schaefer-Klein, Iris Givol, Eugene V Barsov, Jeannette M Whitcomb, Matthew Van-Brocklin, Douglas N Foster, Mark J Federspiel, and Stephen H Hughes. The ev-o-derived cell line df-1 supports the efficient replication of avian leukosis-sarcoma viruses and vectors. Virology, 248(2):305–311, 1998.

[102] Barbara Seidler, Annegret Schmidt, Ulrich Mayr, Hassan Nakhai, Roland M Schmid, Günter Schneider, and Dieter Saur. A cre-loxp-based mouse model for conditional somatic gene expression and knockdown in vivo by using avian retroviral vectors. Proceedings of the National Academy of Sciences, 105(29):10137–10142, 2008.

[103] M. A. Hausburg, J. D. Doles, S. L. Clement, A. B. Cadwallader, M. N. Hall, P. J. Blackshear, J. Lykke-Andersen, and B. B. Olwin. Post-transcriptional regulation of satellite cell quiescence by TTP-mediated mRNA decay. Elife, 4:e03390, 2015.

[104] Yu Xin Wang, Peter Feige, Caroline E. Brun, Bahareh Hekmatnejad, Nicolas A. Dumont, Jean-Marc Renaud, Sharlene Faulkes, Daniel E. Guindon, and Michael A. Rudnicki. Egfr-aurka signaling rescues polarity and regeneration defects in dystrophin-deficient muscle stem cells by increasing asymmetric divisions. Cell Stem Cell, 0(0), 1 2019. PMID: 30713094.

[105] R. W. Hamming. Error detecting and error correcting codes. The Bell System Technical Journal, 29(2):147–160, 1950.

[106] Lukáš Havrlant and Vladik Kreinovich. A simple probabilistic explanation of term frequency-inverse document frequency (tf-idf) heuristic (and variations motivated by this explanation). International Journal of General Systems, 46(1):27–36, 2017.

[107] Zipora Yablonka-Reuveni, Maria E Danoviz, Michael Phelps, and Pascal Stuelsatz. Myogenic-specific ablation of fgfr1 impairs FGF2-mediated proliferation of satellite cells at the myofiber niche but does not abolish the capacity for muscle regeneration. Frontiers in Aging Neuroscience, 7:85, 2015. PMID: 26074812 PMCID: PMC4446549.

[108] Brendan Evano, Sara Khalilian, Gilles Le Carrou, Genevieve Almouzni, and Shahragim Tajbakhsh. Dynamics of asymmetric and symmetric divisions of muscle stem cells in vivo and on artificial niches. Cell reports, 30(10):3195–3206, 2020.

[109] Benjamin D Simons and Hans Clevers. Strategies for homeostatic stem cell self-renewal in adult tissues. Cell, 145(6):851–862, 2011.

[110] Lemonia Chatzeli and Benjamin D. Simons. Tracing the dynamics of stem cell fate. Cold Spring Harbor Perspectives in Biology, 12(6):a036202, 2020.

[111] Shihuan Kuang, Sophie B Chargé, Patrick Seale, Michael Huh, and Michael A Rudnicki. Distinct roles for pax7 and pax3 in adult regenerative myogenesis. The Journal of cell biology, 172(1):103–113, 2006.

[112] Audrey Der Vartanian, Marie Quétin, Stéphanie Michineau, Frédéric Auradé, Shinichiro Hayashi, Christelle Dubois, Didier Rocancourt, Bernadette Drayton-Libotte, Anikó Szegedi, Margaret Buckingham, et al. Pax3 confers functional heterogeneity in skeletal muscle stem cell responses to environmental stress. Cell stem cell, 24(6):958–973, 2019.

[113] Caroline E Brun, Marie-Claude Sincennes, Alexander YT Lin, Derek Hall, William Jarassier, Peter Feige, Fabien Le Grand, and Michael A Rudnicki. Gli3 regulates muscle stem cell entry into galert and self-renewal. Nature Communications, 13(1):3961, 2022.

[114] Thomas Laumonier, Flavien Bermont, Pierre Hoffmeyer, Vincent Kindler, and Jacques Menetrey. Human myogenic reserve cells are quiescent stem cells that contribute to muscle regeneration after intramuscular transplantation in immunodeficient mice. Scientific reports, 7(1):3462, 2017.

[115] Henry E Young, Cecile Duplaa, Marina Romero-Ramos, Marie-Francoise Chesselet, Patrick Vourc'h, Michael J Yost, Kurt Ericson, Louis Terracio, Takayuki Asahara, Haruchika Masuda, et al. Adult reserve stem cells and their potential for tissue engineering. Cell biochemistry and biophysics, 40:1–80, 2004.

[116] Eric D Bankaitis, Andrew Ha, Calvin J Kuo, and Scott T Magness. Reserve stem cells in intestinal homeostasis and injury. Gastroenterology, 155(5):1348–1361, 2018.

[117] Jesse V. Kurland, Alicia A. Cutler, Jacob T. Stanley, Nicole Dalla Betta, Ashleigh Van Deusen, Brad Pawlikowski, Monica Hall, Tiffany Antwine, Alan Russell, Mary Ann Allen, Robin Dowell, and Bradley Olwin. Aging disrupts gene expression timing during muscle regeneration. Stem Cell Reports, 18(6):1325–1339, 2023.

[118] Fabio Demontis, Rosanna Piccirillo, Alfred L. Goldberg, and Norbert Perrimon. Mechanisms of skeletal muscle aging: insights from *Drosophila* and mammalian models. Disease Models & Mechanisms, page dmm.012559, 2013.

[119] Ramkumar Sambasivan, Roseline Yao, Adrien Kissenpfennig, Laetitia Van Wittenberghe, Andras Paldi, Barbara Gayraud-Morel, Hind Guenou, Bernard Malissen, Shahragim Tajbakhsh, and Anne Galy. Pax7-expressing satellite cells are indispensable for adult skeletal muscle regeneration. Development, 138(17):3647–56, 2011.

[120] Mohsen Afshar Bakooshli, Ethan S Lippmann, Ben Mulcahy, Nisha Iyer, Christine T Nguyen, Kayee Tung, Bryan A Stewart, Hubrecht van den Dorpel, Tobias Fuehrmann, Molly Shoichet, Anne Bigot, Elena Pegoraro, Henry Ahn, Howard Ginsberg, Mei Zhen, Randolph Scott Ashton, and Penney M Gilbert. A 3D culture model of innervated human skeletal muscle enables studies of the adult neuromuscular junction. eLife, 8:e44530, 5 2019.

[121] Frederic Dessauge, Cindy Schleder, Marie-Hélène Perruchot, and Karl Rouger. 3D in vitro models of skeletal muscle: myopshere, myobundle and bioprinted muscle construct. Veterinary Research, 52(1):72, 12 2021.

[122] David W. McKellar, Lauren D. Walter, Leo T. Song, Madhav Mantri, Michael F. Z. Wang, Iwijn De Vlaminck, and Benjamin D. Cosgrove. Large-scale integration of single-cell transcriptomic data captures transitional progenitor states in mouse skeletal muscle regeneration. Communications Biology, 4(1):1280, 12 2021.

[123] Katherine Williams, Kyoko Yokomori, and Ali Mortazavi. Heterogeneous skeletal muscle cell and nucleus populations identified by single-cell and single-nucleus resolution transcriptome assays. Frontiers in Genetics, 13:835099, 2022.

[124] Jeffrey R. Moffitt, Emma Lundberg, and Holger Heyn. The emerging landscape of spatial profiling technologies. Nature Reviews Genetics, 7 2022. [Online; accessed 2022-07-26].

[125] Manuel Schmidt, Svenja C. Schüler, Sören S. Hüttner, Björn von Eyss, and Julia von Maltzahn. Adult stem cells at work: regenerating skeletal muscle. Cellular and Molecular Life Sciences, 76(13):2559–2570, 2019.

[126] John Trinick. Understanding the functions of titin and nebulin. FEBS Letters, 307(1):44–48, 7 1992.

[127] Abigail Woodfin, Mathieu-Benoit Voisin, and Sussan Nourshargh. PECAM-1: A multifunctional molecule in inflammation and vascular biology. Arteriosclerosis, Thrombosis, and Vascular Biology, 27(12):2514–2523, 12 2007.

[128] Alma Zernecke, Jürgen Bernhagen, and Christian Weber. Macrophage migration inhibitory factor in cardiovascular disease. Circulation, 117(12):1594–1602, 3 2008.

[129] The Gene Ontology Consortium, Seth Carbon, Eric Douglass, Benjamin M Good, Deepak R Unni, Nomi L Harris, Christopher J Mungall, Siddartha Basu, Rex L Chisholm, Robert J Dodson, Eric Hartline, Petra Fey, Paul D Thomas, Laurent-Philippe Albou, Dustin Ebert, Michael J Kesling, Huaiyu Mi, Anushya Muruganujan, Xiaosong Huang, Tremayne Mushayahama, Sandra A LaBonte, Deborah A Siegele, Giulia Antonazzo, Helen Attrill, Nick H Brown, Phani Garapati, Steven J Marygold, Vitor Trovisco, Gil dos Santos, Kathleen Falls, Christopher Tabone, Pinglei Zhou, Joshua L Goodman, Victor B Strelets, Jim Thurmond, Penelope Garmiri, Rizwan Ishtiaq, Milagros Rodríguez-López, Marcio L Acencio, Martin Kuiper, Astrid Lægreid, Colin Logie, Ruth C Lovering, Barbara Kramarz, Shirin C C Saverimuttu,

Sandra M Pinheiro, Heather Gunn, Renzhi Su, Katherine E Thurlow, Marcus Chibucos, Michelle Giglio, Suvarna Nadendla, James Munro, Rebecca Jackson, Margaret J Duesbury, Noemi Del-Toro, Birgit H M Meldal, Kalpana Paneerselvam, Livia Perfetto, Pablo Porras, Sandra Orchard, Anjali Shrivastava, Hsin-Yu Chang, Robert Daniel Finn, Alexander Lawson Mitchell, Neil David Rawlings, Lorna Richardson, Amaia Sangrador-Vegas, Judith A Blake, Karen R Christie, Mary E Dolan, Harold J Drabkin, David P Hill, Li Ni, Dmitry M Sitnikov, Midori A Harris, Stephen G Oliver, Kim Rutherford, Valerie Wood, Jaqueline Hayles, Jürg Bähler, Elizabeth R Bolton, Jeffery L De Pons, Melinda R Dwinell, G Thomas Hayman, Mary L Kaldunski, Anne E Kwitek, Stanley J F Laulederkind, Cody Plasterer, Marek A Tutaj, Mahima Vedi, Shur-Jen Wang, Peter D'Eustachio, Lisa Matthews, James P Balhoff, Suzi A Aleksander, Michael J Alexander, J Michael Cherry, Stacia R Engel, Felix Gondwe, Kalpana Karra, Stuart R Miyasato, Robert S Nash, Matt Simison, Marek S Skrzypek, Shuai Weng, Edith D Wong, Marc Feuermann, Pascale Gaudet, Anne Morgat, Erica Bakker, Tanya Z Berardini, Leonore Reiser, Shabari Subramaniam, Eva Huala, Cecilia N Arighi, Andrea Auchincloss, Kristian Axelsen, Ghislaine Argoud-Puy, Alex Bateman, Marie-Claude Blatter, Emmanuel Boutet, Emily Bowler, Lionel Breuza, Alan Bridge, Ramona Britto, Hema Bye-A-Jee, Cristina Casals Casas, Elisabeth Coudert, Paul Denny, Anne Estreicher, Maria Livia Famiglietti, George Georghiou, Arnaud Gos, Nadine Gruaz-Gumowski, Emma Hatton-Ellis, Chantal Hulo, Alexandr Ignatchenko, Florence Jungo, Kati Laiho, Philippe Le Mercier, Damien Lieberherr, Antonia Lock, Yvonne Lussi, Alistair MacDougall, Michele Magrane, Maria J Martin, Patrick Masson, Darren A Natale, Nevila Hyka-Nouspikel, Sandra Orchard, Ivo Pedruzzi, Lucille Pourcel, Sylvain Poux, Sangya Pundir, Catherine Rivoire, Elena Speretta, Shyamala Sundaram, Nidhi Tyagi, Kate Warner, Rossana Zaru, Cathy H Wu, Alexander D Diehl, Juancarlos N Chan, Christian Grove, Raymond Y N Lee, Hans-Michael Muller, Daniela Raciti, Kimberly Van Auken, Paul W Sternberg, Matthew Berriman, Michael Paulini, Kevin Howe, Sibyl Gao, Adam Wright, Lincoln Stein, Douglas G Howe, Sabrina Toro, Monte Westerfield, Pankaj Jaiswal, Laurel Cooper, and Justin Elser. The gene ontology resource: enriching a GOld mine. Nucleic Acids Research, 49(D1):D325–D334, 1 2021.

[130] Stamatia Gioftsidi, Frederic Relaix, and Philippos Mourikis. The Notch signaling network in muscle stem cells during development, homeostasis, and disease. Skeletal Muscle, 12(1):9, 12 2022.

[131] Fabien Le Grand, Raphaëlle Grifone, Philippos Mourikis, Christophe Houbron, Carine Gigaud, Julien Pujol, Marjorie Maillet, Gilles Pagès, Michael Rudnicki, Shahragim Tajbakhsh, and Pascal Maire. Six1 regulates stem cell repair potential and self-renewal during skeletal muscle regeneration. Journal of Cell Biology, 198(5):815–832, 9 2012.

[132] B. B. Olwin, K. Arthur, K. Hannon, P. Hein, A. McFall, B. Riley, G. Szebenyi, Z. Zhou, M. E. Zuber, A. C. Rapraeger, and et al. Role of FGFs in skeletal muscle and limb development. Mol Reprod Dev, 39(1):90–100; discussion 100–1, 9 1994.

[133] Xiaojie Qiu, Qi Mao, Ying Tang, Li Wang, Raghav Chawla, Hannah Pliner, and Cole Trapnell. Reversed graph embedding resolves complex single-cell developmental trajectories. Genomics, 2 2017. DOI: 10.1101/110668.

[134] Cole Trapnell, Davide Cacchiarelli, Jonna Grimsby, Prapti Pokharel, Shuqiang Li, Michael Morse, Niall J Lennon, Kenneth J Livak, Tarjei S Mikkelsen, and John L Rinn. The dynamics

and regulators of cell fate decisions are revealed by pseudotemporal ordering of single cells. Nature Biotechnology, 32(4):381–386, 4 2014.

[135] Peter S Zammit, Frederic Relaix, Yosuke Nagata, Ana Pérez Ruiz, Charlotte A Collins, Terence A Partridge, and Jonathan R Beauchamp. Pax7 and myogenic progression in skeletal muscle satellite cells. J Cell Sci, 119(Pt 9):1824–32, 5 2006.

[136] Douglas P. Millay, Jason R. O'Rourke, Lillian B. Sutherland, Svetlana Bezprozvannaya, John M. Shelton, Rhonda Bassel-Duby, and Eric N. Olson. Myomaker is a membrane activator of myoblast fusion and muscle formation. Nature, 499(7458):301–305, 7 2013.

[137] Koen Van den Berge, Hector Roux de Bézieux, Kelly Street, Wouter Saelens, Robrecht Cannoodt, Yvan Saeys, Sandrine Dudoit, and Lieven Clement. Trajectory-based differential expression analysis for single-cell sequencing data. Nature Communications, 11(1):1201, 12 2020.

[138] Sipko van Dam, Urmo Võsa, Adriaan van der Graaf, Lude Franke, and João Pedro de Magalhães. Gene co-expression analysis for functional classification and gene–disease predictions. Briefings in Bioinformatics, page bbw139, 1 2017.

[139] Valeria Fionda. Networks in biology. In Encyclopedia of Bioinformatics and Computational Biology, pages 915–921. Elsevier, 2019. DOI: 10.1016/B978-0-12-809633-8.20420-2.

[140] Tim Stuart, Andrew Butler, Paul Hoffman, Christoph Hafemeister, Efthymia Papalexi, William M. Mauck, Yuhan Hao, Marlon Stoeckius, Peter Smibert, and Rahul Satija. Comprehensive integration of single-cell data. Cell, 177(7):1888–1902.e21, 2019. Publisher: Elsevier.

[141] Wencheng Yin, Luis Mendoza, Jimena Monzon-Sandoval, Araxi O. Urrutia, and Humberto Gutierrez. Emergence of co-expression in gene regulatory networks. PLOS ONE, 16(4):e0247671, 4 2021.

[142] Alexander Lachmann, Denis Torre, Alexandra B. Keenan, Kathleen M. Jagodnik, Hoyjin J. Lee, Lily Wang, Moshe C. Silverstein, and Avi Ma'ayan. Massive mining of publicly available RNA-seq data from human and mouse. Nature Communications, 9(1):1366, 12 2018.

[143] H. Sakoe and S. Chiba. Dynamic programming algorithm optimization for spoken word recognition. IEEE Transactions on Acoustics, Speech, and Signal Processing, 26(1):43–49, 2 1978.

[144] Davide Cacchiarelli, Xiaojie Qiu, Sanjay Srivatsan, Anna Manfredi, Michael Ziller, Eliah Overbey, Antonio Grimaldi, Jonna Grimsby, Prapti Pokharel, Kenneth J. Livak, Shuqiang Li, Alexander Meissner, Tarjei S. Mikkelsen, John L. Rinn, and Cole Trapnell. Aligning single-cell developmental and reprogramming trajectories identifies molecular determinants of myogenic reprogramming outcome. Cell Systems, 7(3):258–268.e3, 2018.

[145] Joshua M. Stuart, Eran Segal, Daphne Koller, and Stuart K. Kim. A gene-coexpression network for global discovery of conserved genetic modules. Science, 302(5643):249–255, 10 2003.

[146] Natasa Miljkovic, Jae-Young Lim, Iva Miljkovic, and Walter R. Frontera. Aging of skeletal muscle fibers. Annals of Rehabilitation Medicine, 39(2):155–162, 4 2015. PMID: 25932410 PMCID: PMC4414960.

[147] Miao Cui, Zhaoning Wang, Kenian Chen, Akansha M. Shah, Wei Tan, Lauren Duan, Efrain Sanchez-Ortiz, Hui Li, Lin Xu, Ning Liu, Rhonda Bassel-Duby, and Eric N. Olson. Dynamic transcriptional responses to injury of regenerative and non-regenerative cardiomyocytes revealed by single-nucleus RNA sequencing. Developmental Cell, page S1534580720301465, 2020.

[148] Ludo Waltman and Nees Jan van Eck. A smart local moving algorithm for large-scale modularity-based community detection. The European Physical Journal B, 86(11):471, 11 2013.

[149] Michael Ashburner, Catherine A. Ball, Judith A. Blake, David Botstein, Heather Butler, J. Michael Cherry, Allan P. Davis, Kara Dolinski, Selina S. Dwight, Janan T. Eppig, Midori A. Harris, David P. Hill, Laurie Issel-Tarver, Andrew Kasarskis, Suzanna Lewis, John C. Matese, Joel E. Richardson, Martin Ringwald, Gerald M. Rubin, and Gavin Sherlock. Gene ontology: tool for the unification of biology. Nature Genetics, 25(1):25–29, 2000.

[150] Edward Y Chen, Christopher M Tan, Yan Kou, Qiaonan Duan, Zichen Wang, Gabriela Meirelles, Neil R Clark, and Avi Ma'ayan. Enrichr: interactive and collaborative HTML5 gene list enrichment analysis tool. BMC Bioinformatics, 14(1):128, 2013.

[151] A J Freemont and J A Hoyland. Morphology, mechanisms and pathology of musculoskeletal ageing. J Pathol, 211(2):252–9, 1 2007.

[152] Marco V. Narici and Nicola Maffulli. Sarcopenia: characteristics, mechanisms and functional significance. British Medical Bulletin, 95(1):139–159, 9 2010.

[153] James G Ryall, Jonathan D Schertzer, and Gordon S Lynch. Cellular and molecular mechanisms underlying age-related skeletal muscle wasting and weakness. Biogerontology, 9(4):213–28, 8 2008.

[154] LaDora V Thompson. Age-related muscle dysfunction. Exp Gerontol, 44(1-2):106–11, 2009.

[155] Benjamin D Cosgrove, Penney M Gilbert, Ermelinda Porpiglia, Foteini Mourkioti, Steven P Lee, Stephane Y Corbel, Michael E Llewellyn, Scott L Delp, and Helen M Blau. Rejuvenation of the muscle stem cell population restores strength to injured aged muscles. Nature Medicine, 20(3):255–264, 2 2014.

[156] Pedro Sousa-Victor, Laura García-Prat, Antonio L Serrano, Eusebio Perdiguero, and Pura Muñoz-Cánoves. Muscle stem cell aging: regulation and rejuvenation. Trends Endocrinol Metab, 4 2015.

[157] I M Conboy, M J Conboy, A J Wagers, E R Girma, I L Weissman, and T A Rando. Rejuvenation of aged progenitor cells by exposure to a young systemic environment. Nature, 433(7027):760–4, 2 2005.

[158] D. D. Cornelison, M. S. Filla, H. M. Stanley, A. C. Rapraeger, and B. B. Olwin. Syndecan-3 and syndecan-4 specifically mark skeletal muscle satellite cells and are implicated in satellite cell maintenance and muscle regeneration. Dev Biol, 239(1):79–94, 11 2001.

[159] Sarah N Cilvik, Joy I Wang, Kory J Lavine, Keita Uchida, Angela Castro, Carolyn M Gierasch, Carla J Weinheimer, Stacey L House, Attila Kovacs, Colin G Nichols, and David M

Ornitz. Fibroblast growth factor receptor 1 signaling in adult cardiomyocytes increases contractility and results in a hypertrophic cardiomyopathy. PLoS One, 8(12):e82979, 2013.

[160] M. C. Naski, Q. Wang, J. Xu, and D. M. Ornitz. Graded activation of fibroblast growth factor receptor 3 by mutations causing achondroplasia and thanatophoric dysplasia. Nat Genet, 13(2):233–7, 1996.

[161] Gusztav Belteki, Jody Haigh, Nikolett Kabacs, Katharina Haigh, Karen Sison, Frank Costantini, Jeff Whitsett, Susan E. Quaggin, and Andras Nagy. Conditional and inducible transgene expression in mice through the combinatorial use of cre-mediated recombination and tetracycline induction. Nucleic Acids Research, 33(5):e51, 3 2005. PMID: 15784609 PMCID: PMC1069131.

[162] N. C. Jones, K. J. Tyner, L. Nibarger, H. M. Stanley, D. D. Cornelison, Y. V. Fedorov, and B. B. Olwin. The p38alpha/beta mapk functions as a molecular switch to activate the quiescent satellite cell. J Cell Biol, 169(1):105–16, 4 2005.

[163] Estela González-Gualda, Andrew G. Baker, Ljiljana Fruk, and Daniel Muñoz-Espín. A guide to assessing cellular senescence in vitro and in vivo. The FEBS Journal, 288(1):56–80, 2021.

[164] Dominik Saul, Robyn Laura Kosinsky, Elizabeth J. Atkinson, Madison L. Doolittle, Xu Zhang, Nathan K. LeBrasseur, Robert J. Pignolo, Paul D. Robbins, Laura J. Niedernhofer, Yuji Ikeno, Diana Jurk, João F. Passos, LaTonya J. Hickson, Ailing Xue, David G. Monroe, Tamara Tchkonia, James L. Kirkland, Joshua N. Farr, and Sundeep Khosla. A new gene set identifies senescent cells and predicts senescence-associated pathways across tissues. Nature Communications, 13(1):4827, 8 2022. number: 1 publisher: Nature Publishing Group.

[165] Tom H. Cheung and Thomas A. Rando. Molecular regulation of stem cell quiescence. Nature reviews. Molecular cell biology, 14(6):10.1038/nrm3591, 6 2013. PMID: 23698583 PMCID: PMC3808888.

[166] Jacob C. Kimmel, Lolita Penland, Nimrod D. Rubinstein, David G. Hendrickson, David R. Kelley, and Adam Z. Rosenthal. Murine single-cell rna-seq reveals cell-identity- and tissue-specific trajectories of aging. Genome Research, 29(12):2088–2103, 12 2019.

[167] Paul D. Thomas, Dustin Ebert, Anushya Muruganujan, Tremayne Mushayahama, Laurent-Philippe Albou, and Huaiyu Mi. Panther: Making genome-scale phylogenetics accessible to all. Protein Science, 31(1):8–22, 2022.

[168] Huaiyu Mi, Anushya Muruganujan, and Paul D. Thomas. Panther in 2013: modeling the evolution of gene function, and other gene attributes, in the context of phylogenetic trees. Nucleic Acids Research, 41(Database issue):D377–386, 1 2013. PMID: 23193289 PMCID: PMC3531194.

[169] Mayank Verma, Yoko Asakura, Bhavani Sai Rohit Murakonda, Thomas Pengo, Claire Latroche, Benedicte Chazaud, Linda K. McLoon, and Atsushi Asakura. Muscle satellite cell cross-talk with a vascular niche maintains quiescence via vegf and notch signaling. Cell Stem Cell, 23(4):530–543.e9, 10 2018. PMID: 30290177 PMCID: PMC6178221.

[170] Cory M. Dungan, Kevin A. Murach, Christopher J. Zdunek, Zuo Jian Tang, Georgia L. VonLehmden, Camille R. Brightwell, Zachary Hettinger, Davis A. Englund, Zheng Liu,

Christopher S. Fry, Antonio Filareto, Michael Franti, and Charlotte A. Peterson. Deletion of sa β-gal+ cells using senolytics improves muscle regeneration in old mice. Aging Cell, n/a(n/a):e13528, 2022.

[171] Lei Liu, Xianlin Yue, Zewei Sun, William S. Hambright, Jianming Wei, Ying Li, Polina Matre, Yan Cui, Zhihui Wang, George Rodney, Johnny Huard, Paul D. Robbins, and Xiaodong Mu. Reduction of senescent fibro-adipogenic progenitors in progeria-aged muscle by senolytics rescues the function of muscle stem cells. Journal of Cachexia, Sarcopenia and Muscle, 13(6):3137–3148, 2022.

[172] Lei Liu, Xianlin Yue, Zewei Sun, William S. Hambright, Qi Feng, Yan Cui, Johnny Huard, Paul D. Robbins, Zhihui Wang, and Xiaodong Mu. Senolytic elimination of senescent macrophages restores muscle stem cell function in severely dystrophic muscle. Aging, 14(19):7650–7661, 9 2022. PMID: 36084954.

[173] Alexandra C Keefe, Jennifer A Lawson, Steven D Flygare, Zachary D Fox, Mary P Colasanto, Sam J Mathew, Mark Yandell, and Gabrielle Kardon. Muscle stem cells contribute to myofibres in sedentary adult mice. Nat Commun, 6:7087, 2015.

[174] Thomas O. Vogler, Katherine E. Gadek, Adam B. Cadwallader, Tiffany L. Elston, and Bradley B. Olwin. Isolation, culture, functional assays, and immunofluorescence of myofiber-associated satellite cells. Methods in Molecular Biology (Clifton, N.J.), 1460:141–162, 2016. PMID: 27492171.

[175] Lucas Encarnacion-Rivera, Steven Foltz, H. Criss Hartzell, and Hyojung Choo. Myosoft: An automated muscle histology analysis tool using machine learning algorithm utilizing fiji/imagej software. PLOS ONE, 15(3):e0229041, 3 2020. publisher: Public Library of Science.

[176] Christopher S Fry, Jonah D Lee, Jyothi Mula, Tyler J Kirby, Janna R Jackson, Fujun Liu, Lin Yang, Christopher L Mendias, Esther E Dupont-Versteegden, John J McCarthy, et al. Inducible depletion of satellite cells in adult, sedentary mice impairs muscle regenerative capacity without affecting sarcopenia. Nature medicine, 21(1):76–80, 2015.

[177] John J McCarthy, Jyothi Mula, Mitsunori Miyazaki, Rod Erfani, Kelcye Garrison, Amreen B Farooqui, Ratchakrit Srikuea, Benjamin A Lawson, Barry Grimes, Charles Keller, et al. Effective fiber hypertrophy in satellite cell-depleted skeletal muscle. Development, 138(17):3657–3666, 2011.

[178] Cédric Debès, Antonios Papadakis, Sebastian Grönke, Özlem Karalay, Luke S Tain, Athanasia Mizi, Shuhei Nakamura, Oliver Hahn, Carina Weigelt, Natasa Josipovic, et al. Ageing-associated changes in transcriptional elongation influence longevity. Nature, pages 1–8, 2023.

[179] Magdalena Rudzińska, Alessandro Parodi, Anastasia V Balakireva, Olga E Chepikova, Franco M Venanzi, and Andrey A Zamyatnin Jr. Cellular aging characteristics and their association with age-related disorders. Antioxidants, 9(2):94, 2020.

[180] Dragomirka Jovic, Xue Liang, Hua Zeng, Lin Lin, Fengping Xu, and Yonglun Luo. Single-cell rna sequencing technologies and applications: A brief overview. Clinical and Translational Medicine, 12(3):e694, 2022.

[181] Sarah Aldridge and Sarah A Teichmann. Single cell transcriptomics comes of age. Nature Communications, 11(1):4307, 2020.

[182] John O Holloszy, John A Faulkner, Susan V Brooks, and Eileen Zerba. Muscle atrophy and weakness with aging: contraction-induced injury as an underlying mechanism. The Journals of Gerontology Series A: Biological Sciences and Medical Sciences, 50(Special_Issue):124–129, 1995.

[183] Lars Larsson, Hans Degens, Meishan Li, Leonardo Salviati, Young il Lee, Wesley Thompson, James L. Kirkland, and Marco Sandri. Sarcopenia: Aging-related loss of muscle mass and function. Physiological Reviews, 99(1):427–511, 2019.